Universität Ulm
Klinik für Neurologie
Ärztlicher Direktor: Prof. Dr. A. C. Ludolph

# Cerebral Correlates of Altered Oculomotor Performance in Parkinson's Disease: A Covariance Analysis between Intrinsic Functional Connectivity Magnetic Resonance Imaging and Video-oculography

**Dissertation**

zur Erlangung des Doktorgrades der Humanbiologie (Dr. hum. biol.)

der Medizinischen Fakultät der Universität Ulm

vorgelegt von

**MARTIN Peter GORGES**

geboren in Bernkastel-Kues

**2014**

| | |
|---|---|
| Amtierender Dekan: | Prof. Dr. Thomas Wirth |
| 1. Berichterstatter: | Prof. Dr. Jan Kassubek |
| 2. Berichterstatter: | Prof. Dr. Volker Rasche |
| Tag der Promotion: | 28. Juli 2014 |

# Table of Contents

# Abbreviations

| | |
|---|---|
| AC | Anterior Commissure |
| ACC | Anterior Cingulate Cortex |
| AD | Alzheimer's Disease |
| ANOVA | Analysis of Variances |
| BA | Brodmann Area |
| BOLD | Blood Oxygenation Level-Dependent |
| BS | Brainstem Network |
| BT | Basal Ganglia Thalamic Network |
| CB | Cerebellar Network |
| CEF | Cingulate Eye Field |
| CG | Cingulate Gyrus |
| DA | Dorsal Attention Network |
| DLPFC | Dorsolateral Prefrontal Cortex |
| DMN | Default Mode Network |
| DTI | Diffusion Tensor Imaging |
| EPI | Echo Planar Imaging |
| F | Female |
| FDR | False Discovery Rate |
| FEF | Frontal Eye Field |
| fMRI | Functional Magnetic Resonance Imaging |
| FOV | Field of View |
| FPC | Frontoparietal Control Network |
| H | Horizontal |
| ICN | Intrinsic Functional Connectivity Network |
| iFC | Intrinsic Functional Connectivity |
| iFCMRI | Intrinsic Functional Connectivity Magnetic Resonance Imaging |
| IFG | Inferior Frontal Gyrus |
| IPL | Inferior Parietal Lobule |
| IR | Infrared |

| | |
|---|---|
| L-FPC | Left Lateralized Frontoparietal Control Network |
| LED | Light Emission Diode |
| LEDD | Levodopa Equivalent Daily Dose |
| M | Male |
| MMSE | Mini Mental State Examination |
| MNI | Montreal Neurological Institute |
| MOT | Motor Network |
| MPRAGE | Magnetization-Prepared Rapid Gradient Echo |
| MRI | Magnetic Resonance Imaging |
| MT | Middle Temporal |
| N/A | Not Applicable |
| PANDA | Parkinson Neuropsychometric Dementia Assessment |
| PC | Posterior Commissure |
| PCC | Posterior Cingulate Cortex |
| PD | Parkinson's Disease |
| PD-CI | Cognitively Impaired Parkinson's Disease Patients |
| PD-Cu | Cognitively Unimpaired Parkinson's Disease Patients |
| PD-D | Parkinson's Disease Associated Dementia |
| PD-MCI | Parkinson's Disease Patients with Mild Cognitively Impairment |
| PEF | Parietal Eye Field |
| PEV | Peak Eye Velocity |
| PHG | Parahippocampal Gyrus |
| R-FPC | Right Lateralized Frontoparietal Control |
| RAVS | Rapid Alternating Voluntary Gaze Shifts |
| RMS | Root Mean Square |
| SC | Superior Colliculus |
| SEF | Supplementary Eye Field |
| SI | Saccadic Intrusions |
| SMG | Supramarginal Gyrus |
| SOG | Superior Occipital Gyrus |
| SPEM | Smooth Pursuit Eye Movement |

| | |
|---|---|
| SPL | Superior Parietal Lobule |
| STG | Superior Temporal Gyrus |
| SWJ | Square Wave Jerks |
| TE | Time Echo |
| TIFT | Tensor Imaging and Fiber Tracking |
| TR | Time Repetition |
| UPDRS | Unified Parkinson's Disease Rating Scale |
| V | Vertical |
| VA | Ventral Attention Network |
| VCP | Vertical Posterior Commissure Plane |
| VGRS | Visually Guided Reactive Saccades |
| VIS | Visuospatial Network |
| VOG | Video-oculography |

# 1. Introduction

## 1.1 Motor and Non-Motor Features of Parkinson's Disease

Parkinson's disease (PD) is the most frequent adult-onset movement disorder in the world. It is accompanied with unremitting neuronal cell loss in the entire human nervous system that can last for decades (Samii et al. 2004, Poewe and Mahlknecht 2014). PD took its name in honor of James Parkinson who initially characterized the disorders as a 'shaking palsy' in his eminent essay in 1817 (Parkinson 1817). The prevalence in the field of neurodegenerative diseases is second most only to Alzheimer's disease (AD) affecting approximately 1 % of the elderly beyond 65 years (Recchia et al. 2004), whereas up to 5 % of the patients display early-onset parkinsonism before the age of 40 years (Schrag and Schott 2006). According to present knowledge, conceivable environmental contributions do not appear to exist (Obeso et al. 2010), however, the last decade has risen evidence for genetic etiology comprising familial parkinsonism and genetic associations in sporadic PD (Trinh and Farrer 2013). In summary, age emerges as an important risk factor, but the mechanisms for developing PD still lack a comprehensive explanation and remain in the spotlight of current research.

Traditionally, PD was characterized as a pure movement disorder with cardinal motor symptoms (Hughes et al. 1992). However, the presence of non-motor manifestations beyond the classical motor presentations has become evident and consistently accepted (Olanow et al. 2011, Chaudhuri et al. 2011)**.** PD motor features mainly included hypokinesia, tremor, rigidity, small handwriting, and postural impairment (Okun 2013) that are accompanied by non-motor conditions categorized into disturbances of sleep, autonomic, sensory and cognition (Park and Stacy 2009, Chaudhuri et al. 2011, Okun 2013). Motor symptoms resulted chiefly from dopamine depletion in the nigro-striatal system whereas the coexisting widespread pathology far beyond the basal ganglia leads to the development of a broad variety of non-motor manifestations (Braak and Del Tredici 2009). Autopsy-controlled studies by Braak and co-workers (Braak et al. 2003, 2006, Braak and Del Tredici 2009) describe PD as a six-stage ascending spreading pathology beginning from

the lower brainstem and the olfactory gyrus (stages 1—2) towards the basal ganglia and mesencephalic structures (stages 3—4) to finally reaching the neo-cortex (stages 5—6). Notably, clinically recognizable motor symptoms manifest not before stage 3 and after an estimated loss of approximately one-third of striatal dopaminergic terminals and 50—80 % of midbrain dopaminergic cells (Braak and Del Tredici 2009). Hence, a much earlier disease onset has become accepted and preclinical biomarkers emerge as an promising investigation tool as the basis for putative disease modifying therapies (Akhtar and Stern 2012). The current diagnostic procedures of PD rely on clinical assessment that is based on the cardinal motor presentation together with a number of non-motor symptoms including cognitive decline (Holmes et al. 1992, Chaudhuri et al. 2011, Kassubek 2014).

Much interest is paid on this domain of therapy-resistant and gradually increasing cognitive impairment in PD that may come into the foreground (Braak et al. 2005, Braak and Del Tredici 2009, Olanow et al. 2011). The vast majority of PD patients develop cognitive deficits in the course of the disease leading to dementia in 83 % of 20 year survivors (Hely et al. 2008). PD patients displaying cognitive impairment (PD-CI) summarize mild cognitively impaired (PD-MCI) and PD-associated demented (PD-D) cases. PD-MCI is a well-described condition characterized mainly by executive and visuospatial difficulties (Litvan et al. 2012) and can be classified as a transient state between cognitively unimpaired PD (PD-Cu) and PD-D. The main clinical aspects of PD-D include pronounced cognitive difficulties in attention, executive and visuospatial control as well as memory problems (Emre et al. 2007). Cognitive difficulties manifest later in the course of PD when the pathological process reaches its full extent and targets the neo-cortex (Braak et al. 2005). Braak and colleagues estimated from their post-mortem neurohistological investigations a non-dopaminergic cell loss of approximately 30-50 % that coexist with pathology in the dopaminergic nigro-striatal system (Braak and Del Tredici 2009).

Other aspects of non-motor symptoms in PD involved a variety of visual dysfunctions including blurred and double vision, contrast insensitivity, disturbed color discrimination, visual hallucinations (Edwards and Bhatia 2011, Sauerbier and Chaudhuri 2013, Kassubek et al. 2013) and almost all facets of eye movement control (Chan et al. 2005, Mosimann et al. 2005, Pinkhardt and Kassubek 2011, Pinkhardt et al. 2012, van Stockum et al. 2013). The

oculomotor system provides a unique opportunity to understand the functional integrity of brain systems and gains insides into several forms of the complex human behavior (Leigh and Zee 2006, Goldberg and Walker 2013). The control of gaze is based upon the processing of the incoming visual stream that requires to foveate a target of interest. About half of the cerebral cortex incorporates wildly distributed and intertwined functionally integrated areas contributing to visual processing and oculomotor control (Gilbert 2013). Thus, the investigation of both oculomotion and functional interaction of brain structures in PD have emerged as promising non-invasive investigation tools in order to expand pathophysiological knowledge in PD (Neggers et al. 2012, Jamadar et al. 2013, Yerram et al. 2013). There is growing awareness that the explanation of the broad spectrum of visual impairment including oculomotor deficits in PD as a pure basal ganglia dysfunction is too narrow and the exact pathological processes outside the dopaminergic system remain to be discovered (Pinkhardt et al. 2012, Kassubek et al. 2013).

## 1.2 Disturbed Oculomotor Control in Parkinson's Diseases

The human eye comprises the photo-sensitive retina which forms an 'image' of the 3-dimensional visual world. The retina comprises the fovea centralis, its most central portion that holds the highest density of photoreceptors and thus provides ultimate visual accuracy compared to the surround peripheral area (Gilbert 2013). In order to bring or to re-fixate an object of interest in the visual scene upon the fovea, humans developed the ability to rotate the eye ball as an optimum strategy than turning the whole head (Walls 1962). Briefly, humans employ the ability to (i) keep the visual image steadily upon the retina in relation of head motion and (ii) to shift the gaze in order to foveate or re-foveate as quickly and as accurately as possible onto an object of interest in the visual surrounding (Anderson and MacAskill 2013). PD patients manifest a broad spectrum of oculomotor dysfunctions that are primarily linked to a lack of attentional control rather than impaired oculomotor nuclei in the brainstem (Pinkhardt and Kassubek 2011, Gorges et al. 2014b).

### 1.2.1 Anticipatory Saccades Interrupt Smooth Pursuit

The ability of sustained movement adaption in a highly predictive manner of a continuously moving target in the visual field is termed *smooth pursuit eye movement* (SPEM) (Fukushima et al. 2013). After a short initial response period, eye velocity settles to an average nearby the target velocity for <20°/s. For higher target velocities (>20°/s), the SPEM gain in healthy humans usually declines. The SPEM system involves large parts of the cerebral cortex comprising primary visual and associative areas, the frontal eye fields (FEFs) and supplementary eye fields (SEFs) (Fukushima et al. 2013) as well as cortical projections into the posterior limb of the internal capsule and into the midbrain and basal pontine nuclei (Dieterich et al. 2009). In addition, the cerebellum is heavily involved in generating pursuit and serves as a major relais by integrating the incoming signals in order to innervate the ocular motor neurons through the medial vestibular nucleus (Kheradmand and Zee 2011).

In patients with PD, SPEM is frequently interrupted or nearby abolished by anticipatory saccades that bring the eyes ahead towards its predicted future position (Pinkhardt et al. 2009). In rare cases small catch-up saccades (correctively moving the eye back onto the target) have also been reported. Notably, even in advanced cases, the patients are fairly able to track the target smoothly whereas the episodes of performing SPEM exclusively shortens with more frequent saccadic intrusions (SI) (Pinkhardt et al. 2012). Thus, the 'genuine' SPEM system appears to be preserved even in advanced cases. This raises the question of whether an executive dysfunction contributes to the characteristic anticipatory saccades interrupting smooth pursuit. A previous study in PD (Pinkhardt et al. 2012) suggested a contribution of extra-dopaminergic processes that may reflect a lack of inhibitory control. As proposed, this pathomechanism could be associated with the dysfunctional integration of the dorsolateral prefrontal cortex (DLPFC) and impaired cortico-striatal projections. It remains an open issue whether this hypothesis is sufficient to explain the circumscribed anticipatory behavior.

### 1.2.2 Hypometric Saccades as a Hallmark in Parkinson's Disease

Conjugated, rapid discontinuous gaze shifts in a step-wise manner are called *saccadic eye movements* (Schall and Thompson 1999) that take their name from the Old French 'saquer' meaning 'a jerk on the reins of a horse'. A prototype saccade produced by a healthy subject is characterized by an eminently abrupt onset of angular acceleration of the eyeball towards its peak (angular) velocity followed by a slightly slower deceleration to stop the eye movement near-instantly. Frequently, these saccadic eye movements end up with marginal under- or overshoot that is immediately compensated by a slow creeping drift defined as a glissadic eye movement (Becker 1989). For target amplitudes approximately larger than 10°, saccades do not almost accurately foveate the target in sense of a slightly undershoot (up to 15 % of the target amplitude) which required a corrective saccade to bring the target finally onto the center of the fovea. Corrective saccades of approximately more than 15 % of target amplitude or multiple immediately consecutive saccades are reported as a 'gaze shift segmentation' phenomenon (Terao et al. 2011) called saccadic hypometria which is a hallmark oculomotor dysfunction in PD. Usually, saccade performance is investigated during visually guided reactive saccades (VGRS) task, that is, tracking a 'jumping' target as quickly and as accurate as possible.

In PD, the dopaminergic nigro-striatal cell degradation in the basal ganglia is critical for locomotion including eye movements. In particular, the substantia nigra pars reticulata tonically inhibits the superior colliculus (SC) via GABA-ergic projections. A prerequisite for saccadic release is given by pausing the inhibition of the SC (Hikosaka and Wurtz 1989). Thus, the SC is an important visuomotor structure and plays a pivotal role in triggering both voluntary and reflexive saccades (Sauleau et al. 2008). Moreover, the SC projects to the cerebellum via the nucleus reticularis tegmenti pontis. The cerebellum contributes to saccadic control in optimizing saccade trajectory by increasing eye acceleration during saccade onset and controls the movement procedure in order to keep the eye on track (Kheradmand and Zee 2011). Unlike the basal ganglia, the SC may remain intact until later stages in the pathological process (Terao et al. 2011), and both the SC and the striatum receive cortical input from the FEF, the SEF, and parietal eye fields (van Stockum et al. 2013). The parietal eye field and several portions of the intraparietal sulcus are located in

the parietal cortex that is associated with oculomotor function and has been demonstrated to be a critical interface for attention and multiple sensory integration from visual and somatosensory modalities (Ptak and Muri 2013). Together, the exact pathomechanisms leading to saccadic hypometria in PD remains unknown, in particular the possible contribution of higher function networks. The peak eye velocity (PEV) is a function of primary saccade amplitude and has consistently reported to be unchanged in PD when patients perform VGRS (Pinkhardt and Kassubek 2011, Anderson and MacAskill 2013). Hence, in PD, the saccadic burst generator in the brainstem is believed to remain intact although the brainstem is heavily involved in the pathological process (Braak and Del Tredici 2009).

Another important measure of saccadic performance it the latency that is commonly determined as the difference in time between new target appearance and primary saccade onset during VGRS task. The literature revealed a mixed picture by reporting normal or shortened latencies in PD (Chambers and Prescott 2010). In contrast, many studies in PD consistently reported prolonged reaction times (Pinkhardt and Kassubek 2011) in support with a comprehensive meta-analysis by Chambers and Prescott (Chambers and Prescott 2010). However, taken the cognitive state into consideration, it appears safe to assume that latencies in PD are prolonged in cognitively impaired patients (PD-MCI, PD-D) and that latencies increase with disease severity (Mosimann et al. 2005, Terao et al. 2011). A recent study demonstrated similar saccadic reaction times in cognitively unimpaired PD patients compared with controls (MacAskill et al. 2012). Abnormal inhibition of the SC by the substantia nigra pars reticulata is also attributed to delayed-saccadic release as well as cell loss in the saccadic generator circuit (Chambers and Prescott 2010). The ‘saccade generator’ innervates the extra-ocular eye muscles directly and it resides in the rostral interstitial nucleus of the medial longitudinal fasciculus and the pontine paramedian reticular formation (Kassubek and Pinkhardt 2011). In summary, the pathological processes leading to prolonged latencies are not fully understood and the possible cortical contribution has not been sufficiently debated, so far.

### 1.2.3 Impaired Executive Eye Movement Control

Beside the *exogenous* tasks such as reflexive saccades or SPEM, voluntary saccades provide another aspect of *endogenous* oculomotor control linked to executive control. Paradigms such as rapidly alternating gaze shifts (RAVS) or the anti-saccades task are conducted to assess cognitive demanding oculomotor performance (Pinkhardt and Kassubek 2011, Anderson and MacAskill 2013). Subjects are asked to withhold their gaze shift upon a new visual stimulus (suppressing the 'visual grasp reflex') either until a 'cue' stimulus is given (delayed-saccades) or by directing their gaze instantaneously into the opposite direction (anti-saccades). Alternatively, subjects are required to produce as much as possible gaze shifts between two fixed targets (RAVS task). PD patients present significant problems in withholding unwanted gaze shifts (hyper-reflexive), resulting in an increased error rate in both delayed- and anti-saccades due to a lack of inhibition control (Pinkhardt and Kassubek 2011, Anderson and MacAskill 2013). In addition, PD patients manifest with initiation problems in performing continuously self-paced gaze shifts back and forth leading to a decreased number of RAVS (Pinkhardt et al. 2012).

The SEF contributes to target selection and visual search (Purcell et al. 2012), and the FEFs are critical in target selection of competing stimuli by mediating their information to the SC and directly to the saccadic generator in the brainstem (Bosch et al. 2013). The main input gait of the basal ganglia, the striatum, evaluates incoming and competing information for appropriate execution, however, with the putamen being involved in PD neurodegeneration, it remains to be discovered to what extent the PD pathology targets this mechanism (Yerram et al. 2013). The striatum also gains incoming streams from the DLPFC which contributes to voluntary eye movements in the sense of inhibition control to prevent unwanted reflexive saccades (Pinkhardt et al. 2012). The cingulate eye field is located in the anterior cingulate cortex and involved in motivation, behavior and executive control as well as saccade generation (Gaymard et al. 1998).

### 1.2.4 Oculomotion Abnormalities During Visual Fixation

Healthy individuals are expected to withhold any unwanted gaze shift during fixation of a steady target in the absence of head motion or any other additional visual stimulus. However, during attempted visual fixation of a single unmoving target, small conjugated (<1°), jerk-like and almost periodically alternating involuntary saccades (microsaccades) ubiquitously manifest in healthy subjects (Abadi and Gowen 2004). Shifting the image on the retina back and forth in small portions of about 0.5° counteracts sensor adaption (visual fading) (Martinez-Conde et al. 2006) due to the property of photoreceptors being optimized for responsiveness to alterations within the incoming visual stream (Martinez-Conde et al. 2004, 2013). Microsaccades are attributed to normal ocular fixation, however, some subjects manifest a second type of interruptive fixational eye movements, i.e. SI that are in some cases pathological. SI with a normal intersaccadic interval can be termed as square wave jerks (SWJ) and 'staircase' SI whereas both have larger amplitude (>1°) than microsaccades (Lemos and Eggenberger 2013). Microsaccades and SWJ preferentially occur in horizontal direction and are thought to share the same neuronal substrate (Otero-Millan et al. 2008, Martinez-Conde et al. 2013) whereas SI are partly somewhat larger (>2°) than SWJ. SI reveal to some extent a consecutive series of 'hypometric' or 'staircase' saccades that compromises steady fixation (Shaikh et al. 2011).

SWJ rarely occur in younger healthy subjects but more frequently in the elderly (Abadi and Gowen 2004) and commonly manifest in PD, in most cases in a pronounced (pathological) manner with respect to amplitude and prevalence. In both pathological state such as PD or in the healthy brain, SWJ are hypothesized to reflect internal 'neuronal noise' in the saccadic control system (Otero-Millan et al. 2013) mediated via the SC, a portion of the upper brainstem that plays a crucial role in the release of saccades by triggering the saccadic pulse generator in the brainstem. The 'neuronal noise' is considered to sporadically release a saccade away from the target due to an impaired triggering of the SC by the substantia nigra pars reticulata (Hikosaka and Wurtz 1989). This undesired saccadic drive yields a position error that is corrected by moving the eye back towards its initial position (Otero-Millan et al. 2013). In addition, the SC might be triggered by an increase in FEF activity that compensates pathological hyper-inhibition of the SC (Shaikh et al. 2011).

More pronounced fixational problems appear to manifest in PD during the fixational periods of VGRS (Shaikh et al. 2011). Both, SWJ and SI interrupt fixational episodes during VGRS. However, it appears speculative to attribute SI exclusively to pure SC associated dysfunction (Shaikh et al. 2011). Donaghy and colleagues covariated the SI rate with cognitive performance scores in non-demented patients with motor neuron disease and demonstrated an association between SI amplitude and frontal lobe dysfunctions. The authors conclude from their findings abnormalities in the frontal-collicular pathway and suggested SI amplitude as a pre-clinical biomarker for frontal lobe impairment (Donaghy et al. 2009).

Steady visual fixation is closely related to the SPEM system, however, evidence for a separate, independent visual fixational system emerges from several electrophysiological investigations. In rhesus macaques, a higher discharging rate in certain neurons located in the parietal lobe during steady fixation compared with SPEM condition has been observed. These findings lead to the assumption that the parietal lobe may play an important role during steady fixation. In addition, those studies suggested a mechanism that suppresses unwanted saccades during both SPEM and attempted visual fixation (Leigh and Zee 2006). In summary, the nature of the underlying pathological processes leading to fixational instabilities still lack a comprehensive explanation. It remains an open issue whether (i) SWJ and SI share a common neural substrate, (ii) SI occur preferentially in horizontal direction like SWJ and (iii) SI and SWJ are related to disturbed higher function networks.

## 1.3 'Resting-State' Functional Magnetic Resonance Imaging

### 1.3.1 Coherent Hemodynamics in the 'Resting' Human Brain

Only a view years after the development of functional magnetic resonance imaging (fMRI) in the early nineties (Kwong et al. 1992, Ogawa et al. 1992), Biswal and co-workers pioneered the intrinsic functional connectivity (iFC)MRI approach by observing spontaneous blood oxygenation level-dependent (BOLD) fluctuation in the absence of specific tasks ('task-free') that oscillate in a correlated manner. Their study demonstrated coherent low frequency (<0.1 Hz) BOLD activations between a portion of the motor cortex and its corresponding contralateral region while subjects stayed motionless 'resting' in the

scanner (Biswal et al. 1995). These results suggest an intrinsic 'ongoing' activity (Fox and Raichle, 2007) in almost those brain regions that become activated during specific tasks (e.g. finger-tapping) or during goal-directed attention. Together, this observations suggested synchronous BOLD fluctuation between functionally connected regions (Buckner 2010). Moreover, the coherence patterns of functionally interconnected regions are mainly constrained by anatomic connectivity (Greicius et al. 2009, Buckner 2010, van Oort et al. 2014), showing convergence between measures of 'resting-state' intrinsic functional connectivity (iFC) and structural connectivity.

Our brain is permanently engaged in intrinsic processes rather than the view of our central nervous system as being only reflexive in the sense of resting on-demand to promptly focus attention to incoming stimuli form the external environment (Raichle 2010). Internal modes of cognitive and emotional processing may comprise information acquisition, storing, interpreting, abstraction, responding to and prediction (Greicius et al. 2003, Raichle and Snyder 2007, Buckner et al. 2008, Raichle 2010). Evidence for the need of intrinsic brain activity also rises from the nearby infinity visual information arriving the human eye each second from the external environment (Raichle 2010). The entropy, a measure of information, is about 10,000,000 kbits/s provided for the retina whereas 'only' approximately 3,000 kbits/s are leaving the retina due to the limited number of available axons of the optic nerve (Gorges et al. 2014b). Finally less than 10 kbits/s are believed to be under attentive scrutiny (Anderson et al. 2004).

The human brain is a very efficient (van den Heuvel and Hulshoff Pol 2010) and an economical network with minimized 'connection costs' (Achard and Bullmore 2007). It consumes approximately 10 times more energy (about 20 % of the human's total energy budget) than predicted by its weight (Clarke and Sokoloff 1999). Since the obtained time-courses reflect a relative measure of the brain's hemodynamics, iFCMRI serves as an indirect proxy for iFC computation (Lee et al. 2013). However, interpreting iFCMRI is complicated by several forms of technical and physiological artifacts as well as by dynamically changed functional couplings (Buckner et al. 2013). Nowadays, 'task-free' functional (f)MRI provides a powerful noninvasive method that copes with the challenge to study the mapping of human's functional integration (Biswal et al. 2010).

A review by Biswal supports the notion that 'task-free' fMRI is a valuable tool for investigating the functional integration of the human brain. He argued that the "the resting-state provides a more general picture of human brain function" than task-induced coactivation (Biswal 2012). Task-induced coactivation corresponds consistently to intrinsic functional connectivity networks (ICNs) in the 'resting' human brain (Di et al. 2013). In a multiparametric study design, iFCMRI may be preferable over 'task-induced' fMRI because other modalities — such as video-oculography (VOG) as worked out here — can be investigated under controlled conditions in the lab rather than in the constrained environment of an MRI-tomograph.

### 1.3.2 Intrinsic Connectivity Networks

ICNs are large scale distributed brain maps organized in a functional topological manner (Yeo et al. 2011). An ICN is thought to comprise individual portions (hubs) that are connected with each other. The ensemble of hubs within the ICN defines a functional interacting network whose iFC between hubs serves as a tool for studying human connectomics (Filippi et al. 2013). An ICN can be computed by the hypothesis-driven seed-based approach (Friston 2011) by defining a seed region based on a priori knowledge. The extracted time-series from one of those seed region is than correlated with the time series from all other voxels yielding a correlation map of coherent BOLD fluctuations – the ICN (Van Dijk et al. 2010). Multiple continuously and dynamically interacting ICNs have been identified 'at rest' by means of iFCMRI (Beckmann et al. 2005, Smith et al. 2009, Laird et al. 2011, Leech and Sharp 2014, Lee et al. 2013) and other modalities such as magnetoencephalography (Brookes et al. 2011, Hall et al. 2013). In iFCMRI, these common ICNs were identified by using data-driven independent component analysis (Beckmann et al. 2005) on the basis of a comprehensive functional explication and behavioral taxonomy (Laird et al. 2011) and were validated by seed-based analysis methods (Buckner et al. 2008, Cole et al. 2010, Van Dijk et al. 2010).

The most prominent and possibly the most studied brain map is the default mode network (DMN) that was firstly described by Marcus Raichle and co-workers (Raichle et al. 2001). The DMN meets the intrinsic activation requirements in a unique manner – that is, the

idling activity (‘baseline’) in the absence of goal-directed attention to an external stimulus is significantly higher than the activity when ones is being engaged in active tasks (Zhang and Raichle 2010). In addition, the brain’s default mode is hypothesized to support broadly exploratory monitoring of the external environment during relaxed attention in a ‘watchfulness’ (Mason et al. 2007, Gilbert et al. 2007) or in manner of a ‘sentinel’ (Buckner et al. 2008).

In this study, common networks were addressed with focus on their contribution to eye movement control and cognitive domains. ICNs comprising the basal ganglia-thalamic, brainstem, and ventral attention system that are strongly related to emotional and autonomic processes (Laird et al. 2011). In particular, the ventral attention system included the cingulate eye field and the interaction between the basal ganglia and the brainstem is crucial for saccade generation (Di Martino et al. 2008). The frontoparietal ICN participate in memory process, attention and executive control and covers the DLPFC (Spoormaker et al. 2012) which is attributed to ocular inhibition control. The cerebellar ICN (Smith et al. 2009) is involved in SPEM generation and refines saccadic gaze shifts. The dorsal attention ICN covers almost all brain areas that are strongly associated with oculomotion (Vincent et al. 2008), whereas the visuospatial systems encompasses associative structures such as the visual motion sensitive middle temporal areas (Beckmann et al. 2005) that play an import role for visual tracking. The motor network is linked to action — execution and somesthesis (Wu et al. 2011). In summary, major brain maps with functionally distinct properties have been clearly identified. Moreover, iFCMRI builds upon ongoing intrinsic functioning when the human brain is ‘at rest’ or even in unconscious state such as sleep, anesthesia or coma (Heine et al. 2012). Learning consolidation, rehearsal and future preparation has been suggested in this context (Smith et al. 2009), however, this fundamental question on the presence of intrinsic activity remains not conclusively explained.

### 1.3.3 Altered Functional Connectivity in Parkinson’s Disease

Some efforts have been made to elucidate the neural functional interactive basis in PD by means of iFCMRI. Altered functional integration of cortico-striatal loops has been reported in PD patients (Kwak et al. 2010, Helmich et al. 2010, Baudrexel et al. 2011, Wu et al. 2012).

Specifically, striatal iFC decline appear to be associated with dopaminergic function loss (Hacker et al. 2012, Luo et al. 2014). Only a few studies investigated cortical iFC characteristics in PD finding disrupted functional integration of the motor cortex (Wu et al. 2009b) and abnormal iFC within the DMN (Tessitore et al. 2012).

Notably, all patients in these aforementioned studies were non-demented, and both increased and decreased iFC changes were observed. The nature of increased iFC is still debated and suggested to be caused by antiparkinsonian treatment (Kelly et al. 2012, Luo et al. 2014) rather than adaptive changes (Mevel et al. 2011). Aging of the healthy brain may possibly manifest in altered functional integration. Damoiseaux and co-workers comprehensively studied changes in iFC within ICNs and demonstrated that the intrinsic activity within the DMN was significantly reduced in the elderly compared with controls (Damoiseaux et al. 2008). The authors suggest the major impact of the brain's DMN on cognitive performance. In agreement with these findings, the cognition-related metabolism hypothesis suggested that the distribution of the Aβ plaques observed in early stages of AD is remarkably similar to the anatomical structure of the DMN – a feature that coincides with cognitive difficulties (Buckner et al. 2005).

Guiding voluntary saccades requires several neural mechanisms under the framework of pre-emptive perception that manifests in activation in the cingulate eye field prior to the release of a saccade (Yerram et al. 2013). Terao and co-workers proposed a possible task-related modulation within the basal ganglia resulting in oscillatory spike activity that may contribute to both 'hyper-reflexivity' and slowed initiation (Terao et al. 2011). Moreover, iFC neuroimaging revealed that connectivity loss in the putamen versus the caudate nucleus follows the same gradient as dopamine depletion, indicating a decoupling of the putamen prior to the caudate nucleus (Hacker et al. 2012). Other imaging studies on functional integration in PD patients (Tessitore et al. 2012, Olde Dubbelink et al. 2013) indicate widespread functional remapping that likely alters connectivity associated with oculomotor function. It is questionable, however, whether these arguments are sufficient to disentangle the – apparently contradictory – pathomechanisms of the coexisting 'hyper-reflexivity' and slowed saccade initiation. Together, the exact neural basis of altered iFC in disease state and their association to the cognitive domain remains an open issue as

well as their relationship to oculomotor control. Moreover, the functional integration of the visuospatial system, the attentional and executive ICNs or the possible cerebellar functional contribution to PD pathology is not fully understood.

## 1.4 Methodological Motivation and Hypotheses of the Present Bimodal Study

There are four main issues of the present study that are subsequently outlined in detail.

### 1.4.1 First Aim: Oculomotor Performance Depending on the Cognitive State

So far, a multitude of studies investigated oculomotor performance in PD (Mosimann et al. 2005, Pinkhardt et al. 2008, 2009, Yugeta et al. 2010, Kassubek and Pinkhardt 2011, MacAskill et al. 2012, Otero-Millan et al. 2013, van Stockum et al. 2013), however, with the exception of saccadic performance (Terao et al. 2011), the influence of cognitive impairment on oculomotor performance have not been investigated systematically. Moreover, the comprehensive investigation of SWJ and SI during visual fixation may be a promising predictor of cognitive difficulties (Donaghy et al. 2009) and may manifest in a pathological fashion in PD patients (Shaikh et al. 2011, Lemos and Eggenberger 2013).

As the first aim, this study aimed to investigate oculomotor control in PD-Cu and PD-CI patients compared with controls in order to quantify oculomotor abnormalities depending on the cognitive status by means of

1) SPEM performance elicited for both single-dot and full-field pattern
2) VGRS task
3) rapid alternating voluntary gaze shifts (RAVS)
4) inhibition control by means of delayed- and anti-saccades
5) attempted visual fixation of a steady target
6) fixation during VGRS task.

The investigation of VGRS entails a comprehensive SI analysis beside the common saccadic performance measures.

### 1.4.2 Second Aim: Challenges in Implementing a Software Package in Order to Investigate Intrinsic Functional Connectivity by Means of Functional Brain Imaging

The analysis of iFCMRI is challenged by several factors, i.e. the raw data of the BOLD sensitive fMRI sequence are predominantly governed by noise as well as physiological artifacts attributed to cardiac, respiratory and head motion confounding (Cole et al. 2010). Freely available software packages allowing iFC analysis yet exists (e.g. resting state toolkit, REST, www.restfmri.net), nevertheless, one issue of this study was to integrate a fully extensible module for iFC analysis into the in-house developed software package *Tensor Imaging and Fiber Tracking* (TIFT) (Müller et al. 2007a). The TIFT software allows multimodal concepts as a special feature that has been concurrently implemented during software development. Beyond this major aspect, TIFT provides a broad level of analysis techniques in one software environment and this application is permanently under further development (Müller and Kassubek 2013).

Thus, the primary methodological goal of the present dissertation was to develop a tool to be integrated into the TIFT software package providing complementary algorithms in order to analyze

1) iFC at the group level and
2) correlations between iFC within ICNs and oculomotor parameters.

### 1.4.3 Third Aim: Intrinsic Functional Connectivity at Group Level

According to the assumption that the brain consists of large scale networks which in turn interact with each other, the present study aimed at working out ICNs in both PD-Cu and PD-CI patients as well as in the healthy control group in terms of their functional interaction. This was accomplished by a voxel-seed based analysis approach in investigating brain maps comprising the following ICNs,

1) default mode
2) left lateralized frontoparietal control
3) right lateralized frontoparietal control

4) visuospatial
5) motor
6) dorsal attention
7) ventral attention
8) basal ganglia-thalamic
9) brainstem
10) cerebellar.

These are well-defined large-scale networks of correlated temporal patterns which have been previously identified in the 'resting-brain' in elderly (Gorges et al. 2014a) and younger adults incorporating the behavioral interpretation (Beckmann et al. 2005, Smith et al. 2009, Laird et al. 2011). The intent of the present study was to examine iFC beyond the subcortical and pure basal ganglia related functional integration whilst taking the cognitive state in PD patients into account in comparison with normal aged brain.

### 1.4.4 Fourth Aim: Covariance Analysis – Association between Altered Oculomotor Control and Functional Integration

Most of our knowledge in terms of oculomotor associated human brain portions emerges from task-based fMRI studies. These studies based upon higher activations in spatially distinct brain areas with respect to the baseline when subjects performing oculomotor tasks in the scanner (Jamadar et al. 2013, Ptak and Muri 2013). However, this does not explain the functional interaction of these areas among themselves. Likewise, a control group is required with respect to pathological conditions such as PD. It appears that no framework exists, that provides a relationship between the level of altered oculomotor performance and functional integration, so far.

Finally, the fourth and overall goal of this dissertation builds upon the three aforementioned issues and was to assess the relationship between altered oculomotor performance in PD and iFC within various ICNs. More specifically, the PD group was pooled from PD-Cu and PD-CI patients in order to provide a continuous spectrum of PD patients ranging from cognitively unimpaired to demented cases. For the correlation analysis,

oculomotor parameters were obtained from conditions mentioned above (**Chapter 1.4.1**) and correlated with iFC in the aforelisted ten ICNs (**Chapter 1.4.3**)**.**

### 1.4.5 Synopsis of the Aims

In summary, this study utilized a bimodal approach in order to expand the knowledge about the pathophysiological correlates of altered oculomotor control in terms of the influence of functional brain networks integration in PD. For this purpose, PD patients with cognitive decline (PD-MCI and PD-D), defined in a detailed neuropsychological assessment according to the recently proposed guidelines (Litvan et al. 2012), were contrasted to cognitively unimpaired PD patients and healthy controls. This study aimed to examine both oculomotor performance and functional integration depending on the patients' cognitive presentation. It is primarily aimed at investigating the relationship between eye movement disturbances and iFC in PD patients presenting with various cognitive states (PD-Cu, PD-CI).

# 2. Methods

## 2.1 Synopsis of the Present Study Design

The study uses a bimodal approach combining assessments of oculomotor performance and of iFC in the 'resting-state' to compare PD patients with age-matched healthy controls. Oculomotor performance was probed by a battery of tests addressing various aspects of oculomotor control, using VOG to record eye movements. 'Task-free' fMRI recordings were used to study iFC by use of a seed based analysis approach. All participants underwent detailed clinical and neuropsychological examinations from which cognitive and clinical scores were obtained. PD patients with and without cognitive deficits were compared with controls and to each other in terms of oculomotor performance and iFC. Possible associations between oculomotor parameters and iFC within various ICNs were examined by means of covariance analysis in all PD patients (PD-Cu, PD-CI).

## 2.2 Characterization of Subjects Participating Experiments

A total number of 49 patients with PD and 25 controls participated in the study. All subjects were native German speakers, right-handed according to the Edinburgh Handedness Inventory (Oldfield 1971) and presented with normal or corrected visual acuity without any moderated or severe eye diseases. The subjects participated in the multicenter LANDSCAPE study (Balzer-Geldsetzer et al. 2011) and were inpatients or outpatients of the Department of Neurology, University of Ulm, Germany. All participants provided written and informed consent with a protocol approved by the central Ethics Committee of the multicenter LANDSCAPE study at the University of Marburg and the local Ethics Committee of the University of Ulm (No. 36/12). The data of 18 patients and 3 control subjects were excluded from the analysis because of severe head movements, or corrupted signals in oculomotor examination or iFCMRI imaging.

**Table 1** summarises demographic data, clinical scores and levodopa equivalent medication of the volunteers included in this study. The analysis were based on 53 subjects comprising patients with the diagnosis of PD (*N*=31, 71 years) and representative age-matched healthy controls that underwent neuropsychological, oculomotor and iFCMRI. The diagnosis of PD

had been established by a board-certificated neurologist (Prof. Dr. J. Kassubek) specialised in movement disorders according to standard clinical criteria while the classification of the PD patients' cognitive state was assessed by a certified clinical psychologist according to the criteria of the Movement Disorder Society Task Force (Emre et al. 2007, Litvan et al. 2012). Exclusion criteria were signs of other neurodegenerative of asymptomatic Parkinsonian syndromes mainly on the basis of dopaminergic responsiveness, dementia with Lewy bodies (McKeith 2002), clinically significant or unstable medical condition, including serious cerebrovascular diseases, psychiatric abnormalities, severe hearing damage and significant white matter lesion load such as periventricular or deep white-matter hyperintensities (Fazekas et al. 1987). Notably, white matter lesions associated with small vessel cerebrovascular disease cause a wide range of oculomotor disturbances (Pinkhardt et al. 2014). All PD patients received antiparkinsonian treatment and were medicated with levodopa equivalent that was computed on individual basis as the total levodopa equivalent daily dose (LEDD) according to the procedure suggested by Tomlinson and co-workers (Tomlinson et al. 2010). The PD patients were subdivided into two groups so that the data from three subject groups were used.

*Group I* comprised PD patients who had been classified as having normal cognition (PD-Cu; *N*=14, 70 years).

*Group II* comprised PD patients diagnosed as cognitively impaired (PD-CI; *N*=17, 72 years) consisting of 11 subjects with PD-MCI and 6 cases with PD-D.

*Group III* comprised of healthy volunteers (controls; *N*=22, 68 years) without any history of neurological or psychiatric disorders or other medical conditions. They were free of significant white matter lesions (see text above). None of them were found as having cognitive problems. A minimum score of 29 (out of 30) in the Mini Mental State Examination (MMSE) (Folstein et al. 1975) and a minimum transformed score of 13 (out of 18) in the sensitive cognitive screening DemTect (Kalbe et al. 2004) was required for inclusion as a control subject.

Motor deficits in all PD patients were quantified utilizing the UPDRS, part III, motor assessment (Fahn and Elton 1987). PD patients were screened for global dementia by

means of the MMSE. For a more detailed characterisation of patients' cognitive and affective dysfunctions, Parkinson's neuropsychometric dementia assessment (PANDA) (Kalbe et al. 2008) was administrated addressing overall performance of the following cognitive domains: executive control, attention, visuospatial functions, episodic and working memory. The PANDA (part B) depression questionnaire was used to rate PD patient's depression state.

Table 1| Subjects (*N*=53) Included in This Study. Data are depicted as median (interquartile range). [a]Statistical significance across both patient groups (PD-Cu, PD-CI) and, if applicable, control subjects in Kruskal-Wallis analysis of variances (ANOVA) on ranks. [b]Under medication. Abbreviations: M, Male; F, Female; UPDRS III, Unified Parkinson's Disease Rating Scale (part III, motor assessment); MMSE, Minimental State Examination; PANDA, Parkinson Neuropsychometric Dementia Assessment; LEDD, Levodopa Equivalent Daily Dose; N/A, Not Applicable.

| PARAMETER | Patients, All | PD-CI | PD-Cu | controls | ANOVA[a] *p* |
|---|---|---|---|---|---|
| **Number**, n | **31** | **17** | **14** | **22** | N/A |
| **Gender**, M/F | **19/12** | **8/9** | **11/3** | **15/7** | N/A |
| **Age** / y | **71** (64-74) | **72** (64-74) | **70** (45-77) | **68** (65-73) | 0.650 |
| **Duration of Disease /** y | **4** (2-8) | **4** (2-10) | **6** (2-8) | N/A | 0.708 |
| **Hoehn & Yahr**, score | **3** (2-3) | **3** (2-3) | **2** (2-3) | N/A | 0.657 |
| **UPDRS III**[b], score | **12** (8-14) | **12** (9-18) | **10** (5-13) | N/A | 0.091 |
| **MMSE**, score | **28** (26-29) | **27** (26-28) | **29** (28-30) | **30** (30-30) | 0.000 |
| **PANDA**, score | **20** (18-25) | **18** (13-20) | **26** (23-27) | N/A | 0.000 |
| **PANDA (depression)**, score | **3** (0-6) | **4** (0-6) | **2** (0-6) | N/A | 0.034 |
| **Duration of Education** / y | **8** (8-10) | **8** (8-10) | **10** (8-10) | **12** (10-13) | 0.001 |
| **LEDD** / mg | **380** (214-659) | **360** (231-620) | **475** (205-880) | N/A | 0.565 |

Both PD patient subpopulations (PD-Cu, PD-CI) and the healthy controls were well age-matched as indicated by Kruskal-Wallis non-parametric one-way analysis of variances (ANOVA, $p$=0.65) (Kruskal and Wallis 1952). Moreover, the patient subgroups revealed matched distributions of disease duration (ANOVA, $p$=0.70) and Hoehn & Yahr rating (ANOVA, $p$=0.66). The UPDRS III motor score were similar ($p$=0.09) in PD-CI compared with PD-Cu patients. Groups significantly differed in years of education (ANOVA, $p$=0.001) and post-hoc analysis indicated similar education years in PD-Cu patients and controls ($p$>0.05) but revealed significantly less educated PD-CI patients compared with both PD-Cu ($p$=0.035) and to the control group ($p$<0.001). Global dementia assessment by means of MMSE (ANOVA, $p$<0.001) revealed the gradient controls>PD-Cu>PD-CI, however, the

outcomes for PD-Cu and controls (MMSE≥27) were in normal range. As expected, PD-CI vs. PD-Cu patients performed significantly worse in PANDA ($p$<0.001) test. PD-CI patients presented with a tendency ($p$=0.034) to be more depressed than the PD-Cu group. Both patient groups received similar levodopa equivalent doses (LEDD, $p$=0.565).

## 2.3 Videooculographic Examination

### 2.3.1 Measurement Device

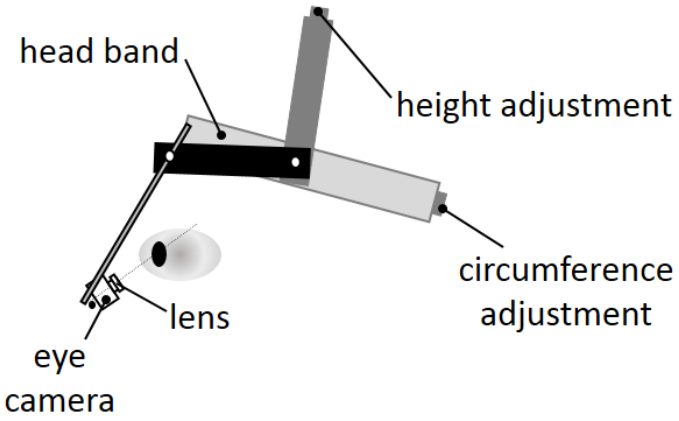


**Figure 1| EyeLink I® Setup.** Schematic setup of the head mounted and freely adjustable video-based eye tracking system.

Eye movements were measured with a head mounted video-based EyeLink I® VOG system (SR Research Ltd., Osgoode, ON, Canada) consisting of two infrared sensitive miniature cameras with additional infrared light emitting diodes (LEDs) mounted on a head-set (**Figure 1**). Fastening this head-set to subjects' heads required a compromise between comfort for the participant and minimal risk of unwanted slipping during measurement. The EyeLink I® system allows robust binocular recording at a temporary sampling rate of 250 Hz and special resolution of 0.005° in a range of at least ±20° horizontal and ±17° vertical at a root mean square noise level of 0.01°, (**Table 2** for detailed specifications). The cameras are adjustable in all 6 degrees of freedom (3 translational, 3 rotational) to facilitate optimal eye tracking which requires a good contrast between pupil and iris and no occlusion of the subject's field of view by any part of the eye tracking system. In addition, the EyeLink I® system provides an on-line display of its measurement so that recording quality and participants' response behaviour could be monitored in real time. The system

outputs uncalibrated horizontal and vertical eye positions of each eye in a camera-centred frame of reference.

Table 2| EyeLink I® Specifications. Abbreviations: H, Horizontal; V, Vertical; RMS, Root Mean Square; IR, Infrared; LED, Light Emission Diode.

| PARAMETER | VALUE |
|---|---|
| **Cameras**, n | 2 |
| **Total Head Mount Weight /** g | 600 |
| **Sampling Rate /** Hz | 250 |
| **Spatial Resolution /** ° | 0.005 |
| **Spatial Range /** ° | >40 (H); >34 (V) |
| **Noise Level**, RMS | 0.01 |
| **Distance Camera-Eye /** mm | 40-70 |
| **IR LED Wavelength /** nm | 940 |
| **IR LED Irradiance /** mW/cm$^2$ | 0.8 (typ); 1.2 (max) |

### 2.3.2 Laboratory Environment

VOG recording took place in a dimly lighted, acoustically shielded room. Participants were comfortably seated in a chair with armrests and viewed a white hemi-cylindrical screen of radius 160 cm. To minimize head movements during measurement, subjects' heads were stabilized by an adjustable chin rest such that the vertex was at the centre of the hemi-cylindrical screen; thus, eyes-to-screen distance amounted to about 150 cm, depending on subjects' head anatomy.

The hemi-cylindrical screen carried identical pairs of vertically adjacent red and green light emitting diodes (LEDs, *d*=0.3°) placed equidistantly every 5° up to ±40° in horizontal and up to ±15° in vertical direction which served as targets for saccades and fixation and were invisible when not lit. Above subjects' head were mounted a projector a (TOSHIBA®, TDP-EX20; lens-to-screen distance, 150 cm) and a mirror galvanometer directing a red laser onto the screen. Both devices served to elicit smooth eye movements by moving either a luminous pattern or a single red spot (*d*=0.15°) across the screen. The inclination of their optical axes with respect to horizontal (by about 30°) was compensated for by appropriate predistortions of their control signals. Both the laser spot and the projector pattern could be moved in a range of at least ±20° and ±15° in both horizontal and vertical direction. In

addition, loudspeakers were placed adjacent to the screen in 90° to the left and right of the centre.

### 2.3.3 Stimuli

The first part of the oculomotor measurement protocol probes basic properties of SPEM and gaze shift performance. Simple 'reflexive' experimental paradigms included (i) SPEM performed by keeping a sinusoidally moving target steadily on the fovea, (ii) tracking a rapid 'jumping' target as fast and as accurate as possible but sustain attempt fixating onto the target when not moving or (iii) to merely fixate a non-moving spot at the primary center position in the visual field. The second part of oculomotor test conditions aims to test executive functions by means of delayed-saccades, anti-saccades, and RAVS. **Table 3** summarizes the full oculomotor measurement protocol in the order of stimulation.

SPEM was elicited in 2 ways: (i) by fullfield-pattern stimulation with a pattern subtending 40° (H) x 30° (V) and consisting of a central yellow spot ($d$=0.8°) embedded in a random cloud pattern of 800 red dots (each of 0.7° diameter) and (ii) by stimulation with a single spot (laser projection). With both methods, four conditions were tested, i.e. sinusoidal motions of

1) horizontal, amplitude ±20°, $f$=0.125 Hz, 6 cycles=48 s
2) horizontal, amplitude ±20°, $f$=0.375 Hz, 12 cycles=32 s
3) vertical, amplitude ±15°, $f$=0.125 Hz, 6 cycles=48 s
4) vertical, amplitude ±20°, $f$=0.375 Hz, 12 cycles=32 s.

In all conditions, subjects were asked to track the central fixation spot as accurately as possible. During the attempted visual fixation paradigm, subjects were requested to quietly fixate the LED light straight ahead for 30 seconds in order to investigate the possible occurrence of square waves and involuntary saccades interrupting the attempted visual fixation.

Table 3| Oculomotor Measurement Protocol. Abbreviations: H, Horizontal; V, Vertical; SWJ, Square Wave Jerks

| TEST | DETAILS | INSTRUCTION | PARAMETERS |
|---|---|---|---|
| **Smooth Pursuit of Fullfield Pattern** | sinusoidal oscillations; *f*=0.125 Hz and *f*=0.375 Hz; amplitude ±15° (V), ±20° (H) | track the spot in the center of the pattern | pursuit gain |
| **Smooth Pursuit of Single Dot** | sinusoidal oscillation; *f*=0.125 Hz, *f*=0.375 Hz; amplitude ±15° (V), ±20° (H) | track the target dot as accurate and as possible | pursuit gain |
| **Attempted Visual Fixation** | central red target led lit | fixate target for 30 seconds | saccade rate (SWJ, intrusions) |
| **Visually Guided Reactive Saccades** (VGRS) | Pseudo-random sequence (spatial and temporal) of target steps of 5-40° (H, ±20°) and 5-30° (V, ±15°). Each step proceeds from target of previous step | track the jumping dot as accurately and as quickly as possible | accuracy, peak eye velocity and latency of primary saccade; saccadic intrusion rate |
| **Rapid Alternating Voluntary Gaze Shifts** (RAVS) | two permanent targets at ±10° (H) and ±10° (V) | shift the eyes as fast as possible back and forth between the two targets for 30 seconds | number of self-paced gaze shifts |
| **Delayed- Saccads** | Pseudo-random sequence (spatial and temporal) of target steps of 5-40° (H, ±20°). The previous target is maintained while acoustic cue is presented after a pseudorandom delay and it is extinguished 1.5 seconds after cue. each step proceeds from position of previous step | withhold reaction to new target until acoustic "go" is sounded | error rate (premature saccades towards the target) |
| **Anti-saccades** | Pseudo-random (spatial and temporal) target steps from the center in range of +-20° (h) | shift the eyes to mirror position of target into the opposite empty half field | error rate (prosaccades) |

VGRS were elicited pseudo-randomly in an unpredictable manner lighting one of the red LEDs as a target such that horizontal target steps of either 3 times of ±5, ±10°, ±15,° ±40° and 4 times of ±20° as well as vertical steps of 4 times of ±5° , ±10°, ±15°, ±30° and 2 times ±20° resulted, respectively. The maximum elongation was ±20° horizontal and ±15° vertical. The targets were presented on average for 2.9 s (range 2.1 – 3.5 s) horizontal and for 2.6 s (2.1 – 3.5 s) in vertical direction, respectively, resulting in acquisition times of 92.8 s and 93.6 s, respectively. Subjects were instructed to re-fixate the target as accurately and as quickly as possible after each target step and to withhold unwanted gaze shifts prior to the next target onset.

**Figure 2** shows delayed-saccades and anti-saccades setup in order to test inhibition control. In the delayed-saccade task (**Figure 2A**), subjects were asked to withhold their reaction to new additive pseudo-random target onset after 1.7 s on average (range 1.1—2.3 s) by lighting a LED in 5, 10, 20, and 40° horizontal distance (either 8 trials to the left and right), until an acoustic 'go' cue was given. The cue was pseudo-randomly presented on average a 2.1 s (range 1.5—2.5s) after the new additive target onset requiring the subject to fixate as accurate and as quickly as possible the new target. The old target varnishes 1.5 s after the cue was given. For both condition, VGRS and delayed-saccades, each target step proceeds with the previous step.

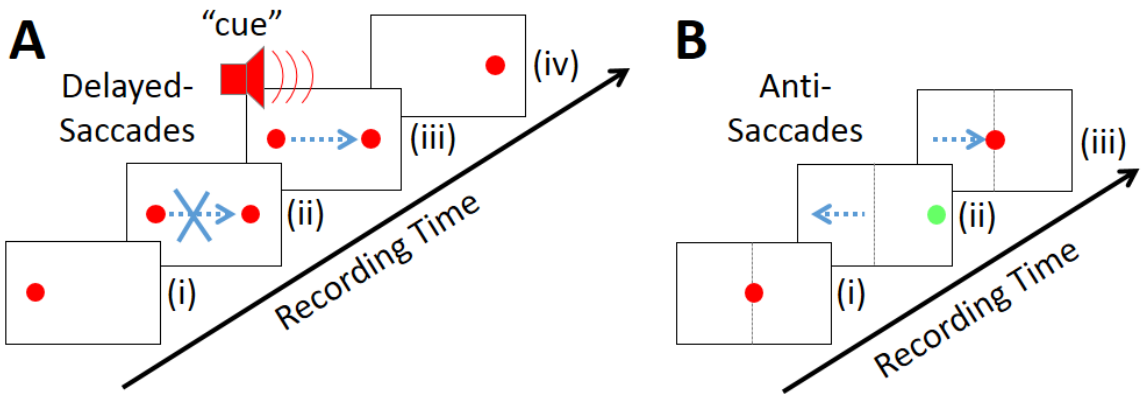


Figure 2| Schematic Illustration of the Oculomotor Stimulus Display for Inhibition Tests. Delayed-saccades (**A**) required the subject to fixate a red spot (i) and withhold their gaze shift onto a new target (ii) until an acoustic 'go' signal is sounded (**iii**). The old target is extinguished (iv) and serves as the new home position for the next sweep. Subjects are asked in the anti-saccade task (**B**) to fixate the home position (i) and move their gaze into the opposite, mirror direction into the second half plane (ii) when a new green target appears at an eccentric position. The gaze has to be shift onto the central position serving as the new home position for the next trial (**iii**). Blue dotted arrows indicate the required gaze shift.

In the anti-saccade paradigm participants are requested to instantly initiated a gaze shift towards the mirror position of the new target into the opposite empty half field (anti-saccade) as illustrated in **Figure 2B**. This is accomplished by lighting a red LED in the centre of the screen as the initial target followed by a pseudo-random target step on average after 2.6 s (range 2.1—3.0 s) by lighting a green LEDs at ±5, ±10 and ±15, and ±20° eccentrical horizontal position (either 8 trials to the left and right). A learning session of five runs was administered prior to the delayed-saccade and anti-saccade conditions.

RAVS were evoked in horizontal and vertical directions by asking subjects to saccade for 30 s as rapidly as possible back and forth between two permanently lit red LEDs arranged symmetrically about the primary direction with 20° horizontal or vertical angular separation. In case of inappropriate behaviour (obvious slowing, saccades too small) subjects were verbally encouraged to try to do better.

### 2.3.4 Preprocessing of Videooculographic Raw Data and Calibration Procedure

The oculomotor recordings were preprocessed and analysed by use of an interactive MATLAB® (The Mathworks Inc, Natick, Massachusetts, USA) based in-house software package developed by Dr. Jürgens and utilized in several studies (Pinkhardt et al. 2008, 2009, 2012, 2014, Gorges et al. 2013). Briefly, preprocessing of the VOG raw data included noise reduction by filtering, cross-talk suppression, calibration and artefact rejection (corrupted signals, blinks). Low pass filtering using a 4th order Bessel filter with cut-off frequency of 30 Hz was applied in order to minimize noise.

The incoming raw signal from the EyeLink® I systems are non-calibrated orthogonalized 'raw' data represented as position, $VOG_x(t)$ and $VOG_y(t)$, with respect to the VOG camera coordinate system. In general, these position stream is given as a non-linear function of the 'true' eye position. In general, exclusively horizontal eye movements do not represented exclusively horizontal, $VOG_x(t)$, but also a cross-talk in the $VOG_y(t)$ signal and vice versa. Hence, a robust and reliable calibration procedure that maps the incoming 'raw' signal with respect to the 'true' eye position is required in order to perform a linearization and elimination of the cross-talk. The mapping of the 'raw' data position stream, $VOG_x(t)$ and $VOG_y(t)$, into the 'true' eye position, $E_x(t)$ and $E_y(t)$ can be expressed by the following equation system:

$$E_x(t) = \sum_{k=0}^{N} c_k^{xx} \cdot \left(VOG_x(t)\right)^k + \sum_{k=0}^{N} c_k^{yx} \cdot \left(VOG_y(t)\right)^k$$
$$E_y(t) = \sum_{k=0}^{N} c_k^{yy} \cdot \left(VOG_y(t)\right)^k + \sum_{k=0}^{N} c_k^{xy} \cdot \left(VOG_x(t)\right)^k \qquad \text{(Equation 1)}$$

**Equation 1** was solved for $N$=5 by means of non-linear least squares in order to obtain the calibration coefficients vectors $c^{xx}$, $c^{yy}$, $c^{xy}$ and $c^{yx}$ as previously applied in our other studies (Pinkhardt et al. 2008, 2009, 2012, 2014, Gorges et al. 2013). Notably, the calibration procedures requires the subject to track the target which was given for 'slow' ($f$=0.125 Hz) single-dot SPEM.

Preprocessing was finalized by removing blinks and periods of corrupted registration by utilizing a threshold-based procedure where episodes exhibiting eye-positions >40°, eye velocities >2,000°/s and eye accelerations >100,000°/s$^2$ were considered as artefacts and discarded for further analysis.

### 2.3.5 Algorithm in Order to Detect Saccadic Eye Movements

Saccades were semi-automatically detected by a recursively data-driven algorithm in order to define the onset and end of a saccade as well as the point in time of PEV. The saccade detection algorithm was as follows:

1) search occurrence of largest PEV within response epoch
2) go back in time from PEV until <10°/s: time of saccade onset
3) go forward in time form PEV until velocity <10°/s: time of saccade termination
4) make sure saccade duration > minimum saccade duration of 10 ms
5) make sure saccade amplitude > minimum saccade amplitude of 0.5°
6) exclude processed time range for further saccade detection
7) repeat step 3 until all detected velocity maxima (step 2) are processed
8) results were visualised on the computer display

In spite of preprocessing (see text above), not all saccades were correctly identified by this algorithm. In this event, the results of the algorithm could be cancelled and the saccade onset and end were manually defined on the display by means of a cursor.

### 2.3.6 Smooth Pursuit Eye Movement Analysis

The SPEM gain was determined from the calibrated and preprocessed pursuit recordings that were decomposed into saccades and 'pure' SPEM. Here, the gain is the fundamental

component of SPEM velocity in relation to the target velocity and was determined by the following steps (Pinkhardt et al. 2014):

1) detect all saccadic velocity peaks exceeding 120°/s according to the previously described ‘saccade detection algorithm’ and discard these saccade-associated episodes
2) fit the remaining ‘desaccadized’ points in time with a sine function by non-linear least square fitting
3) repeat 1) and 2) with a lower peak saccadic velocity threshold of 60°/s
4) repeat 1) and 2) with a lower peak saccadic velocity threshold of 3 times root mean square noise amplitude of interval
5) divide estimated PEV of SPEM component by peak target velocity in order to obtain SPEM gain for each direction

### 2.3.7 Investigation of Square Wave Jerks and Saccadic Intrusions

SI were investigated in recordings of the attempted visual fixation condition and likewise of the VGRS condition where two epochs were distinguished for this purpose: (i) the ‘gaze shift’ epoch comprising a 1-second interval beginning with primary saccade onset and (ii) the ‘fixation epoch’ consisting of the intervals of fixation at the current target position prior to saccade onset an at the new target following the gaze shift epoch. SI rate quantifies the prevalence of SWJ or SI and was measured as degrees per second. The intrusion rate was computed as the accumulated amplitude of saccades divided by considered time interval. In attempted fixation task, all saccades were considered as SWJ or SI. During fixational episodes in VGRS task, saccades <2° amplitude were considered as SWJ and excluded from SI analysis. This prevented a misleading interpretation of small intrusions or SWJ that were attributed to small artefacts that were not detectable during preprocessing. The SI rate in VGRS task was obtained for horizontal and vertical direction separately.

### 2.3.8 Cyclopean Eye Signal

For all oculomotor conditions, the binocular recording was merged into a cyclopean signal since both eyes were considered to reveal no systematic differences in any individual. This

was accomplished by either averaging the data stream of the left and right eye or taken the monocular recording in case of a corrupted measurement in the other eye. This procedure provides a robust strategy in order to overcome potential measurement difficulties in one eye and has been utilized in recent studies, e.g. Pinkhardt and colleagues (Pinkhardt et al. 2014).

### 2.3.9 Postprocessing and Parameter Extraction

Smooth pursuit performance was characterised in terms of its gain; this analysis yielded 16 parameters corresponding to 2 stimuli (single-dot, fullfield-pattern) x 2 frequencies (0.125 Hz, 0.375 Hz) x 4 directions (right, left, up, down). Saccadic gaze shifts recorded during the VGRS task were characterized by the amplitude, the peak velocity and the latency of the primary saccades. From the individual saccades of each participant were calculated:

*Saccade gain* from the linear regression of eye amplitude, $E^{ampl}$, on target step amplitude, $T^{ampl}$, using

$$E^{ampl} = b + m \cdot T^{ampl} . \qquad \text{(Equation 2)}$$

Because term *b* has a positive nonzero value in general (Becker 1989), the gain defined by

$$g(E^{ampl}, T^{ampl}) = \frac{E^{ampl}}{T^{ampl}} \qquad \text{(Equation 3)}$$

is not a constant. As a representative value for the gain, $g(E^{ampl}, T^{ampl}=20°)$ was calculated from **Equation 2** and **Equation 3**.

*Saccade PEV* as a function of saccade amplitude ('main sequence') was obtained by fitting a rational function to the scatter plots of PEV versus $E^{ampl}$ of all primary ('main') saccades:

$$V^{\max}(E^{ampl}) = \frac{a \cdot E^{ampl}}{b + E^{ampl}} \qquad \text{(Equation 4)}$$

Here, parameter *a* represents the asymptotic maximum of PEV reached with large saccades ('saturation') while parameter *b* characterises the onset of the saturation (Becker 1989). In order to characterise PEV by a single figure, the value reaches with saccades of $V^{max}$ ($E^{ampl}$=20°) was calculated from **Equation 4**.

*Saccade latency*, which was available directly from the time stamps of target presentation and main saccade onset, was averaged across all responses irrespective of target step amplitude. The above parameters were calculated separately for each target step direction (right, left, up, down).

In order to quantify inhibition control, the error rate was obtained for both delayed- and anti-saccades. In the delayed-saccade condition, a premature saccade occurring before the acoustic cue was rated as an error. In the anti-saccade condition, the occurrence of a prosaccade was rated as an error. The error rate (percentage of errors) of each of these conditions was determined separately for the horizontal and vertical directions. During RAVS task, the number of gaze shifts exceeding 10° saccade amplitude was determined for horizontal and vertical direction. The number of such shifts was arithmetically averaged for horizontal and vertical directions since the outcomes of both direction were considered to be basically similar (Pinkhardt et al. 2009, 2012).

SIs were characterized as the SI rate and calculated for attempted visual fixation condition as well as for horizontal and vertical VGRS task separately. In order to investigate whether SI occur in a preferred direction, the intrusion rate was computed as orthogonalized components.

## 2.4 'Resting-state' Intrinsic Functional Connectivity Magnetic Resonance Imaging

The subsequently in detail described iFCMRI data processing procedure was performed using the TIFT software package (Müller et al. 2007a, Unrath et al. 2010, Müller and Kassubek 2013) and has recently been published (Gorges et al. 2014a).

### 2.4.1 MRI Scanning Protocol

Magnetic Resonance Imagining (MRI) data were acquired on a 3 Tesla clinical scanner (Magnetom Allegra syngo MR A30, Siemens, Erlangen, Germany). The scanning protocol is summarized in **Table 4** and included the BOLD sensitive (Kwong et al. 1992, Ogawa et al. 1992) 'resting-state' iFCMRI sequence ($T_2$*) and a $T_1$-weighted 3D magnetization-prepared gradient echo image (MPRAGE) sequence. Each subject contributed to either one run of iFCMRI and anatomical high resolution MPRAGE. All participants were asked to stay motionless in the MRI scanner. In addition, all subjects were instructed to keep relaxed with their eyes closed but awake during 'task-free' iFCMRI data acquisition.

Table 4| Magnetic Resonance Imaging (MRI) Scanning Protocols. Abbreviations: ; iFCMRI, Intrinsic Functional Connectivity MRI MPRAGE, Magnetization-Prepared Gradient Echo Image; EPI, Echo Planar Imaging; BOLD, Blood Oxygenation Level-Dependent; TR, Repetition Time, TE, Time to Echo; FOV, Field of View.

| | **iFCMRI** | **MPRAGE** |
|---|---|---|
| **Sequence** | EPI BOLD ($T_2$*) | $T_1$ |
| **Orientation** | transversal | sagittal |
| **Slices**, n | 36 | 192 |
| **Distance Factor /** % | 0 | 50 |
| **Slice Thickness /** mm | 3.5 | 1.0 |
| **Flip Angle /** ° | 80 | 7 |
| **Voxel Size /** mm | 3.5 x 3.5 x 3.5 | 1.0 x 1.0 x 1.0 |
| **TR /** ms | 2200 | 2500 |
| **TE /** ms | 30 | 432 |
| **FOV**, n | 64 x 64 x 36 | 256 x 256 x 192 |
| **FOV /** mm | 224 x 224 x 126 | 256 x 256 x 192 |
| **Slice Averages**, n | 1 | 1 |
| **Repetitions**, n | 200 | 1 |
| **Acquisition Time /** min | 7:24 | 9:22 |
| **Band Width /** Hz/Pixel | 2298 | 140 |
| **Echo Distance /** ms | 0.49 | 10.8 |
| **EPI Factor**, n | 64 | N/A |

### 2.4.2 Preprocessing Procedure

The preprocessing steps applied to the iFCMRI data followed standard practice as recently described (Van Dijk et al. 2010, Whitwell et al. 2011, Lee et al. 2013). Briefly, preprocessing included motion correction, resampling on a 1 mm grid, normalization to Montreal

Neurological Institute (MNI) stereotaxic space (Brett et al. 2002), spatial filtering with Gauss kernel (7 mm full-width at half maximum), temporal linear detrending, and temporal bandpass filtering (0.01<*f*<0.08 Hz) followed by discarding the first 15 of 200 volumes. To insure quality, all volumes of the echo planar imaging (EPI) and MPRAGE images were visually inspected for appropriate registration.

*Step I:* Head motion-correction was directly performed online by the Magnetom Allegra scanner software (syngo MR VA30A, Siemens, Erlangen, Germany) that performed 3-dimensional elastic motion correction in all degrees of freedom. The motion-corrected raw data (released as common Digital Imaging and Communications in Medicine – DICOM files) were used for (further) preprocessing.

*Step II:* The data were than resampled from 3.5 x 3.5 x 3.5 $mm^3$ to a cubic 1 mm grid represented as a 256 x 256 x 256 matrix by means of the nonparametric *k*-nearest neighbor regression approach (Altman 1992). This method used the average voxel intensity of the *k*-nearest neighbor voxels weighted by the inverse of their distance. Notably, this up-sampling procedure yields a 'pseudo'-resolution that has to be kept in mind for both further processing steps and the interpretation of the results on the basis of the (native) scanner resolution. Upsampling to a cubic 1 mm grid has already been performed in previous studies (e.g. (Müller and Kassubek 2013)).The advantage of using the identical voxel resolution for coregistration with the high-resolution MPRAGE anatomical image also in the standardized MNI stereotaxic space is that in this way voxel locations could be easily and unambiguously transferred from one modality to another and vice versa. In addition, performing analysis in a cubic 1 mm grid provides a prerequisite for the utilized seed-voxel approach.

*Step III:* Deformation of the rescaled EPI images (1.0 x 1.0 x 1.0 $mm^3$) into the normalized MNI stereotaxic space were accomplished by a previously described two-stage procedure (Müller et al. 2007a). First, based on the EPI images, eight landmarks were operator defined within the first volume for each subject and validated by a neuroanatomical skilled physicist. These landmarks were placed within the anterior commissure (AC), posterior commissure (PC), vertical PC plane (VCP) superior, VCP inferior, prolonged AC—PC front,

prolonged AC—PC back, prolonged PC—left hemisphere border, prolonged PC—right hemisphere border. An affine transformation in all 6 degrees of freedom (x, y, z, pitch, roll and yaw) into the MNI stereotaxic space was performed according to the coordinates of these landmarks. This procedure was applied for all subjects ($N$=53) in order to compute an EPI template by arithmetically averaging the voxel intensities of all individual MNI-transformed EPI images. The deformation procedure was refined in the second iteration step by normalizing the individual EPI data upon the study-specific template (Müller et al. 2007a). Finally, in order to assure quality, the MNI-normalization was validated by visually comparing each participant's EPI (first volume of data series) overlaid on the Colin Average Brain (Holmes et al. 1998). In a second step, the Pearson's product correlation coefficient (Rodgers and Nicewander 1988) was determined between each individual EPI image (first volume of data series) and the EPI-template as a quantitative measure. The landmarks were refined for each subject whose normalization was unacceptable according to visual inspection or a correlation coefficient of $r$<0.8. The same procedure was applied to the anatomically high resolution MPRAGE images used for seed-voxel location definitions and for illustration purpose (display of results on a morphological background).

*Step IV:* Spatial filtering was applied by using a 7 mm full-width at half maximum Gaussian blur filter (3-dimensional bell shape representing normal distribution) in order to optimize signal to noise ratio. The filter with of 7 mm equals twice the recording voxel size of 3.5mm which is a common choice (Ashby 2011) according to the assumption that the Gauss filter is designed as a 'matched filter'.

*Step V*: Possible scanner-drifts during the iFCMRI data acquisition were voxel-wise removed over each volume by linear detrending (Friman et al. 2004). Linear detrending was performed by subtracting the linear fit of the voxel time-course. The time-courses were further band-pass filtered since iFCMRI data analysis is based on the coherence of low-frequency BOLD fluctuations. The frequency spectrum was band-limited for cut-off frequencies in the range of 0.01<$f$<0.08 Hz (Zou et al. 2008, Van Dijk et al. 2010, van den Heuvel and Hulshoff Pol 2010) using a 6th-order Butterworth bandpass filter design. The first 15 out of 200 volumes of each time course were discarded due to the

transient filter response (**Figure 10C**) and due to scanner oscillations at the beginning of iFCMRI data acquisition. Moreover, this commonly applied procedure allows the participant to adapt to the experimental condition (Song et al. 2011).

### 2.4.3 Seed-Based Correlation Mapping of iFCMRI Data

Large scale correlation maps were computed according to the seed-based approach (Biswal et al. 1995) in accordance with recent studies (Yeo et al. 2011, Choi et al. 2012, Hacker et al. 2012). Ten well-defined ICNs (Smith et al. 2009, Laird et al. 2011, Lee et al. 2013) were computed by placing seed-voxels (i.e., encompassing one voxel only) into regions that had been consistently reported to serve as central hubs for the respective ICN as listed in **Table 5**. Moreover, these seed regions are also linked to oculomotion with the exception of the seed region corresponding to the motor ICN. The exact location of the seed was manually refined based on the subjects' averaged high-resolution $T_1$-images (MPRAGE) according to the standardized MNI atlas (Brett et al. 2002). As a novel aspect, the time series of one single voxel (i.e., the seed-voxel) was extracted in contrast to common approaches such as averaging the time series of voxels within a defined seed-region (Chao-Gan and Yu-Feng 2010, Song et al. 2011, Whitwell et al. 2011) or taking each of the voxels within the given ROI as a seed-voxel (Choi et al. 2012). The extracted time-course of the seed-voxel or the averaged time-course extracted from all voxel within the ROI spheres were correlated with the time series of all other voxels across the whole brain, yielding a corresponding correlation coefficient (*r*-value) for each voxel. The similarity of using a seed-voxel (1.0 x 1.0 x 1.0 $mm^3$) or a spherical ROI with a radius of about 4 mm is illustrated in our recent study (Gorges et al. 2014a). Nevertheless, using ROIs larger than 4 mm, the resulting brain maps slightly differ for 'anatomically small' seed regions as also demonstrated in (Gorges et al. 2014a). Since the time courses were considered to be normally distributed, correlations were computed by use of the parametric Pearson's product moment correlation method (Rodgers and Nicewander 1988). Fisher's *r*-to-*z* transformation (Silver and Dunlap 1987) was applied voxel-wise to improve the normal distribution of the individual's connectivity maps as Z-statistic images (Friston 2011). Each voxel corresponds to a $z(r)$ score representing its connectivity strengths with respect to the seed-voxel of the respective ICN.

Table 5| Definitions of Seed-Voxels with their Corresponding Intrinsic Connectivity Network (ICN). Laterality and location of seed-voxels (1.0 x 1.0 x 1.0 mm) in the Montreal Neurological Institute (MNI) stereotaxic space.

| ICN | R/L | MNI | | | Seed Voxel REGION |
|---|---|---|---|---|---|
| | | *X* | *Y* | *Z* | |
| **Default Mode** (DMN) | - | 0 | -55 | 26 | Posterior Cingulate Cortex |
| **Left Frontoparietal Control** (L-FPC) | L | -50 | -52 | 49 | Left Inferior Parietal Lobule |
| **Right Frontoparietal Control** (R-FPC) | R | 50 | -54 | 49 | Right Inferior Parietal Lobule |
| **Motor** (MOT) | L | -27 | -27 | 68 | Motor Cortex |
| **Visuospatial** (VIS) | R | 47 | -72 | 15 | Middle Temporal Area/Extrastriate Cortex |
| **Dorsal Attention** (DA) | R | 30 | -9 | 54 | Frontal Eye Field |
| **Ventral Attention** (VA) | R | 11 | 13 | 0 | Ventral Striatum |
| **Basal Ganglia-Thalamic** (BT) | R | 18 | 2 | 20 | Caudate Nucleus |
| **Brainstem** (BS) | R | 2 | -31 | -20 | Midbrain |
| **Cerebellum** (CB) | R | 32 | -79 | -34 | Cerebellum |

In order to obtain the ICN at the group level for visualization purpose, the *z*(*r*) scores were arithmetically averaged voxel-wise (Vincent et al. 2008, Choi et al. 2012, Hacker et al. 2012). The brain maps at the group level were statistically validated by also applying a two-sided one-sample *t*-test (Song et al. 2011).

## 2.5 Statistical Analysis

### 2.5.1 Demographics, Clinical Data, and Videooculographic Parameters

Statistical data analysis of the patients' and controls demographic and clinical data as well as video-oculographic parameters were performed utilizing the 'Statistics Toolbox' provided by MATLAB® (The Mathworks Inc, Natick, Massachusetts, USA). The 'average' (and 'range') were described as non-parametric statistics using the median (and the interquartile range) whereas the interquartile range was computed by subtracting the 25% quartile from the 75% quartile (Hyndman and Fan 1996). Kruskal-Wallis non-parametric one-way analysis of variances (Kruskal and Wallis 1952) was applied for all groups (PD-CI, PD-Cu, controls) followed in the event of significance by a Wilcoxon Mann-Whitney-U-Test (Mann and Whitney 1947) in order to detect differences between two groups. All correlations between video-oculographic parameters and cognitive scores were performed using Spearman's rank-order correlation coefficients (Conover and Iman 1981). Correction for multiple comparisons was not applied since contrasts were considered to be driven by

a specific hypothesis. All statistical tests were 2-sided and *p*-values <0.05 indicated statistical significance.

### 2.5.2 Intrinsic Functional Connectivity at Group Level

The iFCMRI data were statistically analyzed by the TIFT software package (Müller et al. 2007a, Unrath et al. 2010, Müller and Kassubek 2013) with use of the previously described preprocessing procedure. The two-sided parametric Student's *t*-test for unequal variances (Ruxton 2006) was used to test voxel-wise differences between two groups in each of the 10 ICNs. Note that each voxel corresponds to a *z(r)* score representing its iFC strengths with respect to the seed voxel of the respective ICN. The resulting *p*-values were corrected for multiple comparisons using the false discovery rate approach (Genovese et al. 2002) at $q$=0.05 level indicating that *p*-values < 0.05 were considered statistical significant. Further correction for multiple comparisons in order to onward reduction of the alpha error were performed by using a parametric correlation-based clustering procedure (Unrath et al. 2010) that discarded isolated clusters not exceeding the minimum size of 343 voxels at 1 mm resolution. This cluster threshold results from a cubic edge length of 7 mm corresponding to twice the 3.5 mm recording resolution. The Brodmann map (Brodmann 1909) was used as an approximate benchmark to locate the resulting brain regions although the observed cluster do not necessarily fully cover the given Brodmann area (BA).

### 2.5.3 Covariance Analysis in Parkinson's Disease Patients between Videooculographic Parameters and Intrinsic Functional Connectivity

The correlation analyses of VOG and iFCMRI modalities were performed using an in-house developed bimodal algorithms integrated in the TIFT software package (Müller et al. 2007a, Müller and Kassubek 2013). To investigate possible relationships between altered oculomotor parameters and iFC within each of the 10 ICN, both PD patient groups (PD-CI and PD-Cu) were pooled. In order to keep the number of correlations manageable, the oculomotor parameters were condensed to a total of 7 most representative quantities, i.e.

1) 'single-dot' SPEM,
2) error rate of inhibition demanding tasks

3) accuracy gain of primary saccades in VGRS task
4) latency of primary saccades in VGRS task
5) number of RAVS
6) rate of SWJ during attempted fixation
7) rate of SI during VGRS.

These 7 scores were considered to be significantly altered in PD (Mosimann et al. 2005, Pinkhardt et al. 2009, 2012, Pinkhardt and Kassubek 2011, Terao et al. 2011, MacAskill et al. 2012, Otero-Millan et al. 2013). The scores were obtained by arithmetically averaging the standard *z*-transformed subscores. Each oculomotor score was correlated with the *z(r)* value in each voxel of the corresponding ICN. This procedure was applied to all 10 ICNs in order to obtain regions which were significantly correlated with the respective oculomotor parameter. All correlations were studied using Spearman's rank-order correlation coefficients (Conover and Iman 1981). To correct for multiple comparisons, the false discovery rate approach was applied followed by the correlation-based clustering approach which was similarly performed for iFCMRI group comparison. Regional effects were only accepted for clusters at an estimated voxel-threshold *z(r)* corresponding to $p$=0.01 (uncorrected) after performing 40 independent Monte Carlo simulation correlations prior to the oculomotor scores for each of the ten ICNs. This procedure for correlation analysis was previously suggested (Tessitore et al. 2012) in order to optimize sensitivity and specificity. BA were used to locate possible significant clusters as described in **Chapter 2.5.2**.

# 3. Results

## 3.1 Altered Oculomotor Performance in Parkinson's Disease

Interference statistics with a paired *t*-test exhibited no significant direction-dependent differences ($p>0.11$) for right and left eye movement performance in terms of SPEM pursuit gain, saccadic accuracy, and PEV in PD patients. Hence, these parameters were arithmetically averaged for the right and left direction for both, PD patients and controls. Likewise, the number of RAVS counts for horizontal and vertical condition did not significantly differ ($p=0.62$) and were arithmetically averaged. Briefly, Kruskal-Wallis ANOVA indicated a significant effect of group (PD-CI, PD-Cu, controls) in almost all of the investigated eye movement parameters, with the exception of the PEV. Post-hoc analysis indicated that these effects were due to significant differences between both PD-Cu and PD-CI on the one hand and controls on the other hand. In rare cases (<10 %), not all parameters could be evaluated due to artefacts or other confounding disturbances.

### 3.1.1 Smooth Pursuit is Preferentially Disturbed by Anticipatory Saccades

Principally, SPEM velocity accuracy decreased clearly upon high-frequency stimulation ($f=0.375$ Hz) in both PD-CI and PD-Cu patients as well as in the controls. As shown in **Figure 3**, the decreased SPEM gain in PD patients results nearly exclusively from SI that interrupt the patients' continuously target tracking of a single-dot stimulus. In particular, at slow ($f=0.125$ Hz) target oscillating frequencies, the SI corrupted periods of perfect SPEM in an anticipating manner that resulted in predictive saccades towards the target motion with a subsequent return onto the target (**Figure 3A—B**). For fast ($f=0.375$ Hz) target motions, the SI pattern somewhat changes in a way that mainly predictive saccades were followed by a slightly back correction rather than a nearly complete return (since there was no time for a return saccade).

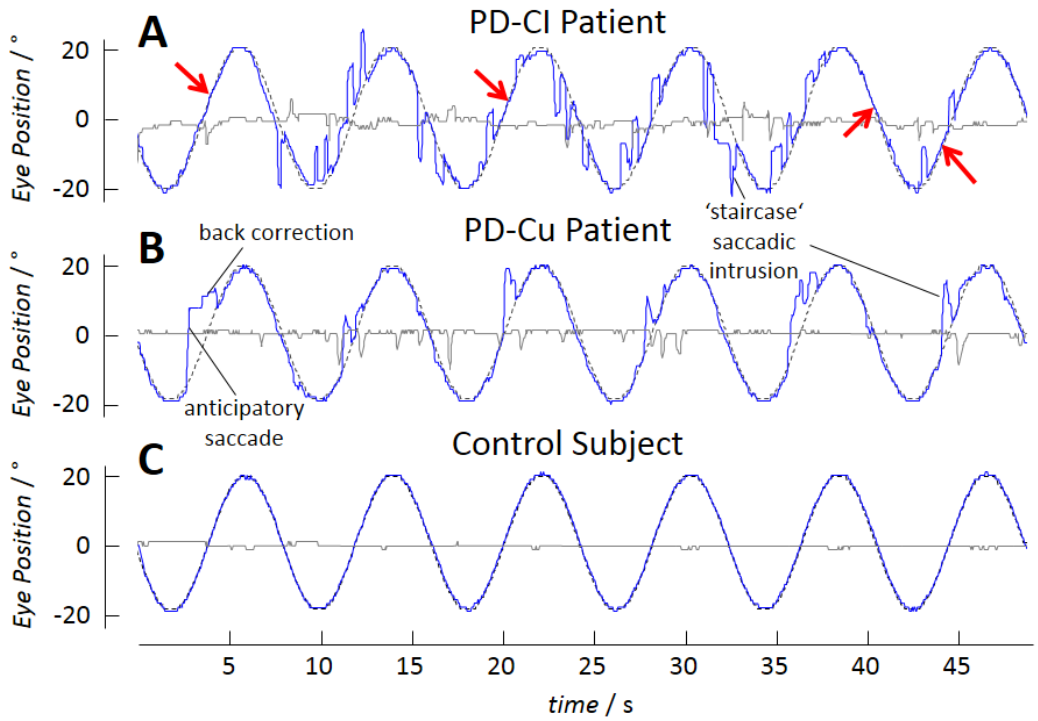


**Figure 3| Sample Recordings of Smooth Pursuit Eye Movement.** Tracks of horizontal (blue) and vertical (**grey**) eye position were elicited by horizontal sinusoidal oscillating (*f*=0.125Hz, ±20°, 6 periods) single-dot (**black dashed**) in Parkinson's disease patient with (PD-CI, **A**) and without cognitive impairment (PD-Cu, **B**) compared with an age-matched healthy control subject (**C**). Typically, smooth pursuit in PD (**A--B**) is interrupted by saccadic intrusions, in particular predominant anticipatory saccades and their back correction in case of improper prediction. Even in PD patients presenting with a high incidence of intrusions, intervals of perfect pursuit manifest (**red arrows**). (**A**) Patient with severely and (**B**) mildly impaired pursuit eye movement compared with a control individual (**C**). Center of the screen at 0°, negative positions are in the **left** or **lower** half-plane, respectively.

The described impairment manifested primarily in the PD-CI group. Notably, cases with severely impaired SPEM are fairly able to track the target at least intermittently smoothly (arrows in **Figure 3**). This impairment manifested in both patient groups (**Figure 3A—B**), PD-CI and PD-Cu compared with controls (ANOVA, $p \leq 0.038$) preferentially due to a reduced gain in the PD-CI patient group in all single-dot SPEM conditions ($p<0.02$) whereas differences between both patient groups (PD-CI, PD-Cu) were found in upward pursuit gain for slow and fast target oscillation frequencies ($p \leq 0.02$). In addition, significant differences between PD-Cu patients and controls ($p \leq 0.046$) were observed for slow horizontal and downward pursuit as well as for fast horizontal pursuit.

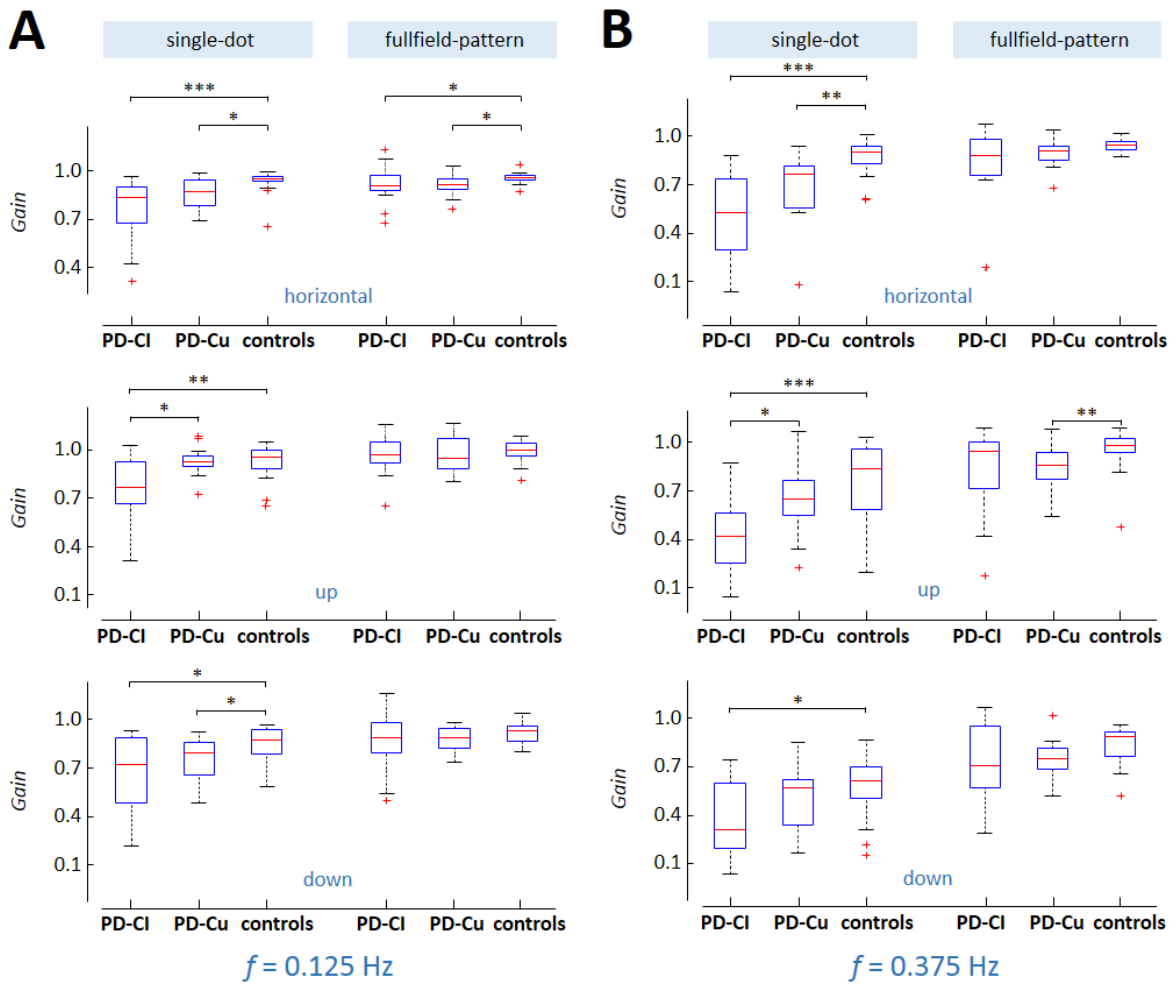


**Figure 4| Boxplots and Group Effects of Smooth Pursuit Performance.** (**A**) Smooth pursuit gain for 'slow' (*f*=0.125 Hz) and (**B**) fast (*f*=0.375 Hz) sinusoidal stimulation elicited by single-dot (**left**) and full-field pattern (**right**); each shown for horizontal, up and downward directions. Triplets of boxes contrasting cognitively impaired (PD-CI, each on the **left**), cognitively unimpaired Parkinson's disease patients (PD-Cu, **center**) and controls (**right**). Medians as red lines within each box; whiskers extended to 1.5 times the interquartile range plus 75 % quartile (upper box edge) and minus 25 % quartile (lower), respectively. Values exceeding maximum whiskers length are considered as outliers (+). Statistical effects were computed across PD-CI, PD-Cu and control groups in Kruskal-Wallis analysis of variances (ANOVA) on ranks and (if ANOVA $p<0.05$ was satisfied) followed by post-hoc Mann-Whitney-*U* rank sum testing. Significance levels are indicated as follows: *$p<0.05$, **$p<0.01$ and ***$p<0.001$.

Full-field pattern stimulation exhibited, if any, weak effects (ANOVA, $p<0.04$), contrasting both groups of patients with controls. ANOVA of all groups indicated significantly altered SPEM gain for slow horizontal and fast upward full-field SPEM. Post-hoc analysis indicated decreased SPEM gain for PD-Cu patients compared with controls ($p<0.02$) for both

conditions and decreased gain in PD-CI compared with controls for slow horizontal direction ($p$<0.05). No effects between both patient groups for full-field pursuit were found. **Figure 4** depicts statistical effects for SPEM performance. Together, as evident from a paired *t*-test contrasting both single-dot and full-field pattern SPEM ($p$<0.008) conditions, PD-patients benefit from extra-foveal stimulation. Single-dot SPEM performance worsens with cognitive decline whereas the 'genuine' ability to perform episodically perfect smooth pursuit is preserved. Anticipatory saccades are markedly suppressed by presenting an oscillating full-field pattern as compared with single-dot.

### 3.1.2 Visually Guided Reflexive Saccades Revealed Hypometric Saccades and Prolonged Latencies

Hypometric saccades as observed during VGS were found to be the hallmark of saccadic impairment in both PD patient groups compared with controls. **Figure 5** illustrates examples of normal (**Figure 5A**, **F**) and impaired (**Figure 5B—E)** horizontal saccades during gaze shift. In particular, ANOVA indicated significantly changed saccadic accuracies ($p$<0.0002) due to hypometric saccades for all groups (PD-CI, PD-Cu, controls). Post-hoc analysis exhibited a marked effect for both patient groups, i.e. PD-CI ($p$<0.002) and PD ($p$<0.006) versus controls. However, all patients presented with the ability to perform primary saccades with inconspicuous amplitudes. ANOVA revealed marked effects in latency investigation ($p$<0.0001) due to prolonged reaction times in PD-Cu ($p$=0.005) and PD-CI ($p$=0.0001) compared with controls. There were no significantly different saccadic accuracies and latencies between both patient groups, PD-CI and PD-Cu. In addition, ANOVA indicated no effect of PEV parameters for any direction as obtained from VGRS ($p$>0.36). As summarized in **Figure 6**, saccadic performance is markedly affected in PD-Cu and PD-CI patients with the exception of the PEV. The observed SWJ and SI during the fixational periods are described below (see also **Figure 9**).

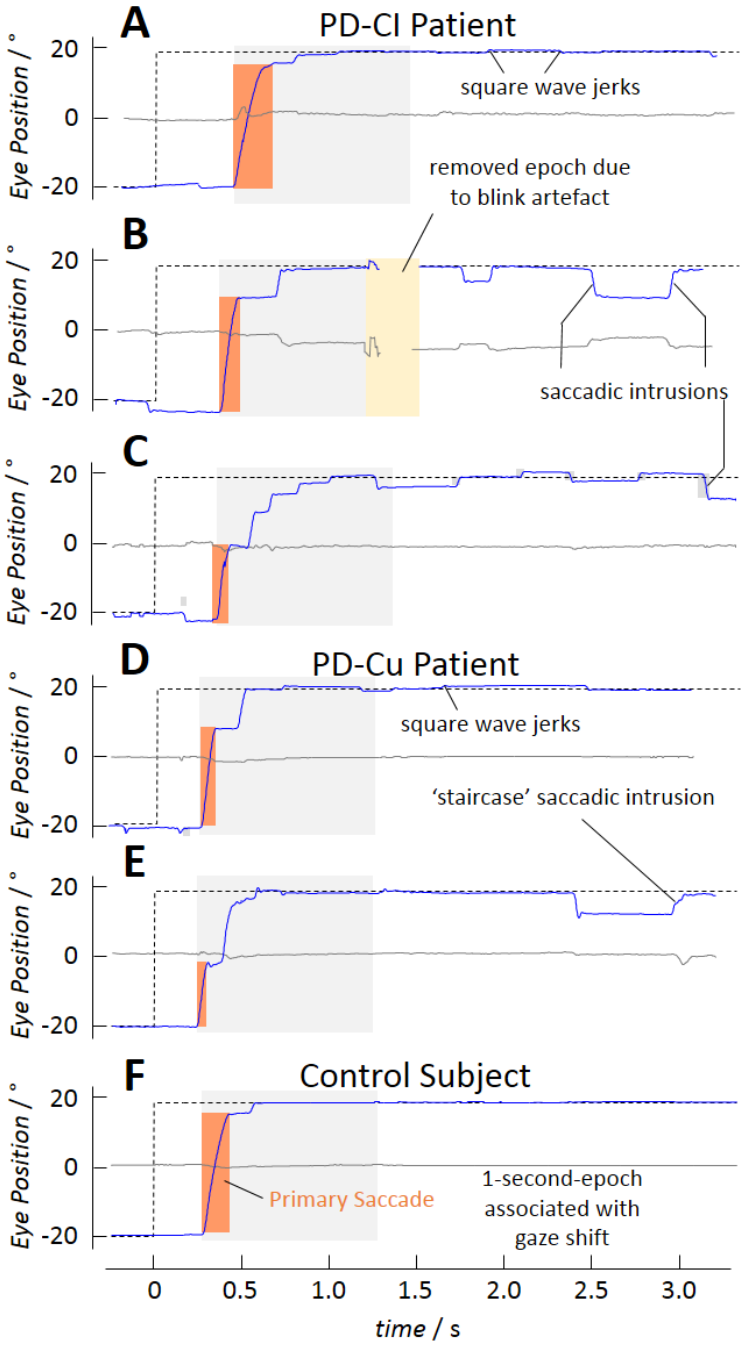


**Figure 5 | Sample Extracts of Visually Guided Reactive Saccades (VGRS) Recordings.** Horizontal (**blue**) and vertical (**grey trace**) eye traces in response to a pseudorandom left to right (-20° to +20°) target step (**black dashed**) exemplified for three Parkinson's disease patients with (PD-CI, **A--C**) and two without cognitive impairment (PD-Cu, **D—E**) compared with one age-matched healthy control subject (**F**). The PD-CI and PD-Cu patient presented with abnormalities both during gaze shift associated epoch (**grey background**) and during fixation. Gaze shifts were party accompanied by reduced accuracy resulting in hypometric saccades (**C**, **E**) whereas a high incidence of saccadic intrusions (**B—C**, **E**) manifested in the PD-CI patient. In all records of VGRS task, latencies were defined as the delay time between new target onset and the initiation of the primary saccade (**orange background**). VGRS were consecutively elicited whereas the new target proceeds with the previous one. The center of the screen at 0°, negative positions are in the left or lower half-plane, respectively.

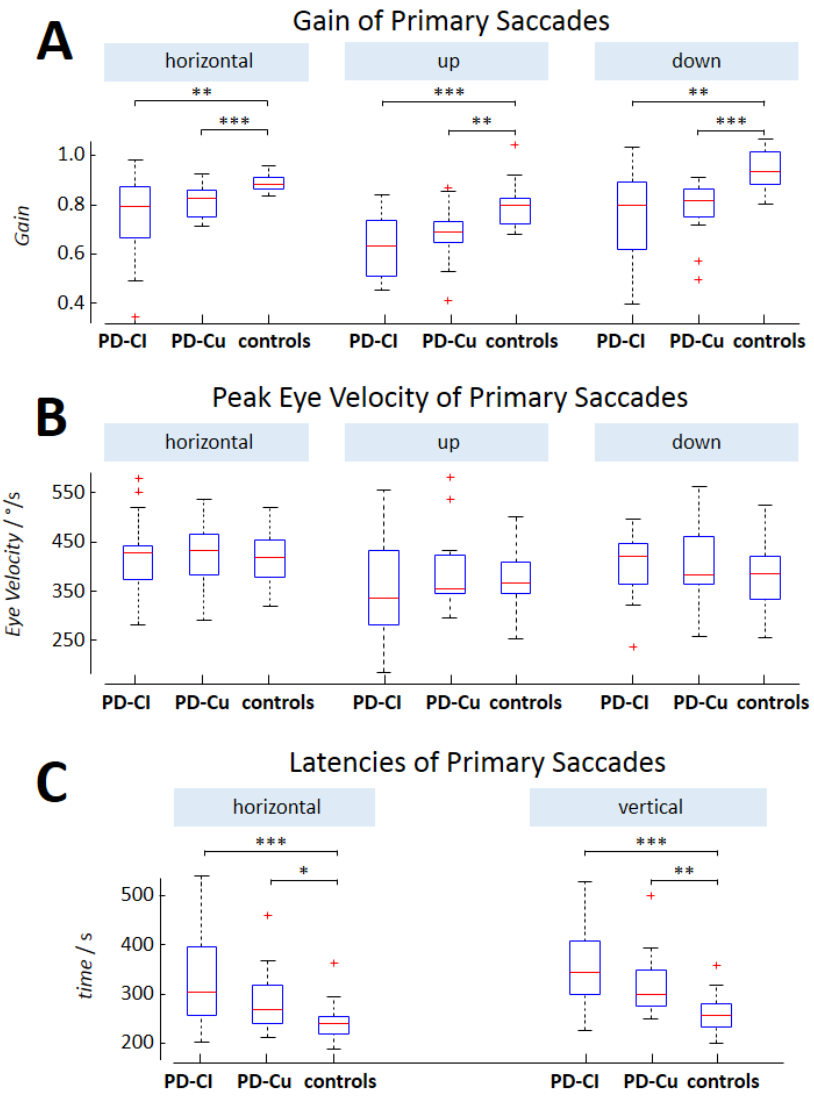


Figure 6| Boxplots and Group Effects of Gaze Shift Performance in Visually Guided Reactive Saccades (VGRS) Task. (A) Gain of primary saccades for horizontal (left), up (center) and downward (right) directions. (B) Peak eye velocity of primary saccades for horizontal (left), up (center) and downward (right) directions. (C) Latencies with respect to primary saccades for horizontal (left) and vertical (right) direction. For boxplots illustration details, see Figure 4.

### 3.1.3 Executive Control is Markedly Affected in both Parkinson's Disease Patient Groups

Executive control was tested in RAVS condition as well as in delayed- and anti-saccades. The results are summarized in **Figure 7**. The number of RAVS was significantly altered as indicated by ANOVA ($p$<0.00001). Post-hoc analysis revealed a marked decreased number of self-paced saccades in PD-Cu ($p$<0.0001) and PD-CI patients ($p$<0.00001) compared with

controls whereas in-between patient groups comparison exhibited no statistical effect. However, a somewhat more reduced number of gaze shifts in PD-CI compared with PD-Cu patients in terms of the median values (**Figure 7A**) was found. Together, the ability to perform self-initiated gaze shifts between to fixed targets is pronounced affected in PD-Cu patients and worsens slightly when cognitive problems manifest.The strongest effects (ANOVA, $p<0.00001$) were found in cognitive demanding conditions where both patient groups, PD-CI ($p<0.0001$) and PD-Cu ($p<0.004$), presented with pronounced difficulties in suppressing unwanted gaze shifts as measured in the error rate in both delayed- and anti-saccades tasks (**Figure 7B**). In addition, PD-CI patients performed significantly worse than PD-Cu patients ($p<0.04$). Hence, the performance in these tasks successively worsens with cognitive decline (controls > PD-Cu > PD-CI).

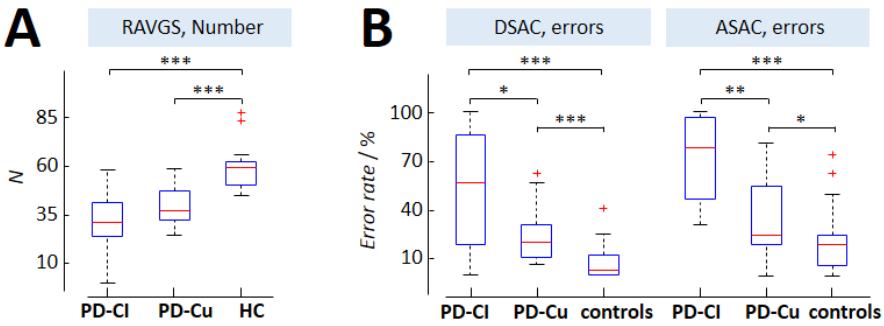


Figure 7| Boxplots and Group Effects of Executive Oculomotor Control. (A) Number of rapid alternating voluntary gaze shifts (RAVS). (B) Error rate in delayed-saccades (DSAC, left) and anti-saccades (ASAC, right). For boxplots illustration details, see Figure 4.

In summary, even when no cognitive problems in PD patients were evident, the lack of attention in the sense of an executive deficit manifested in oculomotor tasks such as RAVS or inhibition tests. Oculomotor inhibition controls deteriorated when cognitive problems in PD patients were present in contrast to the number of RAGVS that were statistically similar between patient groups but revealed a tendency to decline in the PD-CI group.

### 3.1.4 Saccadic Intrusions Frequently Interrupted Fixational Epochs

One contributing factor of impairments during VGRS in PD was the broad spectrum of SI ranging from SWJ to conspicuously large and frequent intrusions in some patients

(**Figure 8**). **Figure 5A—E** illustrates individual examples of SI in the fixational periods of VGRS. PD patients also presented frequently with SWJ during attempted visual fixation, however, no SI were observed within in this condition. Eye movements interrupting normal fixation were observed during attempted fixation task and classified as SWJ with respect to their amplitude and periodical occurrence in back-to-back saccadic manner. SWJ occurred more frequently in both PD-CI ($p$<0.002) and PD-Cu ($p$<0.004) patients compared with controls (ANOVA, $p$<0.001) but manifest somewhat similar in PD-CI compared with PD-Cu patients (**Figure 9**, **left**). Some cases of cognitively impaired patients presented with a high incidence of SWJ, however, the amplitude were not demonstrated to be abnormally large (<2°). The observed SWJ occur almost exclusively in horizontal direction during attempted visual fixation.

Likewise, SWJ were present in the fixational episodes in VGRS, however, SI were observed more prominently within these periods. **Figure 5A—E** depicts examples of PD patients presenting with abnormal SI in horizontal VGRS. Some intrusive saccades comprised a 'staircase' pattern – that is a consecutive series of hypometric saccades that bring the eye away or back onto the target. The amplitude of these saccades were abnormally large (>2°) and, hence, attributed to SI rather than SWJ. The classification between SI and SWJ were based on an empirical threshold of 2° saccade amplitude. Interestingly, SI in horizontal VGRS occur almost exclusively in horizontal direction as illustrated in **Figure 8** (**upper row**). Note that the plots in **Figure 8** show the orientation of interrupting saccade amplitudes for both SI and SWJ. In addition, SI also manifested in vertical direction in contrast to SWJ and manifested nearby exclusively in vertical direction during vertical VGRS (**Figure 8**, **lower row**). Together, in VGRS task, SWJ were consistently observed in exclusively horizontal direction whereas SI manifested in the direction of stimulus – horizontal or vertical. However, no orthogonal or considerable oblique SI were observed. SI appeared to occur randomly but in predictable fashion with respect to their orientation.

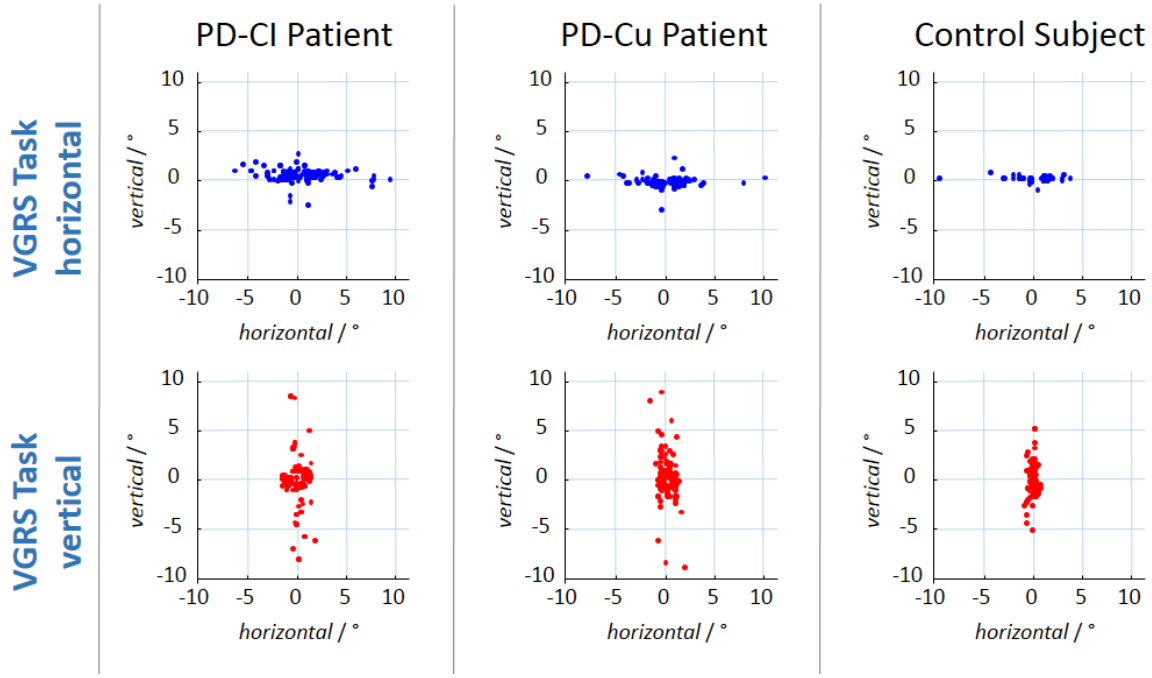


**Figure 8| Scatter Plots of Directions of Saccadic Intrusions in Visually Guided Reactive Saccade (VGRS) Task.** The plots depicted horizontal vs. vertical eye position indicating orientation of all saccades (excluding primary saccades). Horizontal (**upper row**) and vertical (**lower row**) VGRS condition in three representative individuals; a Parkinson's disease patient with (PD-CI, **left column**) and without cognitive impairment (PD-Cu, **center**) as well as one age healthy control subject (**right**) are shown. Saccadic intrusions preferentially occur in the direction of stimulus whereas square wave jerks less than 2° (dots around the centers) manifest also in oblique or orthogonal direction.

Although SI manifested in controls, their frequencies in terms of the intrusion rate were significantly different (ANOVA, $p<0.001$) between groups (PD-CI, PD-CU, controls) in the fixational periods in both horizontal and vertical VGRS conditions. The SI rate in horizontal VGRS task (**Figure 9**, **center**) were similar in PD-Cu patients as compared with controls but increases significantly in PD-CI compared with PD-Cu patients ($p<0.003$) and with controls ($p<0.001$). In vertical VGRS task (**Figure 9**, **right**) an effect was found when contrasting the SI rate for PD-Cu patients and controls ($p<0.01$) as well as for PD-CI patients and controls $p<0.001$). In-between patient groups, no statistically difference was observed, however, the SI rate increased in terms of the medians when cognitive problems in PD patients become evident. In summary, during attempted fixation with no expected alterations in the visual scene, exclusively horizontal SWJ in the absence of SI were demonstrated for the vast majority of PD patients. However, when a 'jumping' target was presented in either

horizontal or vertical direction (VGRS), SI manifested significantly in PD patient preferentially in those with cognitive problems and occurred almost always in the direction of stimulus.

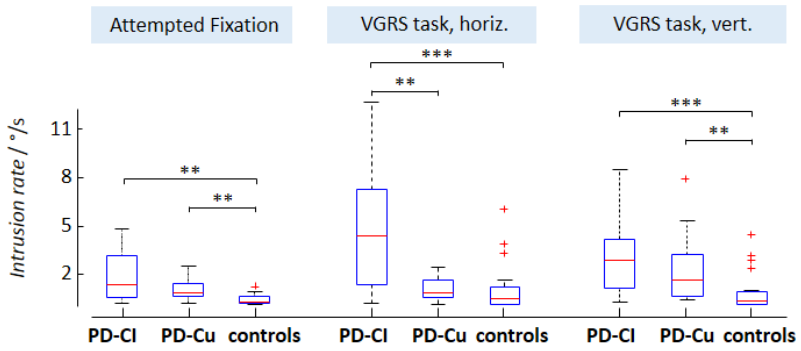


**Figure 9 | Boxplots and Group Effects of Square Wave Jerks (SWJ) and Saccadic Intrusions (SI).** Rate of SWJ during attempted visual fixation (**left**), SI rate in fixational periods in horizontal (**center**) and vertical (**right**) VGRS task. For boxplots illustration details, see **Figure 4**.

### 3.1.5 Oculomotor Performance in Parkinson's Disease Depends only in a few Aspects on Cognitive State

Differences among PD patients, PD-CI and PD-Cu, indicated statistically effects in only a view aspects, the gain of upward single-dot SPEM, the error rate as outcome of inhibition tests (delayed- and anti-saccades) and SI rate in horizontal VGRS tasks. However, oculomotor dysfunction were demonstrated for PD-Cu patients in several conditions with the exception of PEV and generally the full-field SPEM gain. PEV and the ability to perform normal full-field pursuit was preserved in PD patients albeit cognitive difficulties were manifest. In those conditions where significant alterations in PD-Cu patients as compared with controls were demonstrated, oculomotor control was gradually worse in PD-CI compared with PD-Cu patients – if not statically significant – as clearly indicated by tendency of median values. In summary, oculomotor control was disturbed in several aspects due to SI corrupting SPEM and VGRS as well as a lack of inhibition control. These deficits were demonstrated in exclusively all aforementioned aspects for PD-Cu patients; there were no conditions observed where abnormalities in oculomotor control initially manifested together with cognitive problems.

### 3.1.6 PANDA score is Markedly Associated with Error Rate of Inhibitory Oculomotor Tasks

To detect possible relationships between patients' oculomotor parameters and the overall cognition PANDA (Part A, cognition) score, the data of both patient groups PD-Cu and PD-CI were pooled. Tightly negative correlations were observed for the error rate of delayed- ($r$=-0.49, $p$<0.01) and anti-saccades ($r$=-0.79, $p$<0.0001) in the sense of the higher their error rate the poorer the outcome of the PANDA cognition assessment. All other oculomotor parameter exhibited no significant correlations.

## 3.2 Seed-based Correlation Analysis of 'task-free' Functional Connectivity MRI Revealed Large-scale Connectivity Maps

The influence of successive preprocessing steps commonly applied to iFCMRI data on individual basis was explored for the well-studied DMN. Preprocessing has major impact onto the data quality in the sense of substantially increasing signal-to-noise ration as exemplified in **Figure 10** for the effect of filtering for one representative healthy control participant. In particular, after the two-step MNI normalization procedure, all images were well-matched onto the Colin MNI-brain template. Having applied all preprocessing steps, the connectivity map revealed unambiguously the pattern of the DMN on individual basis (**Figure 11A**) and at the group level (**Figure 11B**).

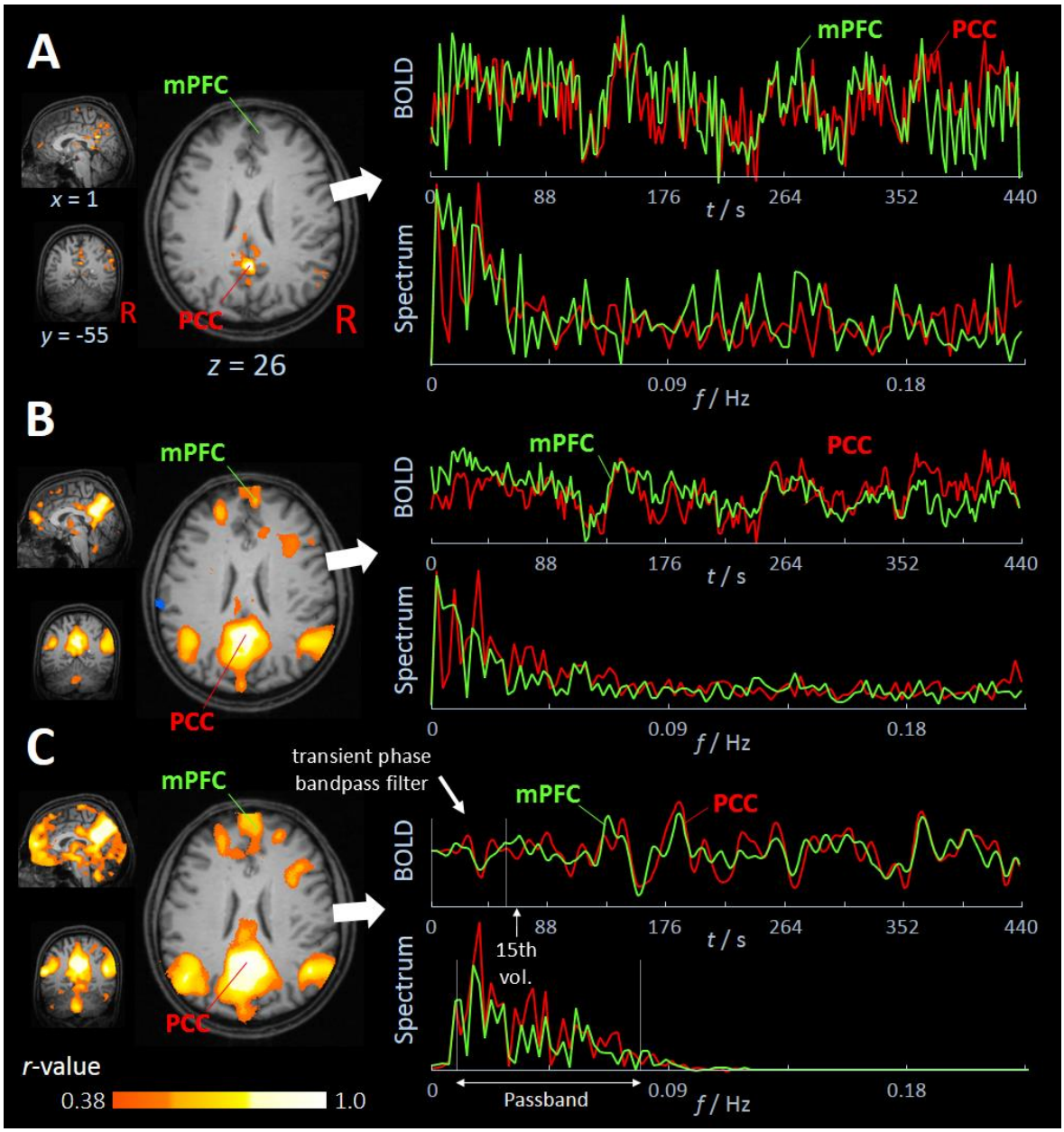


**Figure 10| Effect of Spatial and Temporal Filtering Exemplified in One Representative Healthy Control Subject.** Most informative orthogonal slices (**left column**) show the default mode network (DMN) in standard Montreal Neurological Institute (MNI) stereotaxic brain space. Brain map was computed for a cubic seed-voxel (1 $mm^3$) in the posterior cingulate cortex (PCC; $x$=0, $y$=-55, $z$=26; **red**). Two time series (**right upper panels**) with corresponding frequency spectrum (**right lower panels**) extracted from the PCC (**red**) seed-voxel and a cubic voxel (1 $mm^3$) in the medial prefronal cortex (mPFC; $x$=1, $y$=59, $z$=13; **green**). (**A**) Motion corrected and resampled data to a cubic grid (1 $mm^3$). (**B**) Data after spatial blurring (Gauss kernel at 7 mm full width at half maximum). (**C**) Data after temporal linear detrending and bandpass filtering (6th order Butterworth design, $0.01<f<0.08$ Hz). Connectivity strengths are illustrated in hot colors and thresholded for $|r|>0.38$ corresponding to $p<0.0000001$ superimposed on the subject's MNI-space deformed high-resolution (cubic 1 $mm^3$) structural (MPRAGE) template.

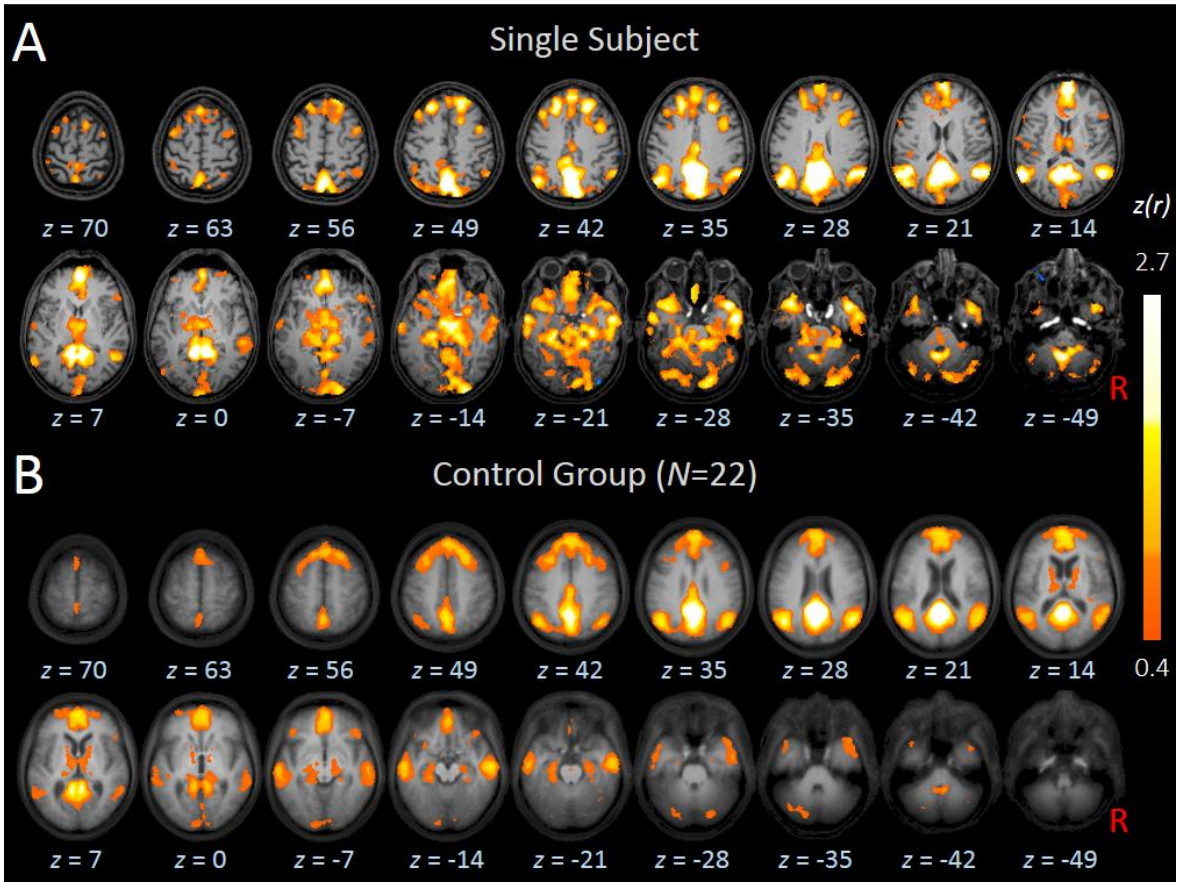


**Figure 11| Axial Slices Showing the Default Mode Network (DMN) at Individual and at Group Level**. Slices displayed in standard Montreal Neurological Institute (MNI) stereotaxic brain space in 1 mm resolution. (**A**) DMN for one representative healthy control subject (male, 60 years) overlaid on its MNI-space deformed high-resolution structural (MPRAGE) image (1.0 x 1.0 x 1.0 $mm^3$). (**B**) Group averaged DMN for all control subjects (*N*=22) on their respective averaged MPRAGE background. The depicted brain maps were computed for a cubic seed-voxel (1 $mm^3$) placed in the posterior cingulate cortex (PCC; *x*=0, *y*=-55, *z*=26). Connectivity strengths are shown in hot colors and thresholded for $|z(r)|>0.4$.

### 3.2.1 Non-Lateralized ICNs Seeds in Either the Left or Right Hemisphere Yields Similar Results

The iFC analysis in this study utilized the seed-based approach by defining seed-voxels (1.0 x 1.0 x 1.0 $mm^3$) in regions serving as major hubs for the corresponding ICN. The ten ICNs were unambiguously identified for the control group (**Figure 12A—J**, **right column**) to evaluate the anatomical plausibility for each ICN whilst taking into account the consistently reported networks in previous studies. The seeds were placed in the right or left hemisphere or medial (see **Table 5**). In all groups (PD-CI, PD-Cu, controls), except for the

frontoparietal ICN, results were generally similar when seeds were placed in either the left or right hemisphere.

### 3.2.2 Identification of Intrinsic Connectivity Networks

All ten investigate large-scale coherent spatial brain maps were identified for the control group (**Figure 12A—J**, **right column**) indicating strong iFC with the defined seed regions (**Table 5**):

The *Default Mode Network* (DMN) (**Figure 12A**, **right**) was identified by seeding the posterior cingulate cortex (PCC) with adjacent precuneus region. The brain map covers the medial parietal cortex comprising bilateral temporal areas around their midline extending to inferior parietal regions. In addition, the medial-frontal cortex reveals activations in ventromedial, anteriormedial, dorsomedial areas, the frontal-pole and the anterior cingulate and paracingulate. Weaker activity was found in bilateral hippocampal formation and parts of DLPFC.

**Figure 12B—C**, **right**, shows the *Left* and *Right Frontoparietal Control ICNs* yielded by seeds in the left and right middle temporal area. These networks exhibited strongest lateralization. Within these spatial maps, activity was observed in several frontoparietal areas comprising the DLPFC, frontal-pole as well as lateral occipital complex and inferior parietal cortex and parts of the posterior cingulate cortex. As a relay between cortical and subcortical areas, bilateral thalamic activity was found.

The *Motor ICN* (**Figure 12D**, **right**) has been computed for a seed-region within the left motor cortex revealing similar activity in both hemispheres comprising the sensory-motor and motor association systems. These included pre- and post-central motor regions and the supplementary motor area. Moreover, weaker activity was also found in the visual association areas in the occipital-pole and the thalamus.

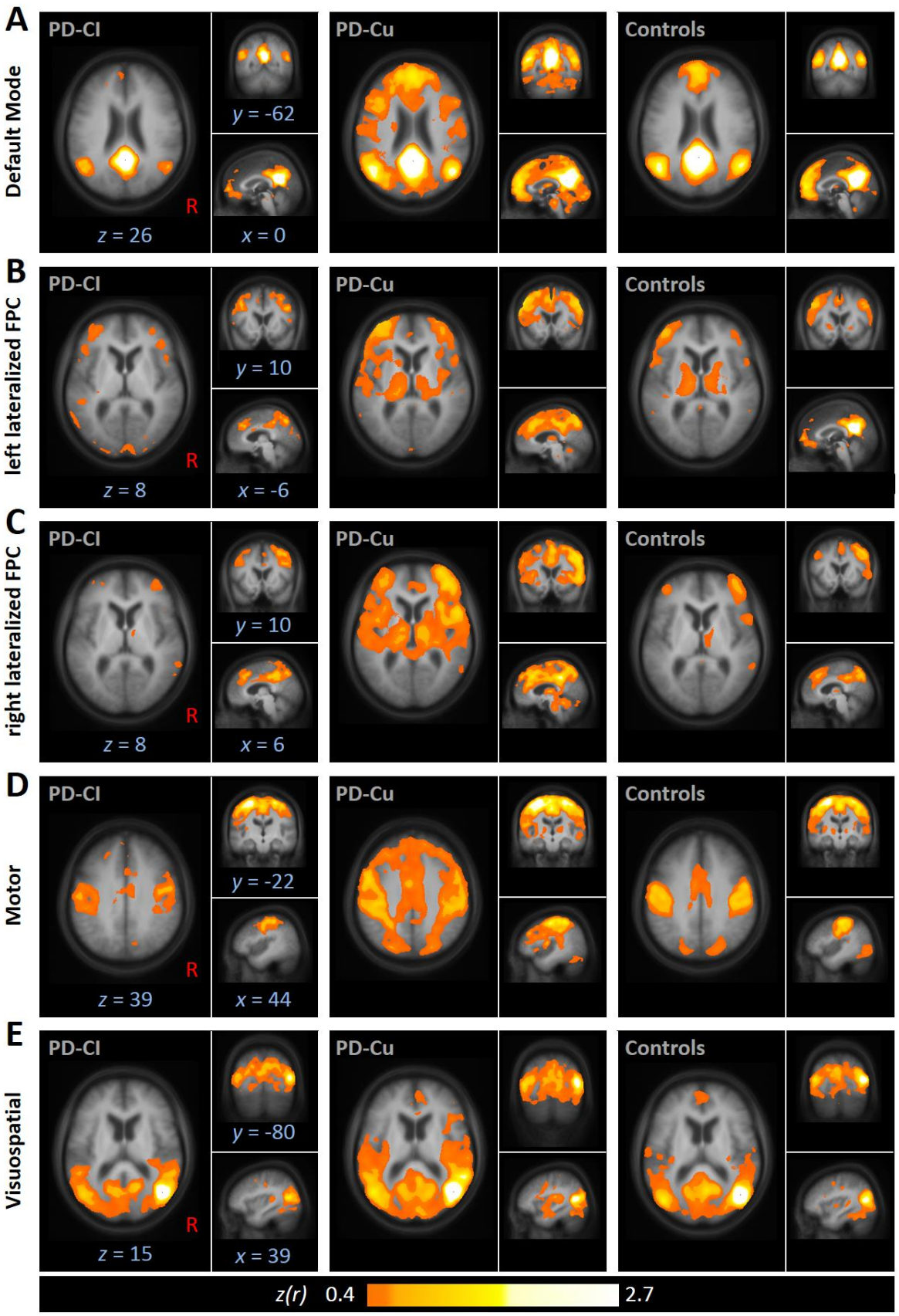


Figure 12 (Continued on the Next Page)

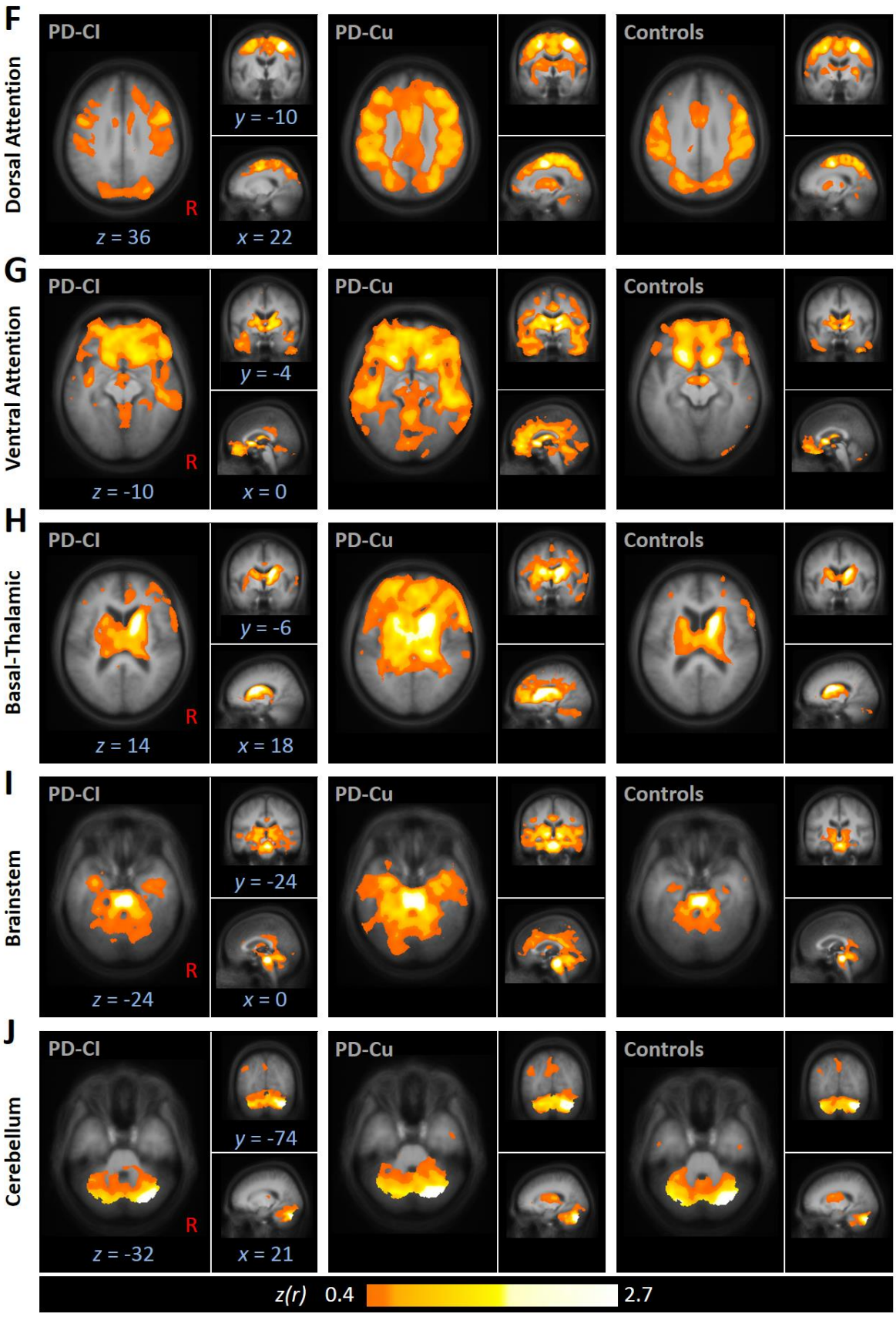
F
Dorsal Attention
PD-CI
PD-Cu
Controls
y = -10
R
z = 36
x = 22
G
Ventral Attention
PD-CI
PD-Cu
Controls
y = -4
R
z = -10
x = 0
H
Basal-Thalamic
PD-CI
PD-Cu
Controls
y = -6
R
z = 14
x = 18
I
Brainstem
PD-CI
PD-Cu
Controls
y = -24
R
z = -24
x = 0
J
Cerebellum
PD-CI
PD-Cu
Controls
y = -74
R
z = -32
x = 21
z(r) 0.4 2.7

Figure 12| Intrinsic Connectivity Networks (ICNs). Most representative orthogonal slices of the 10 investigated ICNs (A-J) displayed in standard Montreal Neurological Institute (MNI) stereotaxic brain space in 1 mm resolution. ICNs were obtained using seed-based intrinsic functional connectivity magnetic resonance imaging iFCMRI for seed-voxels (1.0 x 1.0 x 1.0 $mm^3$) within the (A) default mode (DMN), (B) right (R-FPC) and (C) left lateralized frontoparietal control (L-FPC), (D) motor (MOT), (E) visuospatial (VIS), (F) dorsal (DA) and (G) ventral attention (VA), (H) basal ganglia-thalamic (BT), (I) brainstem (BS), (J) cerebellar (CB) ICNs (computed with seed-voxels from Table 5). Pearson's product correlation coefficient spatial maps for each individual data set were Fisher's z transformed and arithmetically averaged across subjects in the Parkinson's disease patient group with (PD-CI, left column, *N*=17) and without cognitive impairment (PD, center column, *N*=14) as well as the age-matched healthy control group (right column, *N*=22). Connectivity strengths in all ICNs (represented in hot colors) are $|z(r)|>0.4$ corresponding to $p<0.0000001$ and are shown superimposed on the MNI-space deformed high-resolution structural (MPRAGE) template (1.0 x 1.0 x 1.0 $mm^3$) averaged for all subjects (*N*=53). See appendix for extended axial slice wise representation for all ICNs for PD-CI (Figure 20) and PD-Cu patients (Figure 21) as well as healthy controls (Figure 22).

The right extrastriatal seed correspond to a symmetric brain map known as the *Visuospatial ICN* (**Figure 12E**, **right**) that included middle and inferior temporal gyri as well as visual association structures at the temporo-occipital junction and extending laterally towards the primary visual cortex in the posterior and lateral occipital-cortices. Moreover, this ICN map encompasses superior dorsal parietal regions and extra-primary areas of the visual cortex.

The right FEF serves as the seed region for the *Dorsal Attention* system (**Figure 12F**, **right**, and **Figure 13**) displaying a pronounced symmetrical activity in both hemispheres. This brain map encompasses the SEFs, small portions of the DLPFC, the intraparietal cortices including the parietal eye field, association motor areas, and middle temporal structures encompassing visual associative structures. The cingulate gyrus extending from posterior towards anterior portions including the cingulate eye fields revealed also activities. Striatal regions exhibited strong iFC with the FEFs, notably, the putamen displayed the greatest activities whereas the caudate nucleus with adjutant thalamus was found to be less strong functionally connected with the FEFs. In summary, as indicated in detail in **Figure 13**, the dorsal attention ICN chiefly covers areas that are strongly associated with eye movement control.

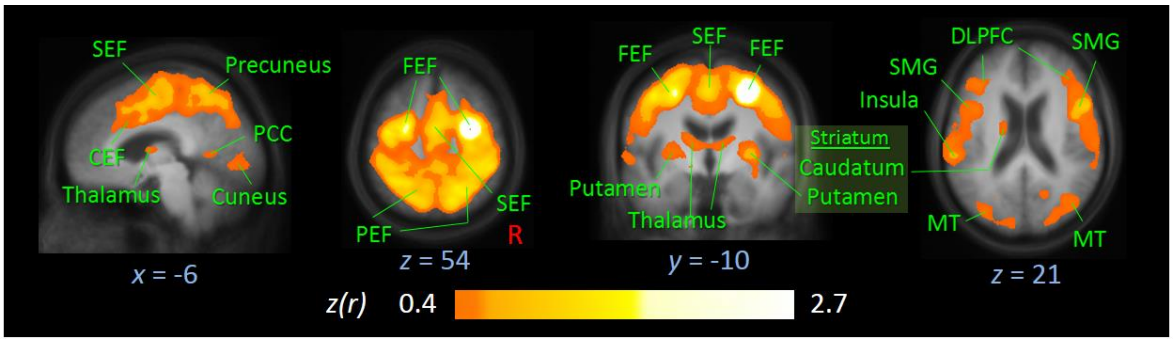


**Figure 13| Dorsal Attention Intrinsic Connectivity Network in Healthy Controls.** Most informative orthogonal slices of the 'oculomotor network' covering areas that are strongly associated with oculomotor control. Slices displayed in standard Montreal Neurological Institute (MNI) stereotaxic brain space in 1 mm resolution and overlaid on the MNI-space deformed high-resolution structural (MPRAGE) template averaged for all subjects (*N*=53). The depicted dorsal attention brain map was computed for a cubic seed-voxel (1 $mm^3$) placed in the right frontal eye field (FEF) and averaged for the control group (*N*=22). Connectivity strengths are shown in hot colors and thresholded for $|z(r)|>0.4$. Abbreviations: SEF, Supplementary Eye Field; CEF, Cingulate Eye Field; PCC, Posterior Cingulate Cortex; PEF, Parietal Eye Field; SMG, Supramarginal Gyrus; DLPFC, Dorsolateral Prefrontal Cortex; MT, Middle Temporal.

The *Ventral Attention ICN* (**Figure 12G**, **right**) has been computed by a basal ganglia seed in the ventral striatum. Its iFC map covers large parts of the limbic system including the nucleus accumbens, basolateral amygdala, the temporo-parietal junction, and ventromedial prefrontal cortex.

A second striatal seed within the caudate nucleus revealed strong activities in the basal ganglia and thalamus and is thus defined as the *Basal Ganglia Thalamic ICN* (BT) (**Figure 12H**, **right**). The spatial pattern indicates weaker iFC with bilateral cerebellar regions and the right DLPFC. Thus, the cortical activities observed in the right hemisphere exhibited lateralization and also an overlap with the right frontoparietal control network.

Placing a seed within the midbrain results in the *Brainstem ICN* (**Figure 12I**, **right**) that included the brainstem extending from mesencephalic areas towards the medulla oblongata. This connectivity map encompasses bilateral thalamic areas.

The *Cerebellar ICN* (**Figure 12J**, **right**) covers the left and right cerebellar hemisphere and has been identified by seeding the right cerebellum. Weaker activities includes middle temporal areas and bilateral thalamus.

### 3.2.3 Hyper-Connectivity in Parkinson's Disease Patients Compared with Healthy Controls

The ten investigated ICN were identified for the group of cognitively unimpaired PD patients whereas the iFC pattern revealed in almost all ICNs a partly extend pattern as compared with controls (**Figure 12A—J**, **center column**). A significantly stronger activity patterns were observed in the DMN, left and right frontoparietal control, ventral attention, motor, basal ganglia-thalamic and brainstem ICN compared with controls (**Figure 14** and **Table 6**). In particular, the DMN differs in PD compared with controls (**Figure 14A**) displaying significantly greater correlation in the medial frontal cortex (BA 8, 10) with respect to the PCC seed region Moreover, the DMN extends towards more dorsal areas showing bilateral activity in DLPFC (BA 45, 46) and in parts of the post-central gyrus (BA 3, 4). The left frontoparietal control system had stronger iFC (**Figure 14B**) between left MTL with bilateral medial frontal gyri (BA 9, 45). More pronounced effects were observed within the right frontoparietal control ICN (**Figure 14C**) indicating stronger iFC with parts of the limbic system including insular cortex (BA 13), hippocampal formation (BA 34, 35), thalamus, and the cingulate gyrus (BA 23, 31). Hyper-connectivity was found in left frontal gyri (BA 9, 10) and left DLPFC (BA 46) indicating a less pronounced lateralization in PD patients. In addition, the iFC with midbrain and anterior cerebellum was found to be greater than in controls. The most prominent effects were observed in the ventral attention ICN (**Figure 14D**) where large regions of the limbic system showed significantly stronger iFC with the seed region placed in the ventral striatum. These limbic regions covered the insular cortex (BA 13) extending into more temporal areas (BA 22, 39, 41, 42). The cingulate gyrus (BA 23) reached from anterior (24, 32) to posterior parts (BA 23) with adjacent precuneus (BA 31) as well as the midbrain, thalamus and the striatal seed region itself. Moreover, the anterior cerebellum and inferior parts of the frontal gyrus (BA 10) revealed significantly greater iFC. The motor ICN encompasses the left DLPFC (BA 46) and the right inferior parietal lobule (BA 7) in PD patients (**Figure 14E**). The limbic areas included in the subcortical basal ganglia-thalamic (**Figure 14F**); the brainstem ICN (**Figure 14G**) was found to be significantly hyper-connected in PD patients compared with controls.

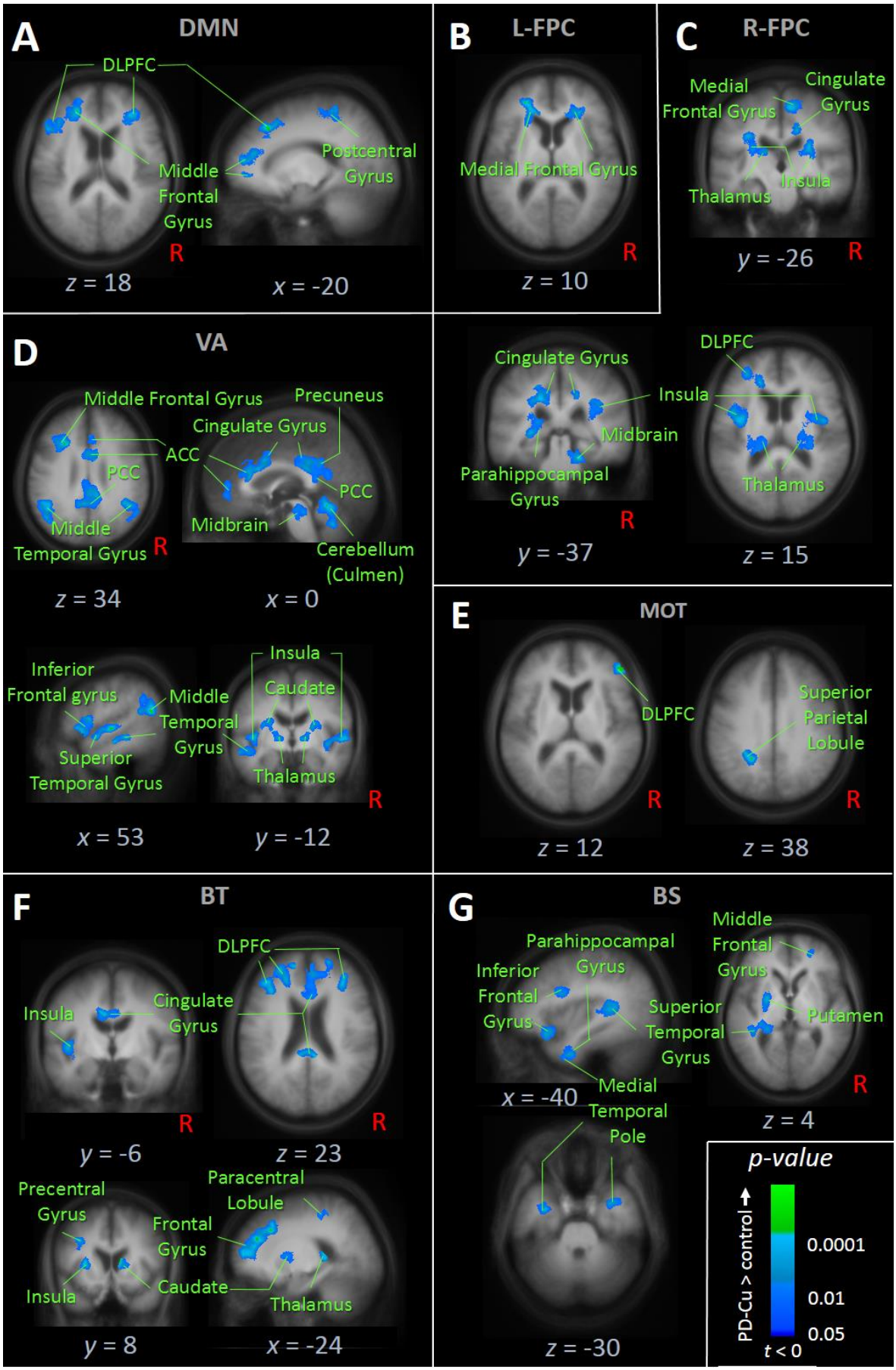
A
DMN
DLPFC
Middle Frontal Gyrus
Postcentral Gyrus
R
z = 18
x = -20
B
L-FPC
Medial Frontal Gyrus
R
z = 10
C
R-FPC
Medial Frontal Gyrus
Cingulate Gyrus
Thalamus
Insula
y = -26
R
D
VA
Middle Frontal Gyrus
Precuneus
Cingulate Gyrus
ACC
PCC
PCC
Middle Temporal Gyrus
R
Midbrain
Cerebellum (Culmen)
z = 34
x = 0
Inferior Frontal gyrus
Middle Temporal Gyrus
Superior Temporal Gyrus
Insula
Caudate
Thalamus
R
x = 53
y = -12
Cingulate Gyrus
Insula
Midbrain
Parahippocampal Gyrus
R
y = -37
DLPFC
Thalamus
z = 15
E
MOT
DLPFC
R
Superior Parietal Lobule
R
z = 12
z = 38
F
BT
DLPFC
Insula
Cingulate Gyrus
R
R
y = -6
z = 23
Precentral Gyrus
Paracentral Lobule
Frontal Gyrus
Insula
Caudate
Thalamus
y = 8
x = -24
G
BS
Parahippocampal Gyrus
Inferior Frontal Gyrus
Middle Frontal Gyrus
Superior Temporal Gyrus
Putamen
R
x = -40
Medial Temporal Pole
z = 4
z = -30
p-value
PD-Cu > control
0.0001
0.01
0.05
t < 0

**Figure 14| Effects Contrasting Intrinsic Connectivity Networks in Cognitively Unimpaired Parkinson's Disease Patients (PD-Cu) versus Age-Matched Healthy Controls.** Most informative orthogonal slices of Student's *t*-statistic maps in Montreal Neurological Institute (MNI) stereotaxic space. Results were corrected at a 5 % false discovery rate (FDR) level with further cluster-wise correction by discarding cluster sizes less than 343 voxels. Cold colors represent positive *t*-values indicating stronger functional connectivity in PD-Cu patients compared with controls within the (**A**) default mode (DMN), (**B**) left (L-PFC) and (**C**) right lateralized frontoparietal control (R-FPC), (**D**) ventral attention (VA), (**E**) motor (MOT), (**F**) basal ganglia-thalamic (BT) as well as the (**G**) brainstem intrinsic connectivity networks (ICNs). Detailed statistics are given in **Table 6**.

**Table 6| Significant Clusters in Intrinsic Connectivity Networks (ICNs) in Cognitively Unimpaired Parkinson's Disease Patients (PD-Cu) Compared with Healthy Controls.** Coordinates in the Montreal Neurological Institute (MNI) stereotaxic space defining the peak cluster activity corresponding to the maximum likelihood. Results were corrected at a 5 % false discovery rate (FDR) level with further cluster-wise correction by discarding cluster sizes less than 343 voxels (see also **Figure 14**). Abbreviations: BA, Brodmann Area; PHG, Parahippocampal Gyrus; IFG, Inferior Frontal Gyrus; STG, Superior Temporal Gyrus; SMG, Supramarginal Gyrus

| ICN | R/L | MNI | | | Cluster | | REGIONS |
|---|---|---|---|---|---|---|---|
| | | *x* | *y* | *z* | *V*/mm3 | *p* | |
| DMN | L | -22 | 23 | 47 | 6603 | 0.000001 | Medial Frontal Gyrus, BA 8 |
| | L | -13 | -38 | 62 | 6154 | 0.000005 | Postcentral Gyrus, BA 3, 4 |
| | L | -26 | 42 | 3 | 4812 | 0.000002 | Superior Frontal Gyrus, BA 10 |
| | L | -42 | 21 | 24 | 2474 | 0.000006 | Inferior Frontal gyrus, BA 45, 46 |
| | R | 30 | 29 | 13 | 1895 | 0.000003 | Inferior Frontal gyrus, BA 46 |
| R-FPC | L | -46 | -5 | 7 | 17912 | 0.000003 | Insula, BA 13; Thalamus; PHG, BA 34, 35 |
| | R | 34 | -8 | 21 | 9076 | 0.000004 | Insula, BA 13; Thalamus |
| | L | -27 | 38 | 8 | 3050 | 0.000001 | Medial Frontal Gyrus, BA 9, 10; IFG, BA 46 |
| | R | 18 | -38 | -23 | 2970 | 0.000004 | Anterior Cerebellum, Culmen; Midbrain |
| | R | 10 | -26 | 63 | 1597 | 0.000002 | Medial Frontal Gyrus, BA 6 |
| | R | 16 | -31 | 40 | 1290 | 0.000003 | Cingulate Gyrus, BA 23, 31 |
| L-FPC | L | -26 | 39 | 6 | 6560 | 0.000002 | Medial Frontal Gyrus, BA 9 |
| | R | 27 | 29 | 9 | 1778 | 0.000005 | Inferior Frontal gyrus, BA 45 |
| MOT | L | -24 | -53 | 38 | 1251 | 0.000002 | Superior Parietal Lobule, BA 7 |
| | R | 49 | 36 | 15 | 1188 | 0.000000 | Inferior Frontal gyrus, BA 46 |
| VA | L | -27 | -55 | -24 | 23856 | 0.000002 | Anterior Cerebellum, Culmen; Midbrain |
| | L | -42 | -20 | -7 | 23610 | 0.000001 | Insula, BA 13; STG, BA 22, 41, 42; Thalamus |
| | R | 42 | -19 | -4 | 20134 | 0.000002 | Insula, BA 13; Inferior frontal gyrus, BA 47 |
| | L | -11 | -51 | 30 | 13377 | 0.000004 | Precuneus, BA 31; Cingulate Gyrus BA 23 |
| | R | 53 | -64 | 22 | 6297 | 0.000002 | Middle/Superior Temporal Gyrus, BA 39 |
| | L | -49 | -64 | 27 | 5701 | 0.000002 | Middle/Superior Temporal Gyrus, BA 39 |

| ICN | R/L | MNI | | | Cluster | | REGIONS |
|---|---|---|---|---|---|---|---|
| | | *x* | *y* | *z* | *V*/mm3 | *p* | |
| | - | 0 | 12 | 27 | 5094 | 0.000005 | Cingulate Gyrus, BA 24,33 |
| | R | 10 | 41 | 3 | 3775 | 0.000004 | Anterior Cingulate, BA 24, 32 |
| | R | 25 | -12 | 19 | 3540 | 0.000008 | Caudate Nucleus |
| | L | -28 | 20 | 33 | 2792 | 0.000004 | Middle Frontal Gyrus, BA 9 |
| | L | -26 | -9 | 21 | 2715 | 0.000005 | Caudate Nucleus |
| | R | 9 | -18 | 3 | 2135 | 0.000004 | Thalamus |
| | L | -38 | 34 | 3 | 1729 | 0.000007 | Inferior Frontal gyrus, BA 10 |
| **BT** | L | -35 | 4 | 37 | 34881 | 0.000002 | Precentral Gyrus, BA 9; Frontal Gyri, BA 8, 9, 10 |
| | R | 9 | -44 | 26 | 7397 | 0.000004 | Cingulate Gyrus, BA 23,33 |
| | L | -42 | -22 | -8 | 7385 | 0.000001 | Insula, BA 13; Superior Temporal Gyrus, BA 22 |
| | R | 38 | 33 | 12 | 4000 | 0.000002 | Inferior Frontal gyrus, BA 46 |
| | L | -41 | 30 | 19 | 2039 | 0.000001 | Middle Frontal Gyrus, BA 46 |
| | L | -23 | -41 | 11 | 1381 | 0.000001 | Thalamus |
| | R | 10 | 9 | 13 | 1189 | 0.000001 | Caudate Nucleus |
| | L | -20 | -46 | 58 | 933 | 0.000004 | Paracentral Lobule, BA 3; SMG, BA 40 |
| **BS** | L | -23 | -39 | 14 | 6234 | 0.000004 | Superior Temporal Gyrus, BA 41 |
| | L | -30 | -3 | 11 | 3343 | 0.000007 | Putamen |
| | L | -32 | 13 | -18 | 2667 | 0.000002 | Inferior Frontal Gyrus, BA 47; PHG, BA 34 |
| | L | -49 | 8 | 21 | 2223 | 0.000004 | Inferior Frontal Gyrus, BA 44 |
| | L | -37 | -3 | -36 | 1979 | 0.000004 | Medial Temporal Pole, BA 38; PHG; BA 34 |
| | R | 33 | 2 | -34 | 1387 | 0.000004 | Medial Temporal Pole, BA 38; PHG, BA 34 |
| | R | 25 | 46 | 0 | 1097 | 0.000006 | Middle Frontal Gyrus, BA 10 |

In more detail, the striatal seed region in the caudate nucleus exhibited stronger connectivity with the insular cortex (BA 13), the thalamus and cingulate cortex (BA 23, 33). Additionally, stronger iFC was observed with cortical regions comprising the frontal gyri (BA 8, 9, 10), the DLPFC (BA 46), temporal regions (BA 22) as well as the paracentral lobule (BA 3) and the supramarginal gyrus (BA 40). The midbrain seed area was stronger correlated with the putamen, the hippocampal formation (BA 34) and cortical areas including temporal and frontal gyri (BA 10, 38, 41, 47). No effect was found in the dorsal attention, visuospatial and cerebellar ICN when comparing PD-Cu patients and controls. In summary, the observed effects in sense of hyper-connectivity in PD patients point towards markedly overlaps of the ICNs in PD-Cu patients compared with controls. The vast majority of ICNs revealed a significantly extended spatial pattern preferentially in the limbic system and frontal areas. Comparing the dorsal and ventral attention system as well as the basal

ganglia-thalamic network with their seed-voxels in the striatum, i.e. putamen, ventral striatum and caudate nucleus, respectively, these ICNs revealed considerably distinct maps in controls, but were nearly similar in PD-Cu patients.

### 3.2.4 Functional Connectivity Decreases in Parkinson's Disease Patients with Cognitive Deficits Preferentially in the Default Mode Network

**Table 7| Significant Clusters in Intrinsic Connectivity Networks (ICNs) in Cognitively Impaired Parkinson's Disease Patients with Compared with Healthy Controls.** Coordinates in the Montreal Neurological Institute (MNI) stereotaxic space defining the peak cluster activity corresponding to the maximum likelihood. Results were corrected at a 5 % false discovery rate (FDR) level with further cluster-wise correction by discarding cluster sizes less than 343 voxels (see also **Figure 15**). Abbreviations: ACC, Anterior Cingulate Cyrus; BA, Brodmann Area

| ICN | R/L | MNI | | | Cluster | | REGIONS |
|---|---|---|---|---|---|---|---|
| | | *x* | *y* | *z* | *V*/mm3 | *p* | |
| DMN | L | -8 | -53 | 21 | 13838 | 0.000001 | Posterior Cingulate, BA 23, 30; Precuneus, BA 31 |
| | - | -5 | 58 | 14 | 6920 | 0.000002 | Middle Frontal Gyrus, BA 10; ACC, BA 24, 32, 33 |
| | R | 12 | 41 | 43 | 2880 | 0.000000 | Superior Frontal Gyrus, BA 8 |
| | R | 26 | 21 | 52 | 1753 | 0.000003 | Middle Frontal Gyrus, BA 8 |
| | L | -25 | -23 | -20 | 1724 | 0.000002 | Hippocampus, Parahippocampal Gyrus, BA 34, 35 |
| MOT | R | 33 | -91 | -1 | 3917 | 0.000003 | Occipital Lobe, BA 18 |
| | - | 4 | -79 | -4 | 915 | 0.000000 | Middle Occipital Lobe, BA 18 |
| DA | L | -13 | -65 | -48 | 1836 | 0.000001 | Posterior Cerebellum, Uvula |
| | L | -50 | -59 | -17 | 1414 | 0.000001 | Fusiform Gyrus, BA 37 |
| VA | R | 12 | -35 | -21 | 1238 | 0.000002 | Pons |

As indicated in **Figure 12A—J**, **left column**, the ICNs in PD-CI patients could be obviously identified. The connectivity pattern displayed to some extent a partly spared pattern as compared with controls indicating a considerable trend towards decreased iFC (hypo-connectivity). This comes obvious, when contrasting PD-CI patients vs. controls resulting in significantly decreased iFC within the DMN, the dorsal attention systems and the motor network. These findings are illustrated in **Figure 15**; detailed cluster statistics is listed in **Table 7**.

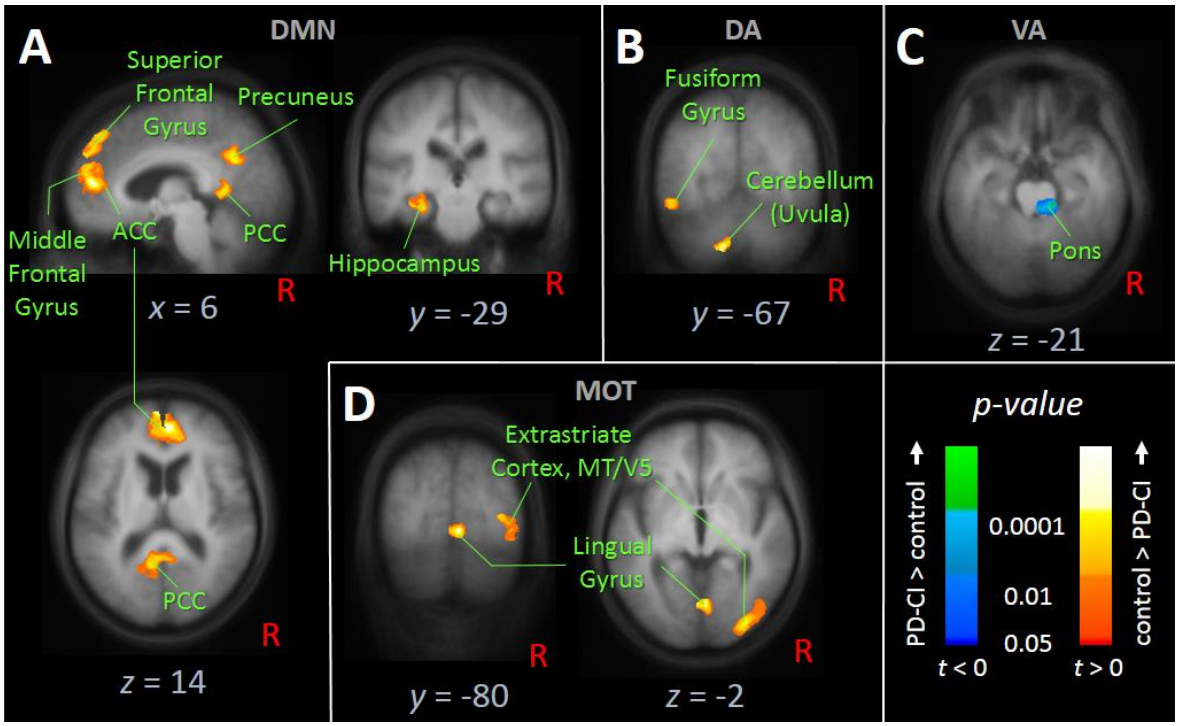


**Figure 15| Effects Contrasting Intrinsic Connectivity Networks in Cognitively Impaired Parkinson's Disease Patients (PD-CI) versus Age-Matched Healthy Controls.** Most informative orthogonal slices of Student's *t*-statistic maps in Montreal Neurological Institute (MNI) stereotaxic space. Results were corrected at a 5 % false discovery rate (FDR) level with further cluster-wise correction by discarding cluster sizes less than 343 voxels. Warm colors represent negative, cold colors represent positive *t*-values indicating weaker and stronger functional connectivity, respectively, in PD-CI patients compared with controls within the (**A**) default mode (DMN), (**B**) dorsal attention (DA), (**C**) ventral attention (VA), and (**D**) motor (MOT) intrinsic connectivity networks (ICNs). Abbreviations: R, Right; PCC, Posterior Cingulate Cortex; ACC, Anterior Cingulate Gyrus; MT, Middle Temporal. Detailed statistics are given in **Table 7**.

Decreased iFC were preferentially observed in brain structures associated with the DMN (**Figure 15A**), preferentially the long-distance midline cores and the hippocampus. Specifically, these regions comprises the middle (BA 8) and superior medial frontal cortex (BA 10) with adjacent anterior cingulate cortex (BA 24, 32, 33), the PCC/precuneus region (BA 23, 30, 31) as well as portions of the hippocampal formation (BA 24, 35). Within the dorsal attention network, the fusiform gyrus (BA 37) and posterior parts of the cerebellum revealed hypo-connectivities (**Figure 15B**). As an exception, a portion of the pons that is functionally connected with the ventral striatum revealed significantly increased iFC (**Figure 15C**). The motor ICN exhibited significantly decreased iFC in small parts of the lingual gyrus (BA 18) and extrastriatal structures (**Figure 15D**). There were no regions within

the frontoparietal control, visual, basal ganglia-thalamic, brainstem and cerebellar ICNs that displayed altered iFC in PD-CI patients compared with controls.

### 3.2.5 Cognitive Decline in the Course of Parkinson's Disease is Accompanied with a Decrease in Functional Connectivity

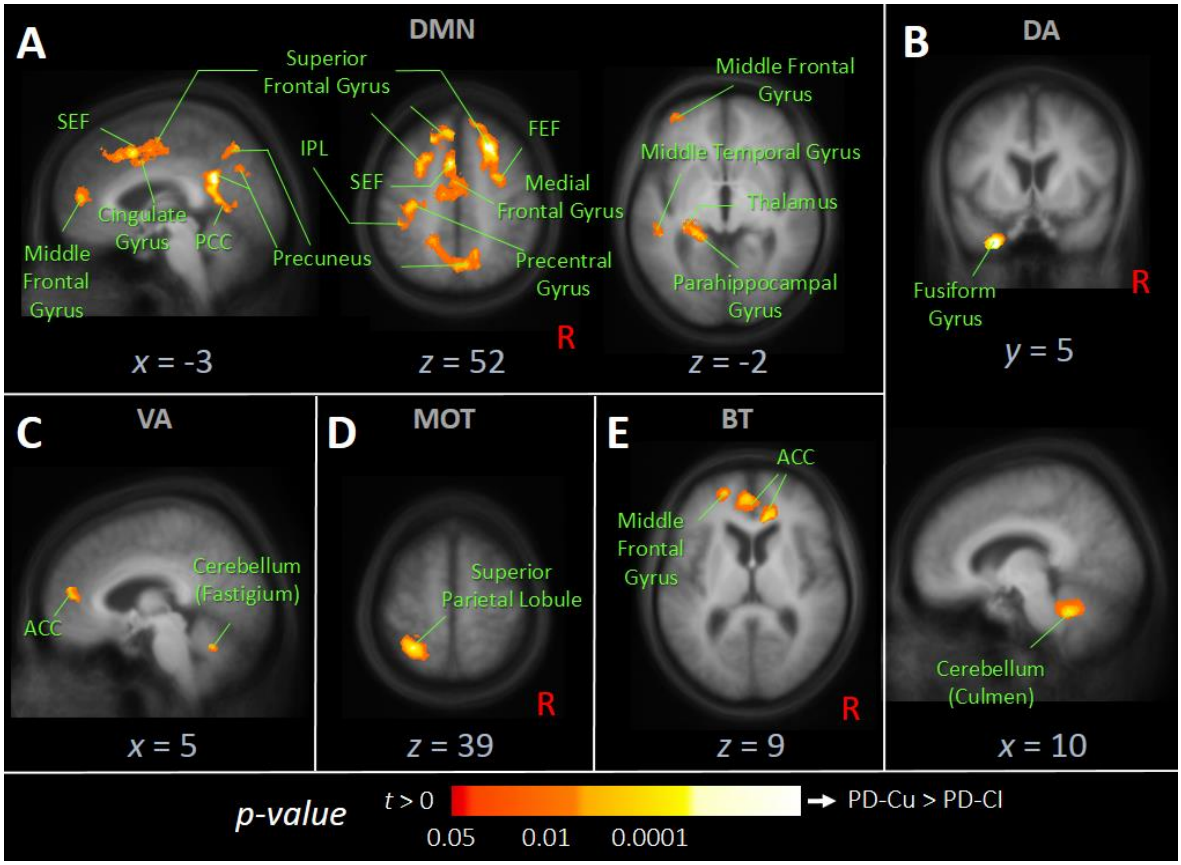


**Figure 16| Effects Contrasting Intrinsic Connectivity Networks in Cognitively Impaired (PD-CI) vs. Unimpaired Parkinson's Disease (PD-Cu) Patients.** Most informative orthogonal slices of Student's *t*-statistic maps in Montreal Neurological Institute (MNI) stereotaxic space. Results were corrected at a 5 % false discovery rate (FDR) level with further cluster-wise correction by discarding cluster sizes less than 343 voxels. Warm colors represent negative *t*-values indicating weaker functional connectivity in PD-CI compared with PD-Cu patients within the (**A**) default mode (DMN), (**B**) dorsal attention (DA), (**C**) ventral attention (VA), (**D**) motor (MOT), and (**E**) basal ganglia-thalamic (BT) intrinsic connectivity networks (ICNs). Abbreviations: R, Right; SEF, Supplementary Eye Field; PCC, Posterior Cingulate Cortex; IPL, Inferior Parietal Lobule; FEF, Frontal Eye Field; ACC, Anterior Cingulate Cortex. Detailed statistics are given in **Table 8**.

Contrasting both patient groups, significant iFC alterations revealed weaker correlations in four out of ten investigated ICNs indicating that iFC declines in the course of the disease

(**Figure 16**). The DMN displayed the greatest effects in iFC alterations (**Figure 16A**), particularly, the memory associated hippocampal formation (BA 34, 35) with adjacent middle temporal areas (BA 22), dorsal parts of the cingulate gyrus (BA 23, 31), the thalamus and the medial prefrontal cortex (BA 6, 8) revealed weaker iFC with the PCC seed. The PCC exhibited less strong iFC in PD-CI compared with PD-Cu patients. In addition, more superior parts of the parietal (BA 4, 5) and frontal gyri (BA 8, 10) including the FEF (BA 8) showed decreased iFC with the PCC seed.

Table 8| Significant Clusters in Intrinsic Connectivity Networks (ICNs) in Cognitively Impaired versus Unimpaired Parkinson's Disease Patients. Coordinates in the Montreal Neurological Institute (MNI) stereotaxic space defining the peak cluster activity corresponding to the maximum likelihood. Results were corrected at a 5 % false discovery rate (FDR) level with further cluster-wise correction by discarding cluster sizes less than 343 voxels (see also Figure 16). Abbreviations: PCC, Posterior Cingulate Cortex; BA, Brodmann Area; PHG, Parahippocampal Gyrus; ACC, Anterior Cingulate Cortex.

| ICN | R/L | MNI | | | Cluster | | REGIONS |
|---|---|---|---|---|---|---|---|
| | | *x* | *y* | *z* | *V*/mm3 | *p* | |
| DMN | R | 22 | 21 | 51 | 20937 | 0.000002 | Superior Frontal Gyrus, BA 8, 10 |
| | - | -5 | -54 | 25 | 15628 | 0.000003 | Cingulate Gyrus, BA 23, 31; PCC, BA 30, 31 |
| | L | -6 | 9 | 51 | 8735 | 0.000007 | Medial Frontal Gyrus, BA 8 |
| | L | -25 | -21 | 45 | 4185 | 0.000005 | Precentral Gyrus, BA 4 |
| | L | -30 | 8 | 47 | 2595 | 0.000006 | Middle Frontal Gyrus, BA 6 |
| | L | -28 | -35 | 2 | 1746 | 0.000003 | Thalamus, PHG BA 34, 35; Precuneus BA 7 |
| | R | 24 | -47 | 60 | 1183 | 0.000007 | Superior Parietal Lobule, BA 5 |
| | L | -52 | -40 | -5 | 996 | 0.000006 | Middle Temporal Gyrus, BA 22 |
| | L | -16 | 49 | 28 | 946 | 0.000002 | Superior Frontal Gyrus, BA 10 |
| MOT | L | -29 | -58 | 66 | 3834 | 0.000002 | Superior Parietal Lobule, BA 7 |
| DA | R | 10 | -51 | -31 | 2272 | 0.000006 | Anterior Cerebellum, Culmen; Midbrain |
| | L | -29 | 9 | -42 | 1307 | 0.000000 | Fusiform Gyrus, BA 36 |
| VA | - | 0 | 43 | 13 | 2222 | 0.000003 | Anterior Cingulate, BA 24, 32 |
| | R | 7 | -61 | -26 | 923 | 0.000006 | Anterior Cerebellum, Fastigium |
| BT | - | -4 | 45 | 9 | 3809 | 0.000005 | Medial Frontal Gyrus, BA 10; ACC, BA 24, 32 |
| | L | -20 | 53 | 15 | 2523 | 0.000006 | Middle Frontal Gyrus, BA 10 |
| | R | 11 | 31 | 8 | 1293 | 0.000002 | ACC, BA 24, 32 |

Within dorsal attention ICN (**Figure 16B**) the iFC of the fusiform gyrus (BA 36) and the cerebellum (Culmen) with the FEF were observed as the regions revealing significant reduced iFC in PD-CI compared with PD patients. The cerebellum (Fastigium) and the

anterior cingulate cortex (BA 24, 32) as portions of the ventral attention ICN exhibited significantly decreased iFC in PD-CI compared with PD-Cu patients (**Figure 16C**). The superior parietal lobe (BA 7) within the motor network (**Figure 16D**) revealed decreased iFC with respect to the seed in the motor cortex in PD-CI compared with PD-Cu patients. As shown in **Figure 16E**, parts of the anterior cingulate cortex (BA 24, 32) and a small area of the middle frontal gyrus revealed decreased iFC with the caudate nucleus seed region of the basal ganglia-thalamic ICN in PD-CI compared with PD-Cu patients. There were no regions within the frontoparietal control, visual, brainstem and cerebellar ICNs that displayed altered iFC when contrasting PD-CI vs. PD-Cu. All significant clusters are listed in **Table 8**.

### 3.2.6 The Cerebellar and Visuospatial Networks Exhibited a Similar Connectivity Map in all Groups

The connectivity pattern of the resulting brain maps in the visuospatial and cerebellar networks were similar in all of the investigated groups (**Figure 12E**, **J**). Hence, no effect was observed when pair-wise comparing groups, i.e. iFC with respect to the seed region in both ICNs revealed relatively similar connectivity strengths in all groups. In addition, the dorsal attention ICN was the only ICN that revealed disturbed iFC in PD-CI but did not display alterations in PD-Cu patients compared with controls. The dorsal attention brain map in both the PD-Cu and control group remained similar as long no cognitive problems occur.

## 3.3 Functional Connectivity in Relation to Altered Oculomotor Performance in Parkinson's Disease

Almost all investigated oculomotor parameters were found to be altered in PD patients in this study excluding the PEV. Eight most informative parameters reflecting changed oculomotor performance in PD patients were used for the covariance analysis, i.e. SPEM gain computed from (i) single-dot and (ii) full-field pattern stimulation, (iii) error rate reflecting inhibitory control in delayed- and anti-saccades, (iv) saccadic gain of primary saccades and (v) latency, both parameters obtained from primary saccade in VGRS, (vi) number of RAVS, (vii) rate of SWJ during attempted visual fixation, and (viii) SI rate during fixational periods in VGRS.

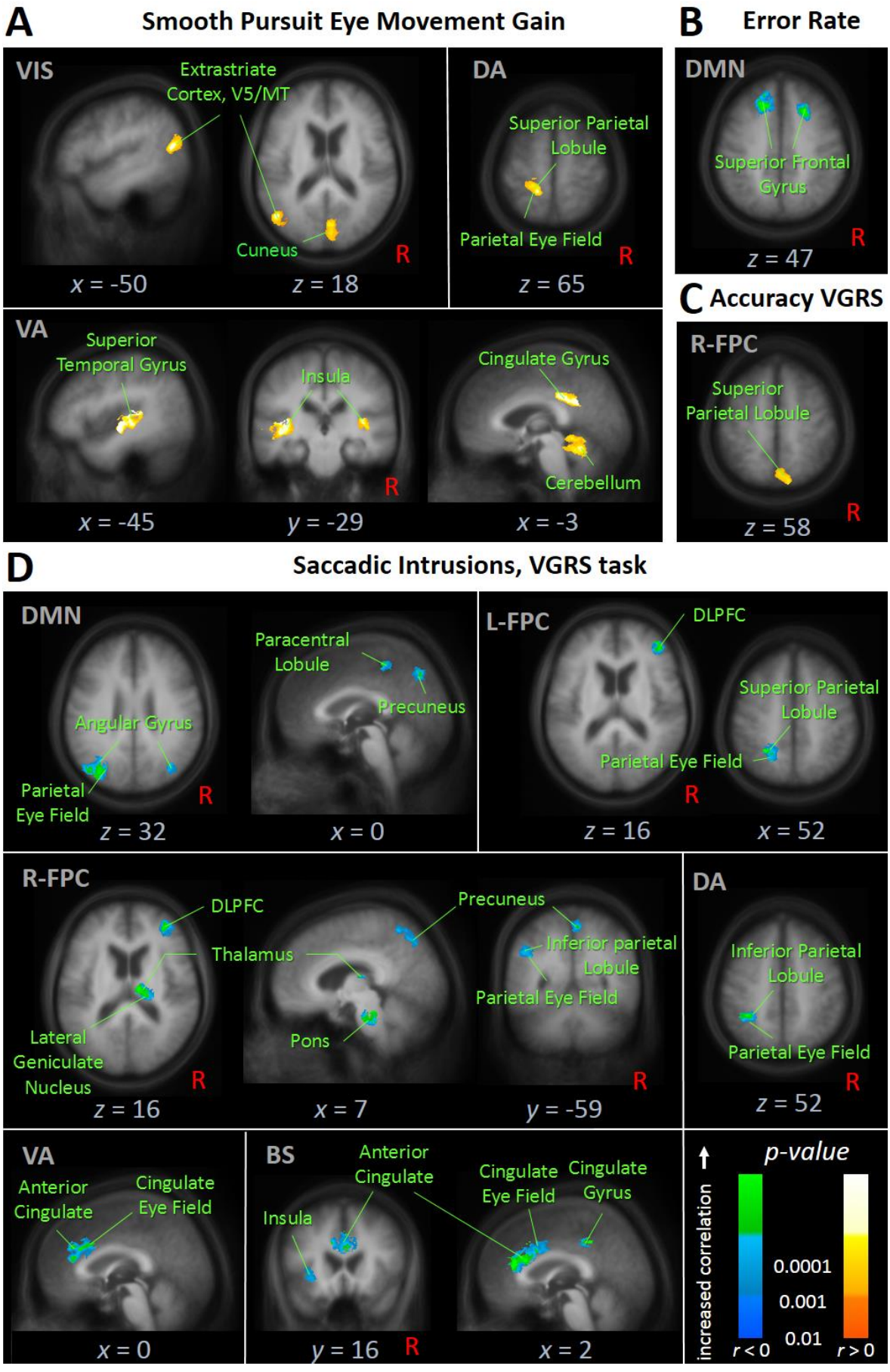
A
Smooth Pursuit Eye Movement Gain
VIS
Extrastriate Cortex, V5/MT
Cuneus
R
x = -50
z = 18
DA
Superior Parietal Lobule
Parietal Eye Field
R
z = 65
VA
Superior Temporal Gyrus
Insula
R
Cingulate Gyrus
Cerebellum
x = -45
y = -29
x = -3
B
Error Rate
DMN
Superior Frontal Gyrus
R
z = 47
C
Accuracy VGRS
R-FPC
Superior Parietal Lobule
R
z = 58
D
Saccadic Intrusions, VGRS task
DMN
Angular Gyrus
Parietal Eye Field
R
z = 32
Paracentral Lobule
Precuneus
x = 0
L-FPC
DLPFC
Superior Parietal Lobule
Parietal Eye Field
R
z = 16
x = 52
R-FPC
DLPFC
Thalamus
Lateral Geniculate Nucleus
R
z = 16
Precuneus
Pons
x = 7
Inferior parietal Lobule
Parietal Eye Field
R
y = -59
DA
Inferior Parietal Lobule
Parietal Eye Field
R
z = 52
VA
Anterior Cingulate
Cingulate Eye Field
x = 0
BS
Anterior Cingulate
Insula
y = 16
R
Cingulate Eye Field
Cingulate Gyrus
x = 2
p-value
increased correlation
0.0001
0.001
0.01
r < 0
r > 0

**Figure 17| Covariance Analysis between Oculomotor Parameters and Voxel-Wise Functional Connectivity Strength within the Intrinsic Connectivity Networks (ICNs) in Parkinson's Disease Patients.** The patients (*N*=31) comprised individuals with (PD-CI) and without cognitive impairment (PD-Cu) that were pooled from both previously defined groups (PD-CI, PD-Cu). Hot and Cold colors represent significant positive or negative Spearman rank correlation coefficients, respectively. Most informative orthogonal slices are shown in Montreal Neurological Institute (MNI) stereotaxic space. Results were corrected at a 1 % false discovery rate (FDR) level with further cluster-wise correction by discarding cluster sizes less than 343 voxels. The mapped quantities were obtained by voxel-wise correlation of intrinsic functional connectivity (iFC) strengths with either one oculomotor parameter as noted below. Note, that iFC is represented as a *z(r)* value for each voxel with respect to the seed-voxel (within the respective ICN). The procedure was applied for each of the ten ICNs. The oculomotor parameters comprises (**A**) smooth pursuit gain evoked by single-dot stimulation, pooled from horizontal and vertical direction as well as both oscillation frequencies (*f*=0.125 Hz and *f*=0.375 Hz), (**B**) pooled error rate from delayed- and anti-saccades conditions, (**C**) accuracy of primary saccade in visually guided reactive saccades (VGRS) pooled for horizontal and vertical direction and (**D**) saccadic intrusion rate during fixational periods pooled for horizontal and vertical VGRS tasks. Detailed statistics are given for **A**, **B**, **C** and **D** in **Table 9**, **Table 10**, **Table 11** and **Table 12**, respectively. Abbreviations: DMN, Default Mode; VIS, Visuospatial; FPC, Frontoparietal Control; VIS, Visuospatial; DA, Dorsal Attention; VA, Ventral Attention; BS, Brainstem; MT, Middle Temporal, DLPFC, Dorsolateral Prefrontal Cortex.

The results of the covariance analysis are summarized in **Figure 17**. In short, significant correlations were found for all PD patients (PD-Cu, PD-CI) between iFC within at least one of the investigate ICNs and (i) 'single-dot' SPEM gain (**Figure 17A**), (ii) error rate of inhibition demanding tasks (**Figure 17B**), (iii) saccadic accuracy gain (**Figure 17C**) and (iv) the SI rate (**Figure 17D**). However, the results indicated no effect for the other oculomotor parameters comprising 'fullfield-pattern', SPEM gain, latencies, number of RAVS and rate of SWJ.

### 3.3.1 Smooth Pursuit Eye Movement Gain Correlates Preferentially with Functional Connectivity of Vision Associated Areas

**Figure 17A** depicts significant relationships in all investigated PD patients between SPEM performance for 'single-dot' stimulation and iFC within the DMN, dorsal and ventral attention ICN. Although the visuospatial ICN revealed similar functional integration in all groups, SPEM was found be significantly correlated with iFC strength between the middle temporal area serving as seed region for visuospatial ICN, the cuneus (BA 18, 19) and the inferior parietal lobule (BA 19, 39, 44) whereas the latter region includes parts of the seed

itself. Within the dorsal attention ICN, iFC between the FEF seed and the superior parietal lobule (BA 3, 5) was positively correlated with pursuit gain.

**Table 9| Clusters of Significant Correlations between 'Single-Dot' Smooth Pursuit Eye Movement (SPEM) and Voxel-Wise Functional Connectivity Strength within Intrinsic Connectivity Networks (ICNs) in Parkinson's Disease Patients.** Coordinates in the Montreal Neurological Institute (MNI) stereotaxic space defining the peak cluster activity corresponding to the maximum likelihood. Results were corrected at a 1 % false discovery rate (FDR) level with further cluster-wise correction (see **Figure 17A**). Averaged correlation coefficients *r* with corresponding *p*-value for given cluster. *Abbreviations*: PCC, Posterior Cingulate Cortex; CG, Cingulate Gyrus; BA, Brodmann Area.

| ICN | R/L | MNI | | | Cluster | | | REGIONS |
|---|---|---|---|---|---|---|---|---|
| | | ***X*** | ***Y*** | ***Z*** | ***V***/mm3 | ***r*** | ***p*** | |
| **VIS** | R | 6 | -84 | 24 | 2623 | 0.61 | 0.0003 | Cuneus; BA 18, 19 |
| | L | -51 | -71 | 16 | 1871 | 0.63 | 0.0002 | Inferior Parietal Lobule, BA 19, 39, 44 |
| **DA** | L | -18 | -48 | 63 | 1854 | 0.64 | 0.0002 | Superior Parietal Lobule, BA 3, 5 |
| **VA** | L | -47 | -18 | -9 | 5553 | 0.71 | 0.0000 | Insula, BA 13 |
| | L | -11 | -45 | -14 | 4299 | 0.68 | 0.0000 | Anterior Cerebellum, Culmen |
| | - | -2 | -43 | 34 | 3534 | 0.68 | 0.0000 | CG, BA 23, 31; PCC, BA 23; Precuneus; BA 30 |
| | L | -53 | 10 | -4 | 1452 | 0.66 | 0.0000 | Superior Temporal Gyrus, BA 22 |
| | R | 39 | -26 | 7 | 1157 | 0.63 | 0.0002 | Insula, BA 13 |

Both regions, FEF and the SPL, play are crucial for oculomotor control. The limbic system as a part of the ventral attention ICN showed great correlations of iFC between the ventro-striatal seed and bilateral insula cortices (BA 13), dorsal and posterior portions of the cingulate gyrus (BA 23, 31) with adjacent cuneus (BA 7) with pursuit gain. In addition, striato-cerebellar and striatal—left superior temporal (BA 22) iFC was found to be significantly linked with pursuit gain. The left superior temporal gyrus encompasses portions of Wernicke's areas residing in the dominant hemisphere which is preferentially left for the right-handed subjects in the investigations. In all other ICNs, i.e. DMN, left and right frontoparietal control, motor, basal ganglia-thalamic, cerebellar and brainstem ICN, exhibited no significant correlated regions. Together, the lower the iFC between each observed significantly correlated cluster and its corresponding seed-region, the lower the SPEM gain. Note, that in this context a reduced gain indicates worse performance in tracking a sinusoidal oscillating 'single-dot'.

### 3.3.2 Inhibition Control is Associated with Functional Integration of the Dorsolateral Prefrontal Cortex as Part of the Default Mode Network

Inhibition control was measured as the rate of erroneous responses in delayed- and anti-saccade conditions. The covariance analysis of the error rate indicated that no ICN other than the DMN revealed clusters whose iFC with its corresponding seed-region were significantly correlated with the error rate (**Figure 17B**). In particular the iFC between bilateral superior frontal gyri (BA 6, 8) with the PCC/precuneus seed exhibited significant negative correlation with the error rate, as in detail illustrated in **Figure 18** and listed in **Table 10**. These findings indicate that the lower the cortico-cortical iFC between the PCC and DLPFC, the higher the error rate in cognitive demanding inhibitory control.

Table 10| Clusters of Significant Correlations between the Error Rate of Oculomotor Inhibition Tasks and Voxel-Wise Functional Connectivity Strength within Intrinsic Connectivity Networks (ICNs) in Parkinson's Disease Patients. Coordinates in the Montreal Neurological Institute (MNI) stereotaxic space defining the peak cluster activity corresponding to the maximum likelihood. Results were corrected at a 1 % false discovery rate (FDR) level with further cluster-wise correction (see Figure 17B). Averaged correlation coefficients *r* with corresponding *p*-value for given cluster. Abbreviations: BA, Brodmann Area.

| ICN | R/L | MNI | | | Cluster | | | REGIONS |
|---|---|---|---|---|---|---|---|---|
| | | ***X*** | ***Y*** | ***Z*** | ***V***/mm3 | ***r*** | ***p*** | |
| **DMN** | L | -17 | 25 | 47 | 4933 | -0.76 | 0.0000 | Superior Frontal Gyrus, BA 6, 8 |
| | R | 20 | 20 | 42 | 2242 | -0.73 | 0.0000 | Superior Frontal Gyrus, BA 6, 8 |

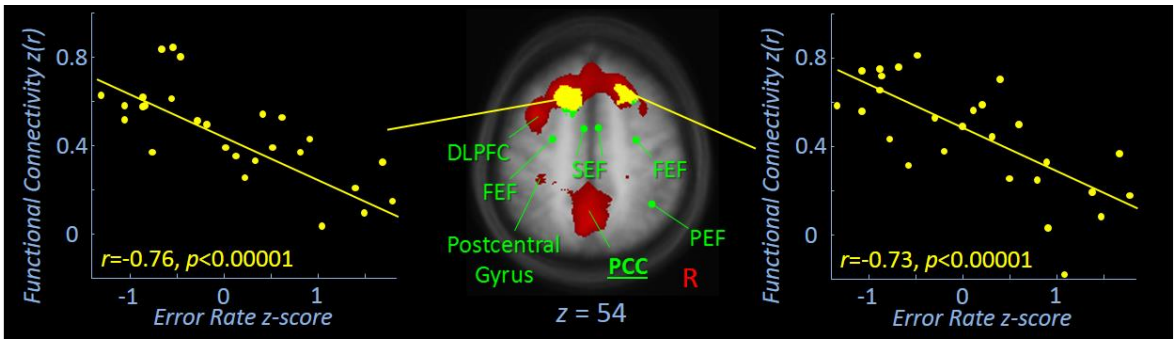


**Figure 18| Scatter Plots Showing Significant Correlations in Parkinson's Disease between Intrinsic Functional Connectivity Strength and the Error Rate in Oculomotor Inhibition Tests.** Two lateralized clusters (**center**, yellow) superimposed on the default mode brain map (red) indicating significant correlations between its connectivity strengths with respect to the posterior cingulate cortex (PCC) and the error rate in oculomotor inhibition tasks (delayed- and anti-saccades). Corresponding scatter plots (**left** and **right**) both showing functional connectivity strengths (*y*-axis) against the error rate represented as *z*-transformed score (*x*-axis) in PD patients. The axial slice (**center**) depicted in standard Montreal Neurological Institute (MNI) stereotaxic brain space in 1 mm resolution and overlaid on the MNI-space deformed high-resolution structural (MPRAGE) template averaged for all subjects (*N*=53). The shown default mode brain map (**center**, red) was computed for the PCC seed-voxel and averaged for all Parkinson's disease patients (*N*=31) and thresholded for minimum $|z(r)|>0.4$ (see also **Figure 23** and **Table 10**). Abbreviations: SEF, Supplementary Eye Field; FEF, Frontal Eye Field; PCC, Posterior Cingulate Cortex; PEF, Parietal Eye Field; DLPFC, Dorsolateral Prefrontal Cortex.

### 3.3.3 Saccadic Accuracy is Related to Temporo-Parietal Connectivity

Primary saccades in VGRS task were found to be hypometric in PD patients resulting in a reduced accuracy gain. **Figure 17C** displayed iFC between the right lateralized fronto-parietal seed region placed in middle temporal area with the depicted cluster showing the superior parietal lobe (BA 7) that is positively correlated with the accuracy gain. Details on cluster statistics are listed in **Table 11**. In summary, these results indicate that the lower is the temporo-parietal iFC between those regions, the lower is the accuracy gain of primary. Moreover, iFC within the other ICN investigated in this dissertation did not reveal any significant relation with saccadic accuracy.

Table 11| Clusters of Significant Correlations between Primary Saccade Gain (Accuracy) and Voxel-Wise Functional Connectivity Strength within Intrinsic Connectivity Networks (ICNs) in Parkinson's Disease Patients. Coordinates in the Montreal Neurological Institute (MNI) stereotaxic space defining the peak cluster activity corresponding to the maximum likelihood. Results were corrected at a 1 % false discovery rate (FDR) level with further cluster-wise correction (see Figure 17C). Averaged correlation coefficients *r* with corresponding *p*-value for given cluster. Abbreviations: BA, Brodmann Area

| ICN | R/L | MNI | | | Cluster | | | REGIONS |
|---|---|---|---|---|---|---|---|---|
| | | *X* | *Y* | *Z* | *V*/mm3 | *r* | *p* | |
| **R-FPC** | R | 8 | -78 | 64 | 1620 | 0.59 | 0.0006 | Superior Parietal Lobule, BA 7 |

### 3.3.4 Saccadic Intrusions

The vast majority of significant correlations with iFC were demonstrated for the SI rate (**Figure 17D**) measured for fixational periods in the VGRS task. The results show for the DMN correlations for bilateral angular gyri (BA 19, 39), the paracentral lobe (BA 5), and the precuneus (BA 7), i.e. the DMN seed region. For the left frontoparietal control, iFC between the left middle temporal area seed with the left precuneus (BA 7) with adjacent superior parietal lobule (BA 7) as well as right DLPFC (BA 46) exhibited significant negative correlations with the intrusion rate. The right DLPFC (BA 10, 46), precuneus (BA 7), the inferior parietal lobule (BA 40), the thalamus including the lateral geniculate nucleus and portions of the pons. Moreover, the results indicate that higher SI rate is significantly correlated with FEF—inferior parietal lobule (BA 19, 39, 44) and ventro-striatal—anterior cingulate cortex (BA 24, 33) iFC within the dorsal and ventral ICN, respectively. Finally, the brainstem ICN revealed SI relationships with iFC strengths between the seed region in the brainstem and portions of the limbic system including the left insula (BA 13), the anterior and superior cingulate gyrus (BA 23, 24, 31, 33). All significant clusters with their corresponding statistics are listed in **Table 12**. No clusters were found within the visuospatial, motor, basal ganglia-thalamic and cerebellar ICNs. Taken together, all clusters showing significant relationships with the SI rate were exclusively found to be negatively correlated. This indicates that the lower the iFC of these clusters with respect to its corresponding seed the higher the presence of SI during the fixational periods in VGRS.

Table 12| **Clusters of Significant Correlations between Saccadic Intrusion Rate in Visually Guided Reactive Saccade Task and Voxel-Wise Functional Connectivity Strength within Intrinsic Connectivity Networks (ICNs) in Parkinson's Disease Patients.** Coordinates in the Montreal Neurological Institute (MNI) stereotaxic space defining the peak cluster activity corresponding to the maximum likelihood. Results were corrected at a 1 % false discovery rate (FDR) level with further cluster-wise correction (see **Figure 17D**). Averaged correlation coefficients *r* with corresponding *p*-value for given cluster. Abbreviations: SOG, Superior Occipital Gyrus; SPL, Superior Parietal Lobule; BA, Brodmann Area.

| ICN | R/L | MNI | | | Cluster | | | REGIONS |
|---|---|---|---|---|---|---|---|---|
| | | ***X*** | ***Y*** | ***Z*** | ***V***/mm3 | ***r*** | ***p*** | |
| **DMN** | L | -35 | -74 | 25 | 5555 | -0.66 | 0.0001 | SOG, BA 19; Angular Gyrus, BA 39 |
| | - | 5 | -75 | 45 | 1320 | -0.68 | 0.0000 | Precuneus, BA 7 |
| | R | 38 | -77 | 38 | 1212 | -0.70 | 0.0000 | SOG, BA 19; Angular Gyrus, BA 39 |
| | - | -1 | -37 | 58 | 882 | -0.65 | 0.0001 | Paracentral Lobule, BA 5 |
| **L-FPC** | L | -27 | -52 | 49 | 1444 | -0.68 | 0.0000 | Precuneus, BA 7; SPL, BA 7 |
| | R | 43 | 40 | 17 | 1085 | -0.73 | 0.0000 | Middle Frontal Gyrus, BA 46 |
| **R-FPC** | - | 5 | -59 | 62 | 2873 | -0.62 | 0.0004 | Precuneus, BA 7 |
| | R | 14 | -23 | 18 | 2028 | -0.69 | 0.0000 | Thalamus |
| | med | 4 | -31 | -27 | 1697 | -0.67 | 0.0000 | Pons |
| | R | 36 | 43 | 17 | 1621 | -0.64 | 0.0002 | Middle Frontal Gyrus, BA 10, 46 |
| | L | -49 | -57 | 36 | 1168 | -0.63 | 0.0003 | Inferior Parietal Lobule, BA 40 |
| **DA** | L | -35 | -49 | 51 | 1360 | -0.69 | 0.0000 | Inferior Parietal Lobule, BA 19, 39, 44 |
| **VA** | L | -6 | 18 | 36 | 3854 | -0.70 | 0.0000 | Anterior Cingulate, BA 24, 33 |
| **BS** | med | 0 | 33 | 17 | 9756 | -0.71 | 0.0000 | Anterior Cingulate, BA 24, 33 |
| | med | 5 | -44 | 45 | 1697 | -0.67 | 0.0000 | Precuneus, BA 7; Cingulate Cyrus, BA 23, 31 |
| | L | -34 | 21 | -2 | 1312 | -0.64 | 0.0002 | Insula, BA 13; Inferior Frontal Gyrus, BA 47 |

# 4. Discussion

Using a novel bimodal methodological approach to covariate oculomotor performance and 'resting-state' fMRI, this study demonstrated PD-associated oculomotor deficits linked to decreasing iFC in brain structures that are associated with oculomotor control including cortical, limbic, thalamic, cerebellar and brainstem regions. Patients that were neuropsychologically confirmed to be free of cognitive problems presented both oculomotor dysfunctions and increased iFC. When cognitive problems in PD manifested, oculomotor performance gradually worsened, and iFC was found to be decreased preferentially in brain structures attributed to the DMN. Hence, increased BOLD coherence (hyper-connectivity) in ICNs apparently diminished towards decreased iFC (hypo-connectivity) as cognitive performance declined. In addition, a combination of non-invasive quantifiable objective measures of (some aspects of) human behavior by means of VOG and *in-vivo* imaging utilizing iFCMRI potentially forms a fundamental groundwork to refine the models of functionally interacting brain areas as parts of large-scale distributed networks. The subsequent discussion considers the implications of the present results with regards to the pathophysiological knowledge of PD.

## 4.1 Oculomotor Alterations Already Manifest in Cognitively Unimpaired Parkinson's Diseases Patients

Performance in oculomotor tasks were investigated in several 'reflexive' (VGRS, SPEM) and cognitively demanding tasks (RAVS, delayed- and anti-saccades) where the patients were categorized with respect to their cognitive presentation and compared with healthy controls. One novelty in this study was the comprehensive oculomotor assessment and a detailed analysis of the SI rate. It is of note that all subjects were controlled for the absence of lesions in MRI or clinical presentations associated with small vessel cerebrovascular disease that has been recently reported to be associated with a broad spectrum of oculomotor dysfunctions (Pinkhardt et al. 2014). The oculomotor phenotype of small vessel cerebrovascular disease is intriguingly similar with the abnormalities observed in PD. The findings when contrasting the VOG data between PD patients and controls were in general agreement with others studies (Mosimann et al. 2005, Pinkhardt et al. 2008, 2012, Terao

et al. 2011, MacAskill et al. 2012, van Stockum et al. 2013). Moreover, almost all aspects of disturbed eye movements including executive oculomotor control manifested already in PD-Cu patients.

### 4.1.1 Anticipatory Behavior During Smooth Pursuit Eye Movement

SPEM was assessed by both single-dot pursuit and fullfield-pattern pursuit at different oscillating frequencies (slow and fast) in horizontal and vertical directions. The former characterize SPEM with foveal stimulation, the latter SPEM with concurrent foveal and extra-foveal stimulation. As demonstrated here and in accordance with other studies, single-dot SPEM is frequently interrupted by anticipatory saccades resulting in a reduced pursuit gain (Pinkhardt et al. 2009, 2012). This deficit already manifested in PD-Cu patients preferentially for horizontal directions whereas upward SPEM was found to be impaired in PD-CI patients. Notably, even in PD-D cases with severely affected SPEM, the patients were fairly able to track the target smoothly whereas the episodes of SPEM obviously shorted with more frequent SI (Pinkhardt et al. 2009). This may lead to the assumption that the 'genuine' SPEM system provides the ability to track a foveal stimulus in a highly predictable fashion. Thus, the 'SPEM system' appears to be unaffected in both PD-Cu and PD-CI patients. This hypothesis receives support from previous studies by our group that attributed the inappropriate release of anticipatory saccades to an executive dysfunction (Pinkhardt et al. 2012).

Nota bene, as the disease progresses together with cognitive decline, the ability of fullfield-pattern pursuit was found to remain intact to a large extent. Hence, the assessment of SPEM with a fullfield-pattern may facilitate attention because unwanted interrupting saccades were mainly suppressed. These findings supported the hypothesis that disturbed SPEM are linked to impaired inhibitory control rather than to an impaired 'genuine' SPEM system (Pinkhardt and Kassubek 2011). The knowledge about the differences between exclusively foveal or concurrent foveal and extra-foveal SPEM stimulation is currently limited and may be addressed in future studies.

### 4.1.2 Impaired Reflexive Gaze Shifts in Parkinson's Disease Patients

Gaze shifts performance was measured in VGRS task where the subject had to track a 'jumping' target in an unpredictable manner. The data underpin the findings of hypometric saccades as a hallmark in PD (Kassubek and Pinkhardt 2011, Anderson and MacAskill 2013). Depending on the patient's clinical state, the amplitudes of reflexive saccades are reported to be decreased in early PD (MacAskill et al. 2012) and not to deteriorate later in the course of the disease (Terao et al. 2011). This is in general agreement with the present results, i.e. the finding of hypometric saccades in VGRS in PD-Cu and PD-CI patients, whereas contrasting both patient groups exhibited no statistical significance but a tendency towards decreasing accuracy gain. In addition, the observed saccadic hypometria in PD-CI patients was consistent with the observations in PD-D patients who display poor saccadic control in reflexive saccades tasks (Mosimann 2005).

In accordance with several other studies (Pinkhardt et al. 2008, 2012, MacAskill et al. 2012), the peak velocities of the primary saccades obtained in the VRGS condition were similar and in the range of normal in all groups (PD-CI, PD-Cu, controls). Moreover, the ability to perform inconspicuous saccades was found to be preserved in all PD patients. Thus, a straightforward conclusion from saccadic performance as measured by VGRS is that the saccadic pulse generator located in portions of the brainstem (Leigh and Zee 2006) seems to remain spared by the pathological process of PD. Saccadic latencies as measured during VGRS are still a matter of controversy in the current literature. In the present study, latencies were measured in terms of the delay time between presenting a new target and the onset of the primary saccades in VGRS condition (MacAskill et al. 2012, Pinkhardt et al. 2014). The results indicate increased reaction times in PD-Cu patients that were slightly more prolonged in PD-CI. This outcome is at odds with the statement by MacAskill and co-workers who reported similar latencies in cognitively unimpaired PD patients compared with controls (MacAskill et al. 2012). However, when cognitive problems in PD become evident, prolonged reaction times have been demonstrated to be consistent to the present findings (Mosimann et al. 2005, MacAskill et al. 2012).

### 4.1.3 Inhibition Control Markedly Worsens with Cognitive Deficits in Parkinson's Disease

Executive functions summarize to a domain of cognitive processes including the control of inhibition and of goal-directed behaviors (Dirnberger and Jahanshahi 2013). Inhibition control tested in the delayed- and anti-saccade task was found to successively worsen with cognitive decline and to be strongly related to overall cognitive scores as assessed by PANDA and MMSE. These results are inline with generally impaired executive control in PD (Dirnberger and Jahanshahi 2013) and affected inhibitory oculomotion (Terao et al. 2011, van Stockum et al. 2013). However, it is remarkable that a lack of oculomotor inhibition control may already manifest in cognitively unimpaired PD patients. As demonstrated in PD-CI patients, inhibition control was reduced which was consistently found in PD-D patients presenting with the decreased ability of inhibitory control, target prediction, and spatial decision making (Mosimann 2005).

Executive control is also addressed by RAVS that reflect the ability to initiate self-paced saccades. The number of gaze shifts was found to be reduced in patients in agreement with our previous study (Pinkhardt et al. 2012); more specifically, in the present study, even PD-Cu patients presented with the impaired ability to perform self-initiated gaze shifts. The disability to suppress unwanted gaze shifts in the sense of 'hyper-reflexive' saccades is apparently at odds with the observed slowed saccade initiation when PD patients are required to perform RAVS. Terao and co-workers attributed this phenomenon to a disturbed input to the 'input gate', the SC, due to abnormal firing patterns mediated by the BG (Terao et al. 2011). Taken together, the disturbed executive oculomotor functions lead to the conclusion that VOG measures provide a valuable and sensitive measure for executive control.

### 4.1.4 Square Wave Jerks and Saccadic Intrusions

Specifically, the present study aimed at the comprehensive investigation of SWJ and SI both during attempted fixation and in fixational periods during VGRS task. During attempted fixation, SWJ manifested preferentially in horizontal direction and were exclusively observed with a pronounced increased rate in PD-Cu and PD-CI patients; with no

differences but a tendency towards more frequent SWJ in PD-CI compared with PD-Cu patients. These data were consistent with recent studies in PD patients (Otero-Millan et al. 2013).

The outcomes of the SI analysis during VGRS exhibited intrusions which were predominantly in the direction of the stimulus for PD-CI and PD-Cu patients. PD patients presented with difficulties in suppressing unwanted gaze shifts when awaiting the next stimulus in the visual scene as given in the fixational periods of VGRS. The SI rate increases with cognitive decline which is in general agreement with a study by Donaghy and co-workers demonstrating the association between properties of SI and deficits in the prefrontal cortex in amyotrophic lateral sclerosis patients (Donaghy et al. 2009). A recent review on SI proposed a dysfunctional inhibitory system responsible for a disturbed suppression of unwanted gaze shifts even in the absence of any targets (Lemos and Eggenberger 2013). It is questionable why SI were observed only in the direction of expected stimulus rather than in towards oblique or orthogonal directions. Further studies are needed to address this open issue. Taken together, the analysis of SI in PD patients depending on their cognitive presentation forms a framework for a diagnostic VOG tool to assess inhibition control in the absence of complex oculomotor task such as anti-saccades that require the patients' insight.

## 4.2 Increased Functional Connectivity in Parkinson's Disease with Normal Cognitive Performance: Pathological Processes or Adaptive Changes?

In this study, ten ICNs in the human brain have been identified for both PD patients and the control group (Beckmann et al. 2005, Smith et al. 2009, Laird et al. 2011). The data for subsequent seed-based iFC analysis were acquired by means of iFCMRI while subjects were quietly 'resting' with their eyes closed but awake in the scanner. The seed-regions for the respective ICNs were placed in areas that were reported to serve as a major hub (van den Heuvel and Hulshoff Pol 2010) and to be strongly associated with oculomotion (Leigh and Zee 2006) with regard to the covariance analysis.

### 4.2.1 Methodological Approach in Identifying Intrinsic Connectivity Networks

A framework has been presented that allows for iFC analysis and ICN identification by a five item preprocessing followed by a three step seed-based correlation analysis in order to obtain ICNs as discussed in (Gorges et al. 2014a). The following algorithm implementations in the *TIFT* software (Müller et al. 2007b, 2007a, Müller and Kassubek 2013) were adapted from diffusion tensor imaging (DTI) analysis and also applied for iFCMRI processing: Data were resampled to a cubic 1 mm grid for further complementary analysis in order to (i) optimize the sensitivity and specificity by spatial Gaussian filtering and (ii) to improve stereotaxic normalization to the EPI-template. Methodological novelties of this study comprises (i) the ICN identification in a sample of elderly subjects which form the basis of the present control group. This is all the more important since it could be shown that age-dependent changes of the cerebral vasculature exist which may alter the neuronal–vascular coupling and thus the BOLD signal also in task-based fMRI investigations (Riecker et al. 2003); (ii) one prerequisite of the seed-voxel approach for ICN identification is an up-sampling to a cubic 1 mm grid. Compared with ROI-seed-based approaches (Shulman et al. 2010, Choi et al. 2012, van Oort et al. 2014), the presently applied seed-voxel approach is supposed to provide some advantages: First, spatial smoothing with sufficient kernel size improves highly correlated time courses of adjacent voxels (Choi et al. 2012) so that the location of the seed-voxel is assumed to be robust against displacements. Second, although the data were stereotaxically normalized in a two-step procedure, small discrepancies in normalization are a common but confounding side-effect due to the slightly different individual's brain anatomy. In particular, for small anatomical ROIs, a larger seed radius may exceed the true ROI by encompassing structures outside. Instead, selecting a single voxel in a 1 mm cubic grid on the basis of the averaged high-resolution image (e.g. MPRAGE) (Hacker et al. 2012) may overcome this problem. Moreover, the proposed approach did not include any kind of brain masking (such as white-matter mask or cerebrospinal fluid-mask).

No nuisance covariates such as whole brain signal, cerebrospinal fluid, white matter signals or head motion parameters have been regressed out, as addressed in the following. In order to correct for non-neuronal BOLD signals (Fox et al. 2005), removing the effect of

nuisance covariates is a common iFCMRI preprocessing step (Chao-Gan and Yu-Feng 2010). However, is remains unclear where the respective data for regressing those covariates should be extracted (Song et al. 2011). In this study, no nuisance covariates were regressed out because the demonstrated ICNs in the elderly were unambiguously identified utilizing the proposed approach. The observed brain maps were remarkably similar compared to previous studies (e.g. Smith et al. 2009, Laird et al. 2011, Gohel and Biswal 2014). The effect of regressing out movement, ventricle and white matter covariates appears to be of minor impact, in agreement with others (Fox et al. 2009, Van Dijk et al. 2010) who systematically investigated and illustrated these effects. However, those authors pointed out the strong influence of utilizing global signal regression that in turn induces the ongoing debated anti-correlated regions (Cole et al. 2010). The identified brain maps did not reveal anti-correlated regions, probably because global mean regression in the data processing procedure was not applied. The global mean regression is thought to induce anti-correlated regions (Murphy et al. 2009) and is therefore still controversial in iFCMRI literature (Song et al. 2011) so that anti-correlated regions and their possible physiological interpretation are a matter of an ongoing debate (Weissenbacher et al. 2009, Cole et al. 2010).

The ten investigated ICNs in this study were (i) the 'task-negative' DMN (Raichle et al. 2001, Greicius et al. 2003, Buckner et al. 2008) as well as the 'task-positive' (ii) left and (iii) right lateralized frontoparietal control (Vincent et al. 2008, Spoormaker et al. 2012), (iv) visuospatial (Smith et al. 2009, Laird et al. 2011), (v) motor (Biswal et al. 1995, Wu et al. 2009b, 2011), (vi) dorsal (Vincent et al. 2008, Van Dijk et al. 2010) and (vii) ventral attention (Di Martino et al. 2008, Hacker et al. 2012), (viii) basal ganglia-thalamic (Di Martino et al. 2008, Laird et al. 2011), (ix) brainstem (Laird et al. 2011, Hacker et al. 2012) and (x) cerebellar (Smith et al. 2009, Laird et al. 2011) ICNs that capture fundamental units of functional organization (Yeo et al. 2011).

The dorsal attention ICN is of particular interest because it has been termed the 'oculomotor system' (Vincent et al. 2008) since this ICN encompasses a vast majority of brain areas closely related to oculomotor control (Leigh and Zee 2006). The FEFs and SEF are thought to mainly project into the caudate nucleus referred to as the 'oculomotor striatum' (Wichmann and DeLong 2013). However, markedly activity in this ICN was

presently found also for the putamen which may serve as a major hub in attentional control and may also be involved in eye movement control. This is in agreement with a recent study in brain connectivity using iFCMRI for functional and DTI for structural imaging of top-down oculomotor pathways, respectively (Neggers et al. 2012). These authors suggested that the oculomotor system may be somewhat different in humans compared with non-human primates. In terms of eye movement control, further investigation in iFC of the dorsal visual pathway could help to present a framework for understanding oculomotor attentional control.

### 4.2.2 The Cerebellar and Visuospatial Brain Maps were Similar in Parkinson's Disease Patients and Controls and thus Defining Reference Networks

In the between-groups comparisons (PD-CI, PD-Cu, controls), the results demonstrate altered iFC in eight out of ten ICNs while only the cerebellar and visuospatial ICN revealed similar activity in all groups. From the methodological point of view, this is of note because measures of iFC by means of iFCMRI are sensitive to confounding factors which could be differentially present within groups (Van Dijk et al. 2012, Buckner et al. 2013). Hence, both ICNs (i.e. cerebellar, visuospatial) also serves as reference networks so that the observed effects may be less likely to emerge as artefacts.

These data lead to the assumption that the pathological process appears to spare cerebellar and small-world visuospatial networks. The finding that the iFC pattern of the visuospatial network in PD resembles that of controls is important to note because a broad spectrum of visual symptoms such as visuospatial dysfunctions, or impaired color discrimination frequently manifest in PD (Sauerbier and Chaudhuri 2013, Kassubek et al. 2013). Hence, iFC between the extrastriate cortex and primary visual areas may not be responsible for these clinical observations. The finding of intact functional integration of associated visual areas is inline with neuropathological evidence that the pronounced myelinated nerve cells and short axoned local circuits within the primary sensory fields are resistant to the selective pathological process in PD (Braak et al. 2004, Braak and Del Tredici 2009, Kassubek et al. 2013). The iFC correlate of the clinical observations of visuospatial abnormalities in PD may be more likely to result from an impaired functional integration of

other brain regions outside the visuospatial ICN, promoting the association areas as a critical relais. This hypothesis receives support from a recent iFCMRI study on extrastriate visual network in PD-D patients where decreased iFC between the caudate nucleus and extrastriatal cortical regions has been reported (Rektorova et al. 2012).

No alteration of cerebellar iFC was demonstrated although there is evidence for the cerebellum to be involved in the pathophysiology and pathoanatomy in PD both in a compensatory and pathological manner, as summarized by Wu and Hallett (Wu and Hallett 2013). These authors attributed cerebellar dysfunction primarily to abnormal dopaminergic mediation by the basal ganglia. This conclusion could be in accordance with our observation that the cerebellar network, mainly covering the cerebellum itself, revealed a normal iFC pattern. The functional communication with other brain areas remains to be addressed in future studies. Again, an explanation emerges from the neuropathological findings by Braak and co-workers who reported lesions in the sensory association areas that manifest in the latest stages of the disorder (Braak et al. 2003, 2005, Braak and Del Tredici 2009). Hubs of the cerebellar circuit are connected by long-axoned nerve cells that are resistant or become involved, in some instances, in the final stages of the disease (Braak et al. 2006). Taken together, the present findings in association with the literature may suggest impaired functional integration within ICNs rather than a cerebellar dysfunction itself.

### 4.2.3 Possible Explanations of Increased and Decreased Functional Connectivity, Respectively

Increased iFC was seen in PD patients who were found to be free of cognitive deficits in the neuropsychological assessments and might be considered as stronger synchronous BOLD fluctuations of the observed clusters with respect to their seed-regions (Mevel et al. 2011). This global hyper-connected state in PD-Cu patients was consistently found in several ICNs beyond the sensorimotor network. It is no surprise that iFC was observed to be decreased in PD patients with evident cognitive problems (Hacker et al. 2012) as a possible consequence of disease-related loss of structural connectivity (Agosta et al. 2014). The transient process from the hyper- towards hypo-iFC state might be considered to be closely

linked to cognitive decline. Since it is commonly assumed that iFC reflects structural connectivity in the brain (Greicius et al. 2009, Damoiseaux and Greicius 2009, Buckner 2010), decreased iFC is most likely the consequence of impaired structural network integrity due to neural cell degeneration. Hence, decreased iFC is consistently explained by functional decoupling of brain areas attributed to ICNs (Buckner et al. 2008, Biswal et al. 2010, Filippi et al. 2013).

In PD-CI patients, the vast majority of clusters indicating decoupling of brain regions from the PCC was strikingly observed for regions that correspond to the DMN. These regions included the midline cores and the memory-associated hippocampus. It must be emphasized that iFC decrease within the DMN does not fully explain the spectrum of cognitive problems clinically evident in PD patients presenting with a range from PD-MCI to PD-D. Regions associated with the DMN are considered to be linked to cognitive decline as suggested from many previous studies on iFC in AD (Greicius et al. 2004, He et al. 2007, Mevel et al. 2011, Lehmann et al. 2013). Hypometabolism in the PCC in AD is related to the mental status (Buckner et al. 2008) and a disrupted DMN also manifests early in the course of AD (Buckner et al. 2005). The authors convincingly argued that the pathological spreading of AD pathology remarkable resembles the pattern of the DMN. Moreover, current theories suggest that the PCC is crucially involved in cognitive functions including memory consolidation, attention and controlling the balance between internal and external thoughts (Leech and Sharp 2014). The medial prefrontal cortex, more specifically its dorsal portion, has been identified as a major hub of the DMN and serves as a relais of the dorsal medial prefrontal cortex subsystem (Andrews-Hanna et al. 2010). In addition, the hippocampal formation characterizes a second and distinct subsystem (Buckner et al. 2008) associated with memory functions in the DMN (Greicius et al. 2004). Both the medial prefrontal and the memory systems of the DMN were found to become functionally disconnected which confirmed the important role of the DMN in cognition. Moreover, these results support the essential role of the prefrontal cortex in higher cognition, e.g. the medial portion is linked to adaptive goal-directed behaviour and learning (Ridderinkhof et al. 2004). These findings received further evidence from DTI investigations in PD-MCI patients that revealed structural disruption between the midline cores (Agosta et al. 2014).

Increased activity in functional networks reflecting a hyper-connectivity state could be revealed in the patient group of PD-Cu patients presumably reflecting adaptive changes as an attempt to sustain cognitive performance (Mevel et al. 2011). When cognition in PD starts to fail as observed here for the PD-CI group, preferentially the hippocampus and regions attributed to the long-distance midline cores comprising medial posterior and anterior parts become functionally disconnected. These areas are associated with portions of the DMN and appear to be crucially involved in several cognitive domains as reported for AD (Greicius et al. 2004, Buckner et al. 2005, 2008) and other neuropathological conditions as reviewed by (Zhang and Raichle 2010). Our previously published pilot study in non-demented PD patients where we found decreased iFC along the midline cores (Gorges et al. 2013) is in accordance with the present outcomes. The results reported for the DMN as observed for PD patients are not fully consistent. Tessitore and co-workers described decreased iFC solely in middle temporal areas in cognitively unimpaired patients (Tessitore et al. 2012), whereas others reported no effect (Krajcovicova et al. 2012). These discrepancies may be due to the differences in cognitive states of PD patients and the utilized methodological approaches.

Increased iFC is difficult to explain. The most obvious explanation is a physiological, compensatory response to disease-related pathology (Mevel et al. 2011, Douaud et al. 2011). Increased iFC reflect highly correlated BOLD fluctuations that could be associated with some (disease-specific) pathological process leading to an excessive pathological firing pattern in 'denial-of-service' fashion, i.e. brain areas excessively communicating with each other are no longer responsible for functional interaction with other structures. This statement is consistent with the notion that dynamic up- and down-regulation of ICN activity may be crucial for normal brain functioning (Leech and Sharp 2014). Douaud and co-workers suggested a loss of the inhibitory influence due to GABA-ergic cell degeneration as part of the pathological process for their results of a positive association of iFC with rate of disease progression in amyotrophic lateral sclerosis (Douaud et al. 2011). The authors also reported structural abnormalities parallel with increasing iFC compared with controls. However, this model may be not sufficient to explain hyper-iFC in PD-Cu patients. First, structural damage appears to be unlikely to manifest in PD-Cu patients as indicated by Agosta and colleagues (Agosta et al. 2014). These authors conducted a structural

connectivity study in neuropsychologically confirmed cognitively unimpaired PD patients compared with controls and showed that anatomical connections (axonal fiber bundles) assessed by DTI remains intact in PD-Cu patients. Second, hyper-iFC diminished towards decreased iFC in PD-CI patients, hence, the relationship of iFC within disease progression in PD appears to be negative. Third, GABA-ergic cell degeneration is not prominent compared to dopaminergic cell loss in PD (Braak and Del Tredici 2009). Thus, the observed wildly distributed pattern of hyper-connectivity may be more likely to be attributed to compensatory mechanisms. The observed effects pointed towards a largely distributed topographical ICN reconfiguration in the sense of 'higher effort' activity or integration of additional areas. The findings demonstrated clusters also located 'outside' the brain maps in PD patients compared with controls. This incorporation of additional network hubs may considerably support the notion of allocating additional resources. The ability to recruit additional resources of networks that are not engaged in the respective function in the healthy brain is related to the concept of cognitive reserve (Stern 2002). Additional cognitive resources may be allocated in reorganizing function networks by bypassing affected regions in a 'more-with-less' fashion until the neuronal reserve is exhausted (Mevel et al. 2011). In addition, it can be hypothesized that ongoing functional remapping accompanies the spreading of the pathological process until the onset of axonal fiber damage. For instance, a hyper-connectivity state in AD was consistently reported to reflect adaptive changes as an attempt to maintain cognitive performance and was found prior to the AD-related symptoms of cognitive decline (Stern 2006, Mevel et al. 2011). Likewise, compensatory processes may also be present in PD (Hacker et al. 2012, Wu and Hallett 2013).

To summarize, the interpretation of decreased iFC, i.e. weak synchronicity of BOLD fluctuations, and increased iFC (strong synchronicity) in terms of the potential functional consequences has not been fully understood and the explanation of hyper-connectivity appears to be disease-specific. In PD, the increased iFC pattern might be interpreted as stronger iFC coupling at expense of less efficient and less dynamic regulation of ICN interactions ('dysregulation'). This reorganisation points to some great extent towards compensatory processes by incorporating additional areas to the respective ICNs. Whilst taking the present findings of increased iFC in PD-Cu patients into account, iFC as measured

by iFCMRI may provide a more sensitive measure for alterations in brain functioning as compared with structural investigations when anatomical connection (axonal fiber bundles) remain intact (Agosta et al. 2014). Whether preclinical alterations in iFC towards a hyper-iFC pattern provide a framework for an imaging surrogate marker for PD provides a promising direction for future research.

## 4.3 Exploring Parkinson's Disease-Specific Functionally Interacting Brain Structure Associated with Oculomotor Control

### 4.3.1 Functional Connectivity and Oculomotor Performance in the Progression of Parkinson's Disease

The results discussed so far comprised the oculomotor performance and iFC depending on the PD patient's cognitive states compared with controls. In order to analyze PD specific iFC alterations linked to oculomotor dysfunctions, both PD patients groups were pooled, spanning a range from cognitively unimpaired to demented PD patients. As illustrated in **Figure 19**, oculomotor performance markedly declined soon after symptom onset even when cognitive deficits have not become neuropsychologically manifest. One strength of the study concept was the comprehensive neuropsychological testing in order to classify PD patients with respect to their cognitive status. PD-Cu patients presented with unimpaired cognition whereas iFC revealed a large-scale distributed pattern of increased iFC. The course of iFC in terms of PD progression seems to be more complex. Together with the oculomotor results, iFC might change before oculomotor impairment manifests in PD. This statement suggests iFC alterations in preclinical stages to be interpreted as a possibly adaptive mechanism until the higher cognitive functions begin to decline. There has been growing awareness that some non-motor symptoms manifest before the cardinal motor symptoms become evident (Chaudhuri et al. 2011). Autopsy-controlled studies provide ample evidence for PD-associated pathology before motor symptoms become recognizable (Del Tredici et al. 2002, Braak et al. 2003, 2004). This raises the question to what extent and where iFC might change in the presymptomatic phases. To address this promising concern, future (longitudinal) iFCMRI investigations are required in subjects prone to develop PD (such as presymptomatic mutation carriers).

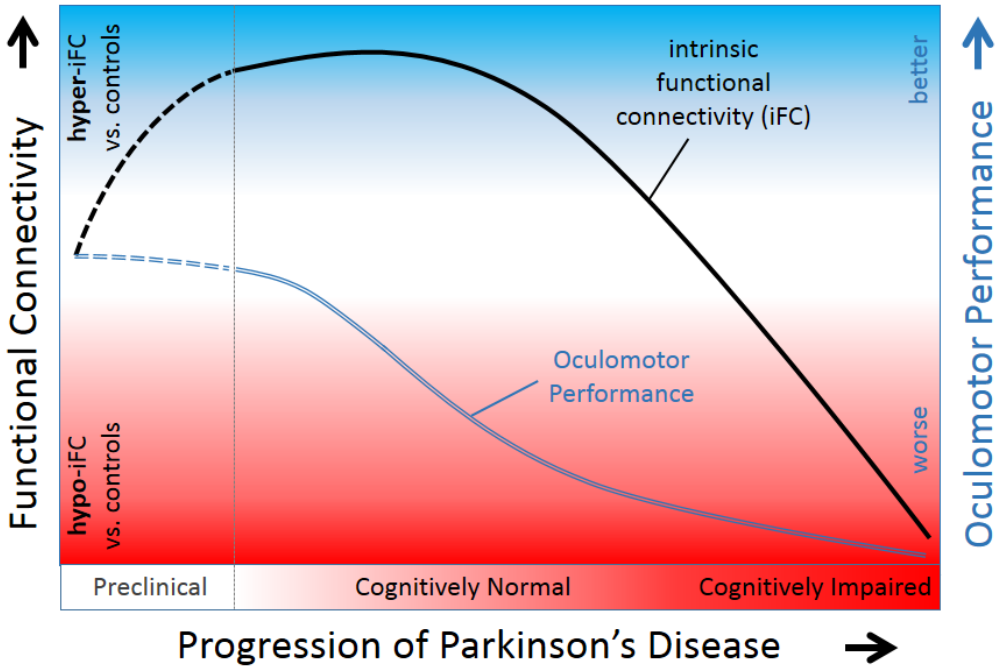


**Figure 19| Hypothetical Model of Intrinsic Functional Connectivity (iFC) and Oculomotion Depending on the Progression of Parkinson's Disease (PD).** The present findings may support the characteristic iFC traces (black) indicating that iFC is hyper-connected in patients without cognitive impairment (PD-Cu) and gradually decreases with upcoming cognitive problems. Pathological state of oculomotion (blue trace) appears to manifest initially in PD-Cu and gradually worsens (red background) as cognitive problems accompanies disease progression. Dashed traces extrapolate the hypothetical model for the presymptomatic phase. In addition, the assumed model based on the comparison with the healthy control group. The observed relationship between oculomotor performance and iFC is in accordance with this model – the more impaired the oculomotion in PD the lower the iFC.

### 4.3.2 Functional Decoupling may Worsen Oculomotor Performance

An intriguing finding of the covariance analysis indicated that all significant clusters, i.e. parts of different ICNs, become functionally disconnected from their major hubs when oculomotor abnormalities presented in PD. The regional iFC which have previously been reported to be significantly related with oculomotor performance were found to be associated with oculomotor control with the exception of the superior temporal and angular gyrus. Notably, the angular gyrus plays a role in language and semantic processing but has recently been proposed to be functionally and structurally connected with the insular cortex and may help to mediate detection of visually salient stimuli (Uddin et al.

2010). The angular gyrus belongs to the DMN (Greicius et al. 2003) and was demonstrated to be associated with the prevalence of SI when its regional iFC value (within the DMN) decreases. Likewise, reduced functional interaction of the precuneus with the adjacent paracentral lobule was found to be related to the release of unmeant SI. The precuneus integrates oculomotor control and plays an essential role in a broad variety of 'highly integrated tasks' including visuospatial imagery (Cavanna and Trimble 2006), and its attribution to oculomotor control receives further evidence from a recent fMRI study by Jamadar and colleagues (Jamadar et al. 2013). These authors reported activations in several cerebral regions including the precuneus in the anti-saccade task compared to pro-saccades. In addition, the authors reported activations in parts of the limbic system comprising the anterior cingulate cortex and the insular cortex. The functional decoupling of the anterior cingulate and the insula might result in a higher SI rate. In oculomotor inhibition demanding tasks such as anti-saccades, the anterior cingulate cortex is critical in error monitoring and preparation for subsequent saccades (Brown et al. 2007, Pa et al. 2014). Accordingly, monitoring oculomotor consequence may also be critical during fixational periods in VGRS when the subject is awaiting the next stimulus. The parietal eye fields were demonstrated to contribute to a higher presence of SI when iFC decreases. This finding is in agreement with the direct role of the parietal eye fields saccade programming (Leigh and Zee 2006), thus, impaired functional communication of the parietal eye fields with other portions of the respective ICNS in a sense of 'false saccade programming' may cause the release of unwanted SI. The parietal cortex is important for shifts of visual attention and has emerged as a relevant interface in integrating multiple sensory signals (Leigh and Zee 2006, Ptak and Muri 2013). This is in general agreement with the demonstrated association of hypometric saccades in the VGRS task and a decrease of parietal iFC. Unwanted gaze shifts as measured by delayed- and anti-saccades were found to increase when iFC of bilateral superior frontal areas decrease in PD patients. Both clusters localized in the DMN confirmed the role of the DMN in higher cognitive functions (Buckner et al. 2008). Nota bene, the DLPFC as part of the frontoparietal ICN was found to be associated with SI during VGRS. Its role concerning inhibition control of unwanted gaze shifts has been consistently described in may studies (Munoz and Everling 2004, Pierrot-Deseilligny et al. 2005, Jamadar et al. 2013, Pa et al. 2014).

The impaired ability in PD to track a single-dot smoothly was found to be related to iFC decreases in the dorsal and ventral attention systems as well as in the visuospatial network. The functional integrity of visual areas V5/MT is crucial for priming the motion direction (Campana et al. 2006, Pavan et al. 2013) and was reported to be a pivotal feature of the visuospatial network (Laird et al. 2011). Although the functional integration of the visuospatial network was not observed to be altered in PD patients, the covariance analysis indicated that decreased iFC of both, the extrastriate cortex and the precuneus, was associated with a higher occurrence of anticipatory saccades disrupting SPEM. This is consistent with an increasing incidence of SI during VGRS task when the precuneus becomes functionally disconnected as demonstrated in this study. Moreover, decreased iFC of the insula was also found to be associated with a higher SI rate supporting the notion that the insular cortex is involved in multiple cognitive domains including eye movement control (Morel et al. 2013). The insular cortex appears also involved in SPEM performance, since decreased iFC in bilateral insular cortices was found to be closely linked to higher occurrence of anticipatory saccades interrupting SPEM in PD. As outlined for the iFC correlate of SI, the parietal eye fields and the anterior portion of the cingulate cortex may implicate undesired saccades. Likewise, decreased iFC in both the cingulate gyrus and the parietal eye field were found to reflect a higher incidence of anticipatory saccades that intrude SPEM in PD. Decreased striato-cerebellar iFC may be associated with impaired SPEM, notably, the cerebellum is spared for the PD-associated pathological process whereas a loss of dopaminergic cells within the nigrostrial system has been frequently considered to be a hallmark of PD (Braak et al. 2003, Braak and Del Tredici 2009). Besides the angular gyrus, the superior temporal gyrus was the second brain region found in the covariance analysis that is not typically concerned with oculomotion. The superior temporal gyrus has reported to be relevant in visual and emotional processing of faces (Radua et al. 2010) but also appears to be attributable to SPEM performance in PD. Together with the regions linked to facilitate the unwanted release of SI, it bears striking evidence for the impression that the observed SPEM disturbances in PD are caused by attentional deficits rather than by the loss of the ability to perform perfect pursuit (Pinkhardt et al. 2012). Further support for this statement emerges from the consistent observation that PD patients are fairly able to track a continuously moving target smoothly

despite of their disease state. In conclusion, a higher incidence of SI during both SPEM and fixational periods of VGRS points towards an impaired functional interaction between broadly distributed cerebral regions.

### 4.3.3 Evidence for Large-Scale Distributed Oculomotor Networks

The covariance analysis of functional integrity and oculomotor performance in PD patients as the focus in this study supported that oculomotor control results from many large-scale distributed networks across the whole brain. As expected, major relais of eye movement control such as FEF or the basal ganglia revealed no significant clusters in the covariance analysis in PD patients. These regions have been consistently reported to be crucially involved in several forms of eye movement control (Grosbras et al. 1999, Dieterich et al. 2009, Purcell et al. 2012, Jamadar et al. 2013, Bosch et al. 2013, Pa et al. 2014) and are parts of complex intertwined oculomotor networks. Both, the FEF and the striatum are major hubs of their corresponding ICN and were defined as seed-regions. Thus, the observed cluster in the covariance analysis in PD patients revealed decreased iFC with respect to their corresponding seed-region which in turn may cause the development of impaired oculomotor control. PD-related pathology progresses in a remarkably predictable manner and may target successively important structures associated with oculomotor control (Braak and Del Tredici 2009). These structures can be seen as hubs of oculomotor networks that functionally interact together. Damage to specific hubs caused by PD-related pathology leads to disturbed topological organization of brain networks that in turn may presented as lack of oculomotor attentional control to finally resulting in overall cognitive decline as more hubs become functionally decoupled from their respective network.

In our pilot study we have demonstrated the relationship between altered eye movements in PD, in particular, the saccadic accuracy gain and the associations with iFC measures within the DMN (Gorges et al. 2013). This pilot study at 1.5 T in a smaller sample and restricted to the DMN formed the bases for the present investigations. Together with the oculomotor findings, it was shown that pathological alterations in PD-Cu patients manifested preferentially in cognitive demanding oculomotor tasks such as anti-saccades. For instance, testing attentional control by means of VOG has been proposed as a

promising procedure (Munoz and Everling 2004) and might also be sensitive to detect possible age-related alterations in the elderly (Pa et al. 2014, Bowling et al. 2014). This leads to the conclusion that the oculomotor system, preferentially the parts responsible for higher functions, appear to be more vulnerable than global cognition. Notably, no significant oculomotor abnormalities appear to be present in presymptomatic patients with Parkin gene mutations whereas symptomatic Parkin-linked compared with early-onset PD patients may presented with different oculomotor dysfunctions (Machner et al. 2010). Although there appears to be no obvious preclinical oculomotor biomarker in PD yet, the results emphasize oculomotor testing with focus on executive control (e.g. anti-saccades, SI during fixation in VGRS) as a promising early biomarker for executive dysfunctions that might be followed by cognitive decline leading to PD-MCI. This conclusion is in agreement with a recent study by Pa and co-workers (Pa et al. 2014) and could be of impact for developing new diseases or neuroprotective therapeutic strategies in order to delay or ultimately prevent non-motor features in PD such as the burdensome cognitive impairment (Olanow and Lang 2011).

## 4.4 Limitations of the Study

### 4.4.1 Parkinson's Disease Patients and Healthy Controls

The study is limited by the relatively small size of PD patients and control subjects. However, this limitation is partly caused by the quality control of the phenotype definition including the broad spectrum of clinical, neuropsychological, oculomotor and imaging assessment, which in turn can be considered as a strength of the investigations. Larger sample sizes in PD patients may permit covariance analysis within the subgroups, i.e. correlations between oculomotor performance and iFC measures. Moreover, larger sample sizes in PD-D patients may allow to distinguish a third subgroup which also might be of great interest to study iFC alterations underlying the development of PD-D.

Another limitation refers to the subject's education level where the control group presented higher educated compared to the PD patients. The level of education is generally associated with a higher cognitive reserve and is thought to provide the ability to recruit additional resources to compensate for brain damage (Stern 2002). The possible effect of

cognitive reserve for both patients groups (PD-CI, PD-Cu) was not regressed out in this study. A higher brain reserve capacity may accompany intellectual performance that in turn was reported to be associated with an increased functional integration based on more efficient utilization of brain networks (van den Heuvel et al. 2009). Thus the effect of subject groups not matched for education may lead to somewhat distinct effects when assessing the iFC of the human brain. In PD, it remains an open issue how the brain responds to the pathological spreading in order to maintain cognitive performance by recruiting additional resources. Higher myelinated and more pronounced bundles of fiber tracts become less vulnerable to the selective PD-associated pathological process (Braak et al. 2004), hence, it might be possible to speculated about the impact of the education level on iFC.

### 4.4.2 Antiparkinsonian Treatment Influences Functional Connectivity and may slightly Improve Oculomotor Performance Preferential in an Early-State

The patients in this study were all medicated and the possible role of antiparkinsonian treatment was not disentangled. Deep-brain stimulation of the subthalamic nucleus as a surgical antiparkinsonian therapy improves motor deficits (Okun 2013) and PD patients in an early disease state tend to benefit more from deep-brain stimulation than more severely affected cases (Schuepbach et al. 2013). However, the benefit for oculomotor performance, in particular reflexive saccade performance, appears to be of no effect (Pinkhardt et al. 2012) or little effect (Yugeta et al. 2010). One explanation for these discrepancies could emerge from the different PD patients' motor symptom manifestation assuming that motor performance progressively worsens during the course of PD and later stages are accompanied by cognitive difficulties when cortical regions become involved (Braak et al. 2005, Braak and Del Tredici 2009).

As demonstrated in this study, decreased functional integrity of the superior parietal lobule within the right frontoparietal control network may contribute to reduced saccadic accuracies in PD and PD-CI patients. In accordance with these findings, hypometric saccades appear to be associated with functional alterations within the DMN in non-demented PD patients (Gorges et al. 2013). Taken together, this may prompt the assumption that saccadic accuracy can be partly improved by deep-brain stimulation in an

early disease stage when cortical contribution is less pronounced. However, when widespread cortical involvement cause abnormal functional interaction in cortical networks, improper saccadic accuracy emerges more likely despite of antiparkinsonian treatment such as deep-brain stimulation. The effects of deep-brain stimulation in terms of cognitively demanding oculomotor tasks such as anti-saccades or SI have not been systematically investigated yet. Some benefit in inhibitory control of eye movements has been reported (Yugeta et al. 2010) that is ascribed to compensatory mechanisms on the functional integration of the SC conveyed by substantia nigra pars reticulata; however, the impact of deep-brain stimulation on SI rates currently unknown. As indicated by this study, SI appear to be mainly attributed to the cognitive domain in PD.

Several iFCMRI studies (Wu et al. 2009b, Krajcovicova et al. 2012, Hacker et al. 2012, Jech et al. 2013) investigated the effects of dopamine substitution (e.g. L-DOPA) by contrasting PD patients in ON vs. OFF-medication state and reported consistently significant effects. In a comprehensive review on iFCMRI in PD, antiparkinsonian treatment was deescribed to have a significant effect on iFC (Prodoehl et al. 2014). In particular, iFC increased in ON-state. The hyper-connectivity in the present study may possibly facilitated from dopamine substitution rather than compensatory mechanisms (Wu et al. 2009a, 2009b, 2010, 2011). However, each of the aforementioned studies incorporated only a few ICNs and did not investigated PD patients without cognitive deficits. Hence, the observed hyper-connectivity in seven out of ten investigated ICNs in PD patients free of cognitive deficits may also be in line with adaptive changes as found in other neurodegenerative conditions such as AD (Mevel et al. 2011). The cerebellum which is almost resistant to develop PD pathology (Braak and Del Tredici 2009) appears to contribute to compensatory mechanisms beyond dopaminergic medication in order to maintain motor and non-motor functions (Wu and Hallett 2013). These aspects underpin the present results demonstrating increased iFC within the ventral attention ICN, in particular large parts of the cingulate gyrus, the cerebellum, the thalamus and ventral striatum. Moreover, it appears that antiparkinsonian medication is not able to completely compensate neuronal cell loss in advanced disease stages in the sense of maintained iFC (Hacker et al. 2012) as indicated by the current results. It is reasonable to interpret the hyper-connectivity state in cortical ICNs such as the DMN or frontoparietal networks in PD patients without cognitive problems as

an attempt to compensate pathological changes. It remains an open issue to comprehensively explain to what extent antiparkinsonian treatment, in particular dopaminergic medication, contribute to iFC alterations.

## 4.5 Conclusions and Outlook

The PD-specific oculomotor phenotype in cognitively impaired and unimpaired PD patients indicates the preserved ability to (i) perform (short-term) perfect smooth pursuit and to (ii) generate saccades with inconspicuous amplitude and proper peak eye velocity. Thus, oculomotor abnormalities in PD are preferentially dysfunctions attributed to a lack of attentional control rather than compromised oculomotor nuclei in the brainstem. The oculomotor nuclei appear to be spared by the PD-related pathological process. Impaired eye movement control already manifested in PD-Cu patients which indicated subtle deficits in executive control that are not detectable by neuropsychological investigation tools.

The cognitively unimpaired status in PD appears to be characterized by widespread increased iFC (hyper-connectivity) that can be considered as the initial sign of altered brain function preceding manifest cognitive deficits. The PD-related pathological process in cognitively unimpaired patients resulted in global topographical remapping of higher function networks. This reorganization could be interpreted as the concept of compensatory mechanisms, i.e. an attempt to maintain cognitive performance as long as possible. Decreased iFC in PD-CI patients, preferentially found in structures related to the DMN, along the midline cores and the hippocampus, appears to indicate a hallmark in iFCMRI for cognitive deficits that may gradually lead to PD-associated dementia.

The covariance analysis revealed that oculomotor performance worsened with disease progression parallel with decreasing iFC. The demonstrated cluster were found in cortical, limbic and brainstem ICNs and encompassed regions which have been consistently reported to be closely related to oculomotor control. However, the superior temporal gyrus and the angular gyrus were also demonstrated to be involved in oculomotor control by their functional interaction with other hubs in oculomotor networks. In PD, a higher incidence of SI may result from decreased iFC of the superior temporal and angular gyrus

within their ICNs. These findings are in agreement with the impression of contributing PD-related pathological mechanisms far beyond the dopaminergic system.

The results presented in this study provide motivation for future studies in PD utilizing complementary video-oculography and iFCMRI as promising non-invasive investigation tools. Such studies might include the identification of different PD-stages on the basis of brain connectivity reflecting the cognitive and oculomotor dysfunctions experienced by PD patients. Models of functional and structural integration in the human brain may enhance pathophysiological understanding of PD in the future by exploiting the nature of intrinsic information flow in cerebral task-associated networks combined with the quantifiable objective measure of eye movements. The development of new *in-vivo* imaging and video-oculographic surrogate markers, or possible preclinical biomarkers is of potentially greater interest. This might form the basis in order to contribute to the design of new therapeutic strategies aiming at modifying the course of the disorder or to ultimately preventing neuronal cell degeneration in PD.

# 5. Summary

Parkinson's disease (PD) is a common movement disorder characterized by a multifaceted clinical spectrum including the well-known motor dysfunctions together with non-motor signs. The pathological process underlying PD spreads from the lower brainstem to the basal ganglia and limbic structures towards the neo-cortex in a topographically predictable manner. Cognitive decline is a burdensome and medication resistant non-motor feature experienced by PD patients; another non-motor aspect comprised disturbed eye movement control with its hallmark in rapid gaze shifts (saccades) interrupting smooth pursuit as well as hypometric reflexive saccades. It remains an open issue to what extent oculomotor deficits are caused by impaired functionally intertwined cerebral networks. Intrinsic functional connectivity (iFC) as assessed by 'resting-state' imaging techniques has indicated alterations in several brain networks in PD previously. The current bimodal study by intrinsic functional connectivity magnetic resonance imaging (iFCMRI) and video-oculography aimed at investigating the influence of cognitive decline in PD depending on (i) the oculomotor performance and (ii) the functional interaction within defined intrinsic connectivity networks. The primary aim was to identify possible relationships between oculomotor dysfunctions and iFC in PD patient that span the cognitive range from unimpaired to PD-associated dementia.

Video-oculography and iFCMRI data from three groups of subjects were used for the analysis: According to detailed neuropsychological assessment, group I included cognitively unimpaired (*N*=14), group II included cognitively impaired PD patients (*N*=17), and group III included age-matched healthy controls (*N*=22). All groups were contrasted with each other for both VOG and iFCMRI modality. PD patients were pooled from both patients groups in order to covariate oculomotor parameters with iFC measures. The oculomotor tasks as measured by means of EyeLink® I comprised smooth pursuit, reflexive saccades and executive control testing (e.g. anti-saccades). The iFCMRI data were acquired at a 3 Tesla scanner (Siemens Magnetom Allegra, 200 vol., 36 slices, 64x64 pixels, slice thickness 3.5 mm, pixel size 3.5 mm x 3.5 mm, *TR*=2.2 s, *TE*=30 ms).

Oculomotor performance depended only in few aspects (inhibition control, saccadic intrusion rate) on the cognitive status. Hence, the broad spectrum of oculomotor deficits manifested already in cognitively unimpaired PD patients (compared with controls). With an exception of the cerebellar and visuospatial intrinsic connectivity networks, the other identified networks were significantly altered in that iFC was increased in cognitively unimpaired and decreased in cognitively impaired patients (each compared with controls). The covariance analysis revealed significant correlations between oculomotor parameters (pursuit and saccadic gain, saccadic intrusion and error rate) and iFC measures, i.e. the worse the oculomotor performance in PD was the more the regional iFC was decreased.

Oculomotor performance worsened with disease progression parallel with decreasing iFC in cortical, limbic and brainstem networks. In PD, dysfunctional oculomotor control is most likely caused by executive deficits rather than compromised oculomotor nuclei in the brainstem. These findings are in agreement with the assumption of contributing PD-related pathological mechanisms beyond the dopaminergic system. The increase in iFC might be the initial manifestation of altered brain function in the sense of adaptive (compensatory) changes preceding neuropsychological assessable cognitive deficits. Together with the lack of attentional oculomotor control, increased iFC in cognitively unimpaired PD patients may be considered an early functional correlate of developing PD-associated cognitive decline. A loss of functional connectivity may be attributed to the development of cognitive deficits in PD. Future studies may also incorporate structural connectivity in order to further guide in the development of *in-vivo* (imaging or video-oculographic) surrogate progression markers which, in turn, could constitute the design of new therapeutic concepts in PD.

# 6. References


1 Abadi, R. V., and E. Gowen. 2004. Characteristics of saccadic intrusions. *Vision R*es. 44:2675–2690.

2 Achard, S., and E. Bullmore. 2007. Efficiency and cost of economical brain functional networks. *PLoS Comput. Bio*l. 3:e17.

3 Agosta, F., E. Canu, E. Stefanova, L. Sarro, A. Tomic, V. Spica, G. Comi, V. S. Kostic, and M. Filippi. 2014. Mild cognitive impairment in Parkinson's disease is associated with a distributed pattern of brain white matter damage. *Hum Brain Mapp* 35:1921–1929.

4 Akhtar, R. S., and M. B. Stern. 2012. New concepts in the early and preclinical detection of Parkinson's disease: therapeutic implications. *Expert Rev Neurother* 12:1429–1438.

5 Altman, N. S. 1992. An Introduction to Kernel and Nearest-Neighbor Nonparametric Regression. *Am Stat* 46:175–185.

6 Anderson, C. H., D. C. Essen, and B. A. Olshausen. 2004. Directed Visual Attention and the Dynamic Control of Information Flow. PP. 11-17 *in* Encyclopedia of Visual Attention. L. Itti, G. Rees, and J. Tsotsos, editors. *Academic Press/Elsevier*. London.

7 Anderson, T. J., and M. R. MacAskill. 2013. Eye movements in patients with neurodegenerative disorders. *Nat Rev Neurol* 9:74–85.

8 Andrews-Hanna, J. R., J. S. Reidler, J. Sepulcre, R. Poulin, and R. L. Buckner. 2010. Functional-anatomic fractionation of the brain's default network. *Neuron* 65:550–562.

9 Ashby, F. G. 2011. Statistical Analysis of FMRI Data. PP. 1-332. 1st edition. *Cambridge*, *Mass.: MIT Press*. Cambridge (Massachusetts) and London.

10 Balzer-Geldsetzer, M., A. S. Costa, M. Kronenburger, J. B. Schulz, S. Roske, A. Spottke, U. Wullner, T. Klockgether, A. Storch, C. Schneider, O. Riedel, H. U. Wittchen, C. Seifried, R. Hilker, N. Schmidt, K. Witt, G. Deuschl, B. Mollenhauer, C. Trenkwalder, I. Liepelt-Scarfone, S. Graber-Sultan, D. Berg, T. Gasser, E. Kalbe, M. Bodden, W. H. Oertel, and R. Dodel. 2011. Parkinson's disease and dementia: a longitudinal study (DEMPARK). *Neuroepidemiology* 37:168–176.

11 Baudrexel, S., T. Witte, C. Seifried, F. von Wegner, F. Beissner, J. C. Klein, H. Steinmetz, R. Deichmann, J. Roeper, and R. Hilker. 2011. Resting state fMRI reveals increased subthalamic nucleus-motor cortex connectivity in Parkinson's disease. *Neuroimage* 55:1728–1738.

12 Becker, W. 1989. The neurobiology of saccadic eye movements. Metrics. *Rev Oculomot Res* 3:13–67.

13 Beckmann, C. F., M. DeLuca, J. T. Devlin, and S. M. Smith. 2005. Investigations into resting-state connectivity using independent component analysis. *Philos Trans R Soc Lond B Biol Sci* 360:1001–1013.

14 Biswal, B. B. 2012. Resting state fMRI: a personal history. *Neuroimage* 62:938–944.

15 Biswal, B. B., M. Mennes, X. N. Zuo, S. Gohel, C. Kelly, S. M. Smith, C. F. Beckmann, J. S. Adelstein, R. L. Buckner, S. Colcombe, A. M. Dogonowski, M. Ernst, D. Fair, M. Hampson, M. J. Hoptman, J. S. Hyde, V. J. Kiviniemi, R. Kotter, S. J. Li, C. P. Lin, M. J. Lowe, C. Mackay, D. J. Madden, K. H. Madsen, D. S. Margulies, H. S. Mayberg, K. McMahon, C. S. Monk, S. H. Mostofsky, B. J. Nagel, J. J. Pekar, S. J. Peltier, S. E. Petersen, V. Riedl, S. A. Rombouts, B. Rypma, B. L. Schlaggar, S. Schmidt, R. D. Seidler, G. J. Siegle, C. Sorg, G. J. Teng, J. Veijola, A. Villringer, M. Walter, L. Wang, X. C. Weng, S. Whitfield-Gabrieli, P. Williamson, C. Windischberger, Y. F. Zang, H. Y. Zhang, F. X. Castellanos, and M. P. Milham. 2010. Toward discovery science of human brain function. *Proc. Natl. Acad. Sci. U.S.A.* 107:4734–4739.

16 Biswal, B., F. Z. Yetkin, V. M. Haughton, and J. S. Hyde. 1995. Functional connectivity in the motor cortex of resting human brain using echo-planar MRI. *Magn Reson Med* 34:537–541.

17 Bosch, S. E., S. F. Neggers, and S. Van der Stigchel. 2013. The role of the frontal eye fields in oculomotor competition: image-guided TMS enhances contralateral target selection. *Cereb. Cortex* 23:824–832.

18 Bowling, A. C., P. Lindsay, B. G. Smith, and K. Storok. 2014. Saccadic eye movements as indicators of cognitive function in older adults. *Neuropsychol Dev Cogn B Aging Neuropsychol Cogn* (in press). doi:10.1080/13825585.2014.901290

19 Braak, H., and K. Del Tredici. 2009. Neuroanatomy and pathology of sporadic Parkinson's disease. *Adv Anat Embryol Cell Biol* 201:1–119.

20 Braak, H., K. Del Tredici, U. Rub, R. A. de Vos, E. N. Jansen Steur, and E. Braak. 2003. Staging of brain pathology related to sporadic Parkinson's disease. *Neurobiol. Aging* 24:197–211.

21 Braak, H., E. Ghebremedhin, U. Rub, H. Bratzke, and K. Del Tredici. 2004. Stages in the development of Parkinson's disease-related pathology. *Cell Tissue Res.* 318:121–134.

22 Braak, H., C. M. Müller, U. Rub, H. Ackermann, H. Bratzke, R. A. de Vos, and K. Del Tredici. 2006. Pathology associated with sporadic Parkinson's disease–where does it end? *J. Neural Transm. Suppl.*:89–97.

23 Braak, H., U. Rub, E. N. Jansen Steur, K. Del Tredici, and R. A. de Vos. 2005. Cognitive status correlates with neuropathologic stage in Parkinson disease. *Neurology* 64:1404–1410.

24 Brett, M., I. S. Johnsrude, and A. M. Owen. 2002. The problem of functional localization in the human brain. *Nat. Rev. Neurosci.* 3:243–249.

25 Brodmann, K. 1909. Vergleichende Lokalisationslehre der Großhirnrinde in ihren Prinzipien dargestellt auf Grund des Zellenbaues. Johann Ambrosius Barth, Leipzig.

26 Brookes, M. J., M. Woolrich, H. Luckhoo, D. Price, J. R. Hale, M. C. Stephenson, G. R. Barnes, S. M. Smith, and P. G. Morris. 2011. Investigating the electrophysiological basis of resting state networks using magnetoencephalography. *Proc. Natl. Acad. Sci. U.S.A.* 108:16783–16788.

27 Brown, M. R., T. Vilis, and S. Everling. 2007. Frontoparietal activation with preparation for antisaccades. *J. Neurophysiol.* 98:1751–1762.

28 Buckner, R. L. 2010. Human functional connectivity: new tools, unresolved questions. *Proc. Natl. Acad. Sci. U.S.A.* 107:10769–10770.

29 Buckner, R. L., J. R. Andrews-Hanna, and D. L. Schacter. 2008. The brain's default network: anatomy, function, and relevance to disease. *Ann. N. Y. Acad. Sci.* 1124:1–38.

30 Buckner, R. L., F. M. Krienen, and B. T. Yeo. 2013. Opportunities and limitations of intrinsic functional connectivity MRI. *Nat. Neurosci.* 16:832–837.

31 Buckner, R. L., A. Z. Snyder, B. J. Shannon, G. LaRossa, R. Sachs, A. F. Fotenos, Y. I. Sheline, W. E. Klunk, C. A. Mathis, J. C. Morris, and M. A. Mintun. 2005. Molecular, structural, and functional characterization of Alzheimer's disease: evidence for a

relationship between default activity, amyloid, and memory. *J. Neurosci.* 25:7709–7717.

32 Campana, G., A. Cowey, and V. Walsh. 2006. Visual area V5/MT remembers "what" but not "where". *Cereb. Cortex* 16:1766–1770.

33 Cavanna, A. E., and M. R. Trimble. 2006. The precuneus: a review of its functional anatomy and behavioural correlates. *Brain* 129:564–583.

34 Chambers, J. M., and T. J. Prescott. 2010. Response times for visually guided saccades in persons with Parkinson's disease: a meta-analytic review. *Neuropsychologia* 48:887–899.

35 Chan, F., I. T. Armstrong, G. Pari, R. J. Riopelle, and D. P. Munoz. 2005. Deficits in saccadic eye-movement control in Parkinson's disease. *Neuropsychologia* 43:784–796.

36 Chao-Gan, Y., and Z. Yu-Feng. 2010. DPARSF: A MATLAB Toolbox for "Pipeline" Data Analysis of Resting-State fMRI. *Front Syst Neurosci* 4:13.

37 Chaudhuri, K. R., P. Odin, A. Antonini, and P. Martinez-Martin. 2011. Parkinson's disease: the non-motor issues. *Parkinsonism Relat. Disord.* 17:717–723.

38 Choi, E. Y., B. T. Yeo, and R. L. Buckner. 2012. The organization of the human striatum estimated by intrinsic functional connectivity. *J. Neurophysiol.* 108:2242–2263.

39 Clarke, D. D., and L. Sokoloff. 1999. Circulation and Energy Metabolism of the Brain. PP. 637-670 *in* Basic Neurochemistry. Siegel GJ, Agranoff BW, Alberts RW, et al., editors., 6th edition. *Lippincott-Raven.* Philadelphia.

40 Cole, D. M., S. M. Smith, and C. F. Beckmann. 2010. Advances and pitfalls in the analysis and interpretation of resting-state FMRI data. *Front Syst Neurosci* 4:8.

41 Conover, W. J., and R. L. Iman. 1981. Rank Transformations as a Bridge Between Parametric and Nonparametric Statistics. *Am Stat* 35:124–129.

42 Damoiseaux, J. S., C. F. Beckmann, E. J. Arigita, F. Barkhof, P. Scheltens, C. J. Stam, S. M. Smith, and S. A. Rombouts. 2008. Reduced resting-state brain activity in the "default network" in normal aging. *Cereb. Cortex* 18:1856–1864.

43 Damoiseaux, J. S., and M. D. Greicius. 2009. Greater than the sum of its parts: a review of studies combining structural connectivity and resting-state functional connectivity. *Brain Struct Funct* 213:525–533.

44 Del Tredici, K., U. Rub, R. A. De Vos, J. R. Bohl, and H. Braak. 2002. Where does parkinson disease pathology begin in the brain? *J. Neuropathol. Exp. Neurol.* 61:413–426.

45 Di, X., S. Gohel, E. H. Kim, and B. B. Biswal. 2013. Task vs. rest-different network configurations between the coactivation and the resting-state brain networks. *Front Hum Neurosci* 7:493.

46 Di Martino, A., A. Scheres, D. S. Margulies, A. M. Kelly, L. Q. Uddin, Z. Shehzad, B. Biswal, J. R. Walters, F. X. Castellanos, and M. P. Milham. 2008. Functional connectivity of human striatum: a resting state FMRI study. *Cereb. Cortex* 18:2735–2747.

47 Dieterich, M., S. Müller-Schunk, T. Stephan, S. Bense, K. Seelos, and T. A. Yousry. 2009. Functional magnetic resonance imaging activations of cortical eye fields during saccades, smooth pursuit, and optokinetic nystagmus. *Ann. N. Y. Acad. Sci.* 1164:282–292.

48 Dirnberger, G., and M. Jahanshahi. 2013. Executive dysfunction in Parkinson's disease: a review. *J Neuropsychol* 7:193–224.

49 Donaghy, C., R. Pinnock, S. Abrahams, C. Cardwell, O. Hardiman, V. Patterson, R. C. McGivern, and J. M. Gibson. 2009. Ocular fixation instabilities in motor neurone disease. A marker of frontal lobe dysfunction? *J. Neurol.* 256:420–426.

50 Douaud, G., N. Filippini, S. Knight, K. Talbot, and M. R. Turner. 2011. Integration of structural and functional magnetic resonance imaging in amyotrophic lateral sclerosis. *Brain* 134:3470–3479.

51 Edwards, M. J., and K. P. Bhatia. 2011. Other Non-Motor Symptoms of Parkinson's Disease. PP. 387–393 *in* Parkinson's Disease: Non-Motor and Non-Dopaminergic Features. C. W. Olanow, F. Stocchi, and A. E. Lang, editors. *John Wiley & Sons*. New Delhi.

52 Emre, M., D. Aarsland, R. Brown, D. J. Burn, C. Duyckaerts, Y. Mizuno, G. A. Broe, J. Cummings, D. W. Dickson, S. Gauthier, J. Goldman, C. Goetz, A. Korczyn, A. Lees, R. Levy, I. Litvan, I. McKeith, W. Olanow, W. Poewe, N. Quinn, C. Sampaio, E. Tolosa, and B. Dubois. 2007. Clinical diagnostic criteria for dementia associated with Parkinson's disease. *Mov. Disord.* 22:1689–1707.

53 Fahn, S., and R. L. Elton. 1987. UPDRS Development Committee. The Unified Parkinson's Disease Rating Scale. *Recent Developments in Parkinson's Disease*:153–163, 293–304.

54 Fazekas, F., J. B. Chawluk, A. Alavi, H. I. Hurtig, and R. A. Zimmerman. 1987. MR signal abnormalities at 1.5 T in Alzheimer's dementia and normal aging. *AJR Am J Roentgenol* 149:351–356.

55 Filippi, M., M. P. van den Heuvel, A. Fornito, Y. He, H. E. Hulshoff Pol, F. Agosta, G. Comi, and M. A. Rocca. 2013. Assessment of system dysfunction in the brain through MRI-based connectomics. *Lancet Neurol* 12:1189–1199.

56 Folstein, M. F., S. E. Folstein, and P. R. McHugh. 1975. Mini-mental state". A practical method for grading the cognitive state of patients for the clinician. *J Psychiatr Res* 12:189–198.

57 Fox, M. D., A. Z. Snyder, J. L. Vincent, M. Corbetta, D. C. Van Essen, and M. E. Raichle. 2005. The human brain is intrinsically organized into dynamic, anticorrelated functional networks. *Proc. Natl. Acad. Sci. U.S.A.* 102:9673–9678.

58 Fox, M. D., D. Zhang, A. Z. Snyder, and M. E. Raichle. 2009. The global signal and observed anticorrelated resting state brain networks. *J. Neurophysiol.* 101:3270–3283.

59 Friman, O., M. Borga, P. Lundberg, and H. Knutsson. 2004. Detection and detrending in fMRI data analysis. *Neuroimage* 22:645–655.

60 Friston, K. J. 2011. Functional and effective connectivity: a review. *Brain Connect* 1:13–36.

61 Fukushima, K., J. Fukushima, T. Warabi, and G. R. Barnes. 2013. Cognitive processes involved in smooth pursuit eye movements: behavioral evidence, neural substrate and clinical correlation. *Front Syst Neurosci* 7.

62 Gaymard, B., S. Rivaud, J. F. Cassarini, T. Dubard, G. Rancurel, Y. Agid, and C. Pierrot-Deseilligny. 1998. Effects of anterior cingulate cortex lesions on ocular saccades in humans. *Exp Brain Res* 120:173–183.

63 Genovese, C. R., N. A. Lazar, and T. Nichols. 2002. Thresholding of statistical maps in functional neuroimaging using the false discovery rate. *Neuroimage* 15:870–878.

64 Gilbert, C. D. 2013. The Constructive Nature of Visual Processing. PP. 556–576 *in* Principles of Neural Science. James H. Schwartz, Thomas M. Jessell, Steven A. Siegelbaum, Eric R. Kandel editor. 5th edition. *McGraw-Hill*. New York.

65 Gilbert, S. J., I. Dumontheil, J. S. Simons, C. D. Frith, and P. W. Burgess. 2007. Comment on "Wandering minds: the default network and stimulus-independent thought. *Science* 317:43; author reply 43.

66 Gohel, S. R., and B. B. Biswal. 2014. Functional integration between brain regions at 'rest' occurs in multiple-frequency bands. *Brain Connect* (in press). doi:10.1089/brain.2013.0210

67 Goldberg, M. E., and M. F. Walker. 2013. The Control of Gaze. PP. 894–916 *in* Principles of Neural Science. James H. Schwartz, Thomas M. Jessell, Steven A. Siegelbaum, Eric R. Kandel, editor. 5th edition. McGraw-Hill, USA, New York.

68 Gorges, M., H. P. Müller, D. Lule, A. C. Ludolph, E. H. Pinkhardt, and J. Kassubek. 2013. Functional connectivity within the default mode network is associated with saccadic accuracy in Parkinson's disease: a resting-state FMRI and videooculographic study. *Brain Connect* 3:265–272.

69 Gorges, M., H.-P. Müller, A. C. Ludolph, V. Rasche, and J. Kassubek. 2014a. Intrinsic functional connectivity networks in healthy elderly subjects: a multiparametric approach with structural connectivity analysis. *Biomed Res Int* (accepted for publication). http://www.hindawi.com/journals/bmri/aip/947252

70 Gorges, M., E. H. Pinkhardt, and J. Kassubek. 2014b. Alterations of Eye Movement Control in Neurodegenerative Movement Disorders. *J Ophthalmol* (in press). doi:10.1155/2014/658243

71 Greicius, M. D., B. Krasnow, A. L. Reiss, and V. Menon. 2003. Functional connectivity in the resting brain: a network analysis of the default mode hypothesis. *Proc. Natl. Acad. Sci. U.S.A.* 100:253–258.

72 Greicius, M. D., G. Srivastava, A. L. Reiss, and V. Menon. 2004. Default-mode network activity distinguishes Alzheimer's disease from healthy aging: evidence from functional MRI. *Proc. Natl. Acad. Sci. U.S.A.* 101:4637–4642.

73 Greicius, M. D., K. Supekar, V. Menon, and R. F. Dougherty. 2009. Resting-state functional connectivity reflects structural connectivity in the default mode network. *Cereb. Cortex* 19:72–78.

74 Grosbras, M. H., E. Lobel, P. F. Van de Moortele, D. LeBihan, and A. Berthoz. 1999. An anatomical landmark for the supplementary eye fields in human revealed with functional magnetic resonance imaging. *Cereb. Cortex* 9:705–711.

75 Hacker, C. D., J. S. Perlmutter, S. R. Criswell, B. M. Ances, and A. Z. Snyder. 2012. Resting state functional connectivity of the striatum in Parkinson's disease. *Brain* 135:3699–3711.

76 Hall, E. L., S. E. Robson, P. G. Morris, and M. J. Brookes. 2013. The relationship between MEG and fMRI. *Neuroimage* (in press). doi:10.1016/j.neuroimage.2013.11.005

77 He, Y., L. Wang, Y. Zang, L. Tian, X. Zhang, K. Li, and T. Jiang. 2007. Regional coherence changes in the early stages of Alzheimer's disease: a combined structural and resting-state functional MRI study. *Neuroimage* 35:488–500.

78 Heine, L., A. Soddu, F. Gomez, A. Vanhaudenhuyse, L. Tshibanda, M. Thonnard, V. Charland-Verville, M. Kirsch, S. Laureys, and A. Demertzi. 2012. Resting state networks and consciousness: alterations of multiple resting state network connectivity in physiological, pharmacological, and pathological consciousness States. *Front Psychol* 3:295.

79 Helmich, R. C., L. C. Derikx, M. Bakker, R. Scheeringa, B. R. Bloem, and I. Toni. 2010. Spatial remapping of cortico-striatal connectivity in Parkinson's disease. *Cereb. Cortex* 20:1175–1186.

80 Hely, M. A., W. G. Reid, M. A. Adena, G. M. Halliday, and J. G. Morris. 2008. The Sydney multicenter study of Parkinson's disease: the inevitability of dementia at 20 years. *Mov. Disord.* 23:837–844.

81 Hikosaka, O., and R. H. Wurtz. 1989. The basal ganglia. Rev Oculomot Res 3:257–281.

82 Holmes, C. J., R. Hoge, L. Collins, R. Woods, A. W. Toga, and A. C. Evans. 1998. Enhancement of MR images using registration for signal averaging. *J Comput Assist Tomogr* 22:324–333.

83 Hughes, A. J., S. E. Daniel, L. Kilford, and A. J. Lees. 1992. Accuracy of clinical diagnosis of idiopathic Parkinson's disease: a clinico-pathological study of 100 cases. *J. Neurol. Neurosurg. Psychiatr.* 55:181–184.

84 Hyndman, R. J., and Y. Fan. 1996. Sample Quantiles in Statistical Packages. *Am Stat* 50:361–365.

85 Jamadar, S. D., J. Fielding, and G. F. Egan. 2013. Quantitative meta-analysis of fMRI and PET studies reveals consistent activation in fronto-striatal-parietal regions and cerebellum during antisaccades and prosaccades. *Front Psychol* 4:1–15.

86 Jech, R., K. Mueller, M. L. Schroeter, and E. Ruzicka. 2013. Levodopa increases functional connectivity in the cerebellum and brainstem in Parkinson's disease. *Brain* 136:e234.

87 Kalbe, E., P. Calabrese, N. Kohn, R. Hilker, O. Riedel, H. U. Wittchen, R. Dodel, J. Otto, G. Ebersbach, and J. Kessler. 2008. Screening for cognitive deficits in Parkinson's disease with the Parkinson neuropsychometric dementia assessment (PANDA) instrument. *Parkinsonism Relat. Disord.* 14:93–101.

88 Kalbe, E., J. Kessler, P. Calabrese, R. Smith, A. P. Passmore, M. Brand, and R. Bullock. 2004. DemTect: a new, sensitive cognitive screening test to support the diagnosis of mild cognitive impairment and early dementia. *Int J Geriatr Psychiatry* 19:136–143.

89 Kassubek, J. 2014. Diagnostic procedures during the course of Parkinson's Disease. *Basal Ganglia* (in press). doi:10.1016/j.baga.2014.02.001

90 Kassubek, J., A. Danek, K. Del Tredici-Braak, M. W. Greenlee, and E. H. Pinkhardt. 2013. Das Auge als Zugang zur Pathophysiologie von Parkinson-Syndromen. *Nervenarzt* 84:909–917.

91 Kassubek, J., and E. H. Pinkhardt. 2011. Neuro-ophthalmological alterations in patients with movement disorders. PP. 306–315 *in* Uncommon Causes of Movement Disorders. N. Gálvez-Jiménez and P. Tuite, editors., 1st edition. *Cambridge University Press*. Cambridge (England).

92 Kelly, C., B. B. Biswal, R. C. Craddock, F. X. Castellanos, and M. P. Milham. 2012. Characterizing variation in the functional connectome: promise and pitfalls. *Trends Cogn. Sci.* (Regul. Ed.) 16:181–188.

93 Kheradmand, A., and D. S. Zee. 2011. Cerebellum and ocular motor control. *Front Neurol* 2.

94 Krajcovicova, L., M. Mikl, R. Marecek, and I. Rektorova. 2012. The default mode network integrity in patients with Parkinson's disease is levodopa equivalent dose-dependent. *J Neural Transm* 119:443–454.

95 Kruskal, W. H., and W. A. Wallis. 1952. Use of Ranks in One-Criterion Variance Analysis. *J Am Stat Assoc* 47:583–621.

96 Kwak, Y., S. Peltier, N. I. Bohnen, M. L. Müller, P. Dayalu, and R. D. Seidler. 2010. Altered resting state cortico-striatal connectivity in mild to moderate stage Parkinson's disease. *Front Syst Neurosci* 4:143.

97 Kwong, K. K., J. W. Belliveau, D. A. Chesler, I. E. Goldberg, R. M. Weisskoff, B. P. Poncelet, D. N. Kennedy, B. E. Hoppel, M. S. Cohen, and R. Turner. 1992. Dynamic magnetic resonance imaging of human brain activity during primary sensory stimulation. *Proc. Natl. Acad. Sci.* U.S.A. 89:5675–5679.

98 Laird, A. R., P. M. Fox, S. B. Eickhoff, J. A. Turner, K. L. Ray, D. R. McKay, D. C. Glahn, C. F. Beckmann, S. M. Smith, and P. T. Fox. 2011. Behavioral interpretations of intrinsic connectivity networks. *J Cogn Neurosci* 23:4022–4037.

99 Lee, M. H., C. D. Smyser, and J. S. Shimony. 2013. Resting-state fMRI: a review of methods and clinical applications. *AJNR Am J Neuroradiol* 34:1866–1872.

100 Leech, R., and D. J. Sharp. 2014. The role of the posterior cingulate cortex in cognition and disease. *Brain*. 137:12-32.

101 Lehmann, M., C. M. Madison, P. M. Ghosh, W. W. Seeley, E. Mormino, M. D. Greicius, M. L. Gorno-Tempini, J. H. Kramer, B. L. Miller, W. J. Jagust, and G. D. Rabinovici. 2013. Intrinsic connectivity networks in healthy subjects explain clinical variability in Alzheimer's disease. *Proc. Natl. Acad. Sci. U.S.A.* 110:11606–11611.

102 Leigh, R. J., and D. S. Zee. 2006. The Neurology of Eye Movements. (W. J. H. Sid Gilman, Ed.), 4th edition. *Oxford University Press*. New York.

103 Lemos, J., and E. Eggenberger. 2013. Saccadic intrusions: review and update. *Curr. Opin. Neurol.* 26:59–66.

104 Litvan, I., J. G. Goldman, A. I. Troster, B. A. Schmand, D. Weintraub, R. C. Petersen, B. Mollenhauer, C. H. Adler, K. Marder, C. H. Williams-Gray, D. Aarsland, J. Kulisevsky, M.

C. Rodriguez-Oroz, D. J. Burn, R. A. Barker, and M. Emre. 2012. Diagnostic criteria for mild cognitive impairment in Parkinson's disease: Movement Disorder Society Task Force guidelines. *Mov. Disord.* 27:349–356.

105 Luo, C., W. Song, Q. Chen, Z. Zheng, K. Chen, B. Cao, J. Yang, J. Li, X. Huang, Q. Gong, and H. F. Shang. 2014. Reduced functional connectivity in early-stage drug-naive Parkinson's disease: a resting-state fMRI study. *Neurobiol. Aging* 35:431–441.

106 MacAskill, M. R. M. R.skill, C. F. Graham, T. L. Pitcher, D. J. Myall, L. Livingston, S. van Stockum, J. C. Dalrymple-Alford, and T. J. Anderson. 2012. The influence of motor and cognitive impairment upon visually-guided saccades in Parkinson's disease. *Neuropsychologia* 50:3338–3347.

107 Machner, B., C. Klein, A. Sprenger, P. Baumbach, P. P. Pramstaller, C. Helmchen, and W. Heide. 2010. Eye movement disorders are different in Parkin-linked and idiopathic early-onset PD. *Neurology* 75:125–128.

108 Mann, H. B., and D. R. Whitney. 1947. On a Test of Whether one of Two Random Variables is Stochastically Larger than the Other. *Ann Math Statist* 18.

109 Martinez-Conde, S., S. L. Macknik, and D. H. Hubel. 2004. The role of fixational eye movements in visual perception. *Nat. Rev. Neurosci.* 5:229–240.

110 Martinez-Conde, S., S. L. Macknik, X. G. Troncoso, and T. A. Dyar. 2006. Microsaccades counteract visual fading during fixation. *Neuron* 49:297–305.

111 Martinez-Conde, S., J. Otero-Millan, and S. L. Macknik. 2013. The impact of microsaccades on vision: towards a unified theory of saccadic function. *Nat. Rev. Neurosci.* 14:83–96.

112 Mason, M. F., M. I. Norton, J. D. Van Horn, D. M. Wegner, S. T. Grafton, and C. N. Macrae. 2007. Wandering minds: the default network and stimulus-independent thought. *Science* 315:393–395.

113 McKeith, I. G. 2002. Dementia with Lewy bodies. *Br J Psychiatry* 180:144–147.

114 Mevel, K., G. Chetelat, F. Eustache, and B. Desgranges. 2011. The default mode network in healthy aging and Alzheimer's disease. *Int J Alzheimers Dis* 2011:535816.

115 Morel, A., M. N. Gallay, A. Baechler, M. Wyss, and D. S. Gallay. 2013. The human insula: Architectonic organization and postmortem MRI registration. *Neuroscience* 236:117–135.

116 Mosimann, U. P., R. M. Muri, D. J. Burn, J. Felblinger, J. T. O'Brien, and I. G. McKeith. 2005. Saccadic eye movement changes in Parkinson's disease dementia and dementia with Lewy bodies. *Brain* 128:1267–1276.

117 Müller, H. P., and J. Kassubek. 2013. Diffusion tensor magnetic resonance imaging in the analysis of neurodegenerative diseases. *J Vis Exp* 77. doi:10.3791/50427

118 Müller, H. P., A. Unrath, A. C. Ludolph, and J. Kassubek. 2007a. Preservation of diffusion tensor properties during spatial normalization by use of tensor imaging and fibre tracking on a normal brain database. *Phys Med Biol* 52:99–109.

119 Müller, H. P., A. Unrath, A. D. Sperfeld, A. C. Ludolph, A. Riecker, and J. Kassubek. 2007b. Diffusion tensor imaging and tractwise fractional anisotropy statistics: quantitative analysis in white matter pathology. *Biomed Eng Online* 6:42.

120 Munoz, D. P., and S. Everling. 2004. Look away: the anti-saccade task and the voluntary control of eye movement. *Nat. Rev. Neurosci.* 5:218–228.

121 Murphy, K., R. M. Birn, D. A. Handwerker, T. B. Jones, and P. A. Bandettini. 2009. The impact of global signal regression on resting state correlations: are anti-correlated networks introduced? *Neuroimage* 44:893–905.

122 Neggers, S. F., R. M. Diepen, B. B. Zandbelt, M. Vink, R. C. Mandl, and T. P. Gutteling. 2012. A functional and structural investigation of the human fronto-basal volitional saccade network. *PLoS ONE* 7:e29517.

123 Obeso, J. A., M. C. Rodriguez-Oroz, C. G. Goetz, C. Marin, J. H. Kordower, M. Rodriguez, E. C. Hirsch, M. Farrer, A. H. Schapira, and G. Halliday. 2010. Missing pieces in the Parkinson's disease puzzle. *Nat. Med.* 16:653–661.

124 Ogawa, S., D. W. Tank, R. Menon, J. M. Ellermann, S. G. Kim, H. Merkle, and K. Ugurbil. 1992. Intrinsic signal changes accompanying sensory stimulation: functional brain mapping with magnetic resonance imaging. *Proc. Natl. Acad. Sci. U.S.A.* 89:5951–5955.

125 Okun, M. S. 2013. Deep-brain stimulation for Parkinson's disease. *N. Engl. J. Med.* 368:483–484.

126 Olanow, C. W., and A. E. Lang. 2011. Prospects for Neuroprotective Therapies that can Modulate Non-Dopaminergic Features in Parkinson's Disease. PP. 455–461 *in*

Parkinson's Disease: Non-Motor and Non-Dopaminergic Features. C. W. Olanow, F. Stocchi, and A. E. Lang, editors. *John Wiley & Sons*. New Delhi.

127 Olanow, C. W., F. Stocchi, and A. E. Lang. 2011. The Dopaminergic and Non-Dopaminergic Features of Parkinson's Disease. PP. 1–14 *in* Parkinson's Disease: Non-Motor and Non-Dopaminergic Features. C. W. Olanow, F. Stocchi, and A. E. Lang, editors. *John Wiley & Sons*. New Delhi.

128 Olde Dubbelink, K. T., D. Stoffers, J. B. Deijen, J. W. Twisk, C. J. Stam, and H. W. Berendse. 2013. Cognitive decline in Parkinson's disease is associated with slowing of resting-state brain activity: a longitudinal study. *Neurobiol. Aging* 34:408–418.

129 Oldfield, R. C. 1971. The assessment and analysis of handedness: the Edinburgh inventory. *Neuropsychologia* 9:97–113.

130 Otero-Millan, J., R. Schneider, R. J. Leigh, S. L. Macknik, and S. Martinez-Conde. 2013. Saccades during attempted fixation in parkinsonian disorders and recessive ataxia: from microsaccades to square-wave jerks. *PLoS ONE* 8:e58535.

131 Otero-Millan, J., X. G. Troncoso, S. L. Macknik, I. Serrano-Pedraza, and S. Martinez-Conde. 2008. Saccades and microsaccades during visual fixation, exploration, and search: foundations for a common saccadic generator. *J Vis* 8:1–18.

132 Pa, J., S. Dutt, J. B. Mirsky, H. W. Heuer, P. Keselman, E. Kong, A. Trujillo, A. Gazzaley, J. H. Kramer, W. W. Seeley, B. L. Miller, and A. L. Boxer. 2014. The functional oculomotor network and saccadic cognitive control in healthy elders. *Neuroimage* 95C:61–68.

133 Park, A., and M. Stacy. 2009. Non-motor symptoms in Parkinson's disease. *J. Neurol.* 256 Suppl 3:293–298.

134 Parkinson, J. 1817. An essay on the shaking palsy. *Sherwood Neely and Jones*, London.

135 Pavan, A., D. Langgartner, and M. W. Greenlee. 2013. Visual short-term memory for global motion revealed by directional and speed-tuned masking. *Neuropsychologia* 51:809–817.

136 Pierrot-Deseilligny, C. h., R. M. Muri, T. Nyffeler, and D. Milea. 2005. The role of the human dorsolateral prefrontal cortex in ocular motor behavior. *Ann. N. Y. Acad. Sci.* 1039:239–251.

137 Pinkhardt, E. H., H. Issa, M. Gorges, R. Jürgens, D. Lule, J. Heimrath, H. P. Müller, A. C. Ludolph, W. Becker, and J. Kassubek. 2014. Do eye movement impairments in patients with small vessel cerebrovascular disease depend on lesion load or on cognitive deficits? A video-oculographic and MRI study. *J. Neurol.* 261:791–803.

138 Pinkhardt, E. H., R. Jürgens, W. Becker, F. Valdarno, A. C. Ludolph, and J. Kassubek. 2008. Differential diagnostic value of eye movement recording in PSP-parkinsonism, Richardson's syndrome, and idiopathic Parkinson's disease. *J. Neurol.* 255:1916–1925.

139 Pinkhardt, E. H., R. Jürgens, D. Lule, J. Heimrath, A. C. Ludolph, W. Becker, and J. Kassubek. 2012. Eye movement impairments in Parkinson's disease: possible role of extradopaminergic mechanisms. *BMC Neurol* 12.

140 Pinkhardt, E. H., and J. Kassubek. 2011. Ocular motor abnormalities in Parkinsonian syndromes. *Parkinsonism Relat. Disord.* 17:223–230.

141 Pinkhardt, E. H., J. Kassubek, S. Sussmuth, A. C. Ludolph, W. Becker, and R. Jürgens. 2009. Comparison of smooth pursuit eye movement deficits in multiple system atrophy and Parkinson's disease. *J. Neurol.* 256:1438–1446.

142 Poewe, W., and P. Mahlknecht. 2014. Movement disorders: new insights into disease mechanisms and treatment. *Lancet Neurol* 13:9–11.

143 Prodoehl, J., R. G. Burciu, and D. E. Vaillancourt. 2014. Resting state functional magnetic resonance imaging in Parkinson's disease. *Curr Neurol Neurosci Rep* 14:448.

144 Ptak, R., and R. M. Muri. 2013. The parietal cortex and saccade planning: lessons from human lesion studies. *Front Hum Neurosci* 7:254.

145 Purcell, B. A., P. K. Weigand, and J. D. Schall. 2012. Supplementary eye field during visual search: salience, cognitive control, and performance monitoring. *J. Neurosci.* 32:10273–10285.

146 Radua, J., M. L. Phillips, T. Russell, N. Lawrence, N. Marshall, S. Kalidindi, W. El-Hage, C. McDonald, V. Giampietro, M. J. Brammer, A. S. David, and S. A. Surguladze. 2010. Neural response to specific components of fearful faces in healthy and schizophrenic adults. *Neuroimage* 49:939–946.

147 Raichle, M. E. 2010. Two views of brain function. *Trends Cogn Sci* 14:180–190.

148 Raichle, M. E., A. M. MacLeod, A. Z. Snyder, W. J. Powers, D. A. Gusnard, and G. L. Shulman. 2001. A default mode of brain function. *Proc. Natl. Acad. Sci. U.S.A.* 98:676–682.

149 Raichle, M. E., and A. Z. Snyder. 2007. A default mode of brain function: a brief history of an evolving idea. *Neuroimage* 37:1083–1090.

150 Recchia, A., P. Debetto, A. Negro, D. Guidolin, S. D. Skaper, and P. Giusti. 2004. Alpha-synuclein and Parkinson's disease. *FASEB J.* 18:617–626.

151 Rektorova, I., L. Krajcovicova, R. Marecek, and M. Mikl. 2012. Default mode network and extrastriate visual resting state network in patients with Parkinson's disease dementia. *Neurodegener Dis* 10:232–237.

152 Ridderinkhof, K. R., M. Ullsperger, E. A. Crone, and S. Nieuwenhuis. 2004. The role of the medial frontal cortex in cognitive control. *Science* 306:443–447.

153 Riecker, A., W. Grodd, U. Klose, J. B. Schulz, K. Groschel, M. Erb, H. Ackermann, and A. Kastrup. 2003. Relation between regional functional MRI activation and vascular reactivity to carbon dioxide during normal aging. *J. Cereb. Blood Flow Metab.* 23:565–573.

154 Rodgers, J. L., and W. A. Nicewander. 1988. Thirteen Ways to Look at the Correlation Coefficient. *Am Stat* 42:59–66.

155 Ruxton, G. D. 2006. The unequal variance t-test is an underused alternative to Student's t-test and the Mann–Whitney U test. *Behav Ecol* 17:688–690.

156 Samii, A., J. G. Nutt, and B. R. Ransom. 2004. Parkinson's disease. *Lancet* 363:1783–1793.

157 Sauerbier, A., and K. R. Chaudhuri. 2013. Parkinson's disease and vision. *Basal Ganglia* 3:159–163.

158 Sauleau, P., P. Pollak, P. Krack, J. H. Courjon, A. Vighetto, A. L. Benabid, D. Pelisson, and C. Tilikete. 2008. Subthalamic stimulation improves orienting gaze movements in Parkinson's disease. *Clin Neurophysiol* 119:1857–1863.

159 Schall, J. D., and K. G. Thompson. 1999. Neural selection and control of visually guided eye movements. *Annu. Rev. Neurosci.* 22:241–259.

160 Schrag, A., and J. M. Schott. 2006. Epidemiological, clinical, and genetic characteristics of early-onset parkinsonism. *Lancet Neurol* 5:355–363.

161 Schuepbach, W. M., J. Rau, K. Knudsen, J. Volkmann, P. Krack, L. Timmermann, T. D. Hälbig, H. Hesekamp, S. M. Navarro, N. Meier, D. Falk, M. Mehdorn, S. Paschen, M. Maarouf, M. T. Barbe, G. R. Fink, A. Kupsch, D. Gruber, G. H. Schneider, E. Seigneuret, A. Kistner, P. Chaynes, F. Ory-Magne, C. Brefel Courbon, J. Vesper, A. Schnitzler, L. Wojtecki, J. L. Houeto, B. Bataille, D. Maltete, P. Damier, S. Raoul, F. Sixel-Doering, D. Hellwig, A. Gharabaghi, R. Krüger, M. O. Pinsker, F. Amtage, J. M. Regis, T. Witjas, S. Thobois, P. Mertens, M. Kloss, A. Hartmann, W. H. Oertel, B. Post, H. Speelman, Y. Agid, C. Schade-Brittinger, G. Deuschl, V. Czernecki, F. Pineau, V. Negovanska, M. L. Welter, J. C. Corvol, P. Cornu, B. Moller, A. Nebel, K. Witt, J. Raethjen, I. G. Meister, J. Kuhn, K. Donner, J. Kessler, A. Kuhn, B. Müller, K. Faust, S. Chabardes, P. Pollak, V. Fraix, O. Rascol, C. Arbus, L. Danet, S. J. Groiss, S. Elben, C. Hartmann, M. Sudmeyer, S. Ledily, A. Sauvaget, C. Trenkwalder, W. Richter-Dreske, T. Wachter, D. Weiss, A. Eusebio, J. P. Azulay, G. Polo, S. Pinto, J. Levin, S. Dornier, F. Pene, D. Hourton, M. Quintin, C. Hoffart-Jourdain, H. Brocvielle, M. Partowinia-Peters, K. Balthasar, M. Stein, S. Harnisch, A. Reuss, B. Aminossadati, C. Nasemann, V. Stoker, H. C. Diener, W. Lehmacher, Y. Keravel, K. Roosen, G. Deuschl, Y. Agid, C. Schade-Brittinger, A. Reuss, N. Burchardi, J. L. Houeto, P. Krack, and M. Schupbach. 2013. Neurostimulation for Parkinson's disease with early motor complications. *N. Engl. J. Med.* 368:610–622.

162 Shaikh, A. G., M. Xu-Wilson, S. Grill, and D. S. Zee. 2011. Staircase' square-wave jerks in early Parkinson's disease. *Br J Ophthalmol* 95:705–709.

163 Shulman, G. L., D. L. Pope, S. V. Astafiev, M. P. McAvoy, A. Z. Snyder, and M. Corbetta. 2010. Right hemisphere dominance during spatial selective attention and target detection occurs outside the dorsal frontoparietal network. *J. Neurosci.* 30:3640–3651.

164 Silver, N. C., and W. P. Dunlap. 1987. Averaging correlation coefficients: Should Fisher's z transformation be used? *J Appl Psychol* 72:146–148.

165 Smith, S. M., P. T. Fox, K. L. Miller, D. C. Glahn, P. M. Fox, C. E. Mackay, N. Filippini, K. E. Watkins, R. Toro, A. R. Laird, and C. F. Beckmann. 2009. Correspondence of the brain's functional architecture during activation and rest. *Proc. Natl. Acad. Sci. U.S.A.* 106:13040–13045.

166 Song, X. W., Z. Y. Dong, X. Y. Long, S. F. Li, X. N. Zuo, C. Z. Zhu, Y. He, C. G. Yan, and Y. F. Zang. 2011. REST: a toolkit for resting-state functional magnetic resonance imaging data processing. *PLoS ONE* 6:e25031.

167 Spoormaker, V. I., P. M. Gleiser, and M. Czisch. 2012. Frontoparietal Connectivity and Hierarchical Structure of the Brain's Functional Network during Sleep. *Front Neurol* 3:80.

168 Stern, Y. 2002. What is cognitive reserve? Theory and research application of the reserve concept. *J Int Neuropsychol Soc* 8:448–460.

169 Stern, Y. 2006. Cognitive reserve and Alzheimer disease. *Alzheimer Dis Assoc Disord* 20:112–117.

170 Terao, Y., H. Fukuda, A. Yugeta, O. Hikosaka, Y. Nomura, M. Segawa, R. Hanajima, S. Tsuji, and Y. Ugawa. 2011. Initiation and inhibitory control of saccades with the progression of Parkinson's disease - changes in three major drives converging on the superior colliculus. *Neuropsychologia* 49:1794–1806.

171 Tessitore, A., F. Esposito, C. Vitale, G. Santangelo, M. Amboni, A. Russo, D. Corbo, G. Cirillo, P. Barone, and G. Tedeschi. 2012. Default-mode network connectivity in cognitively unimpaired patients with Parkinson disease. *Neurology* 79:2226–2232.

172 Tomlinson, C. L., R. Stowe, S. Patel, C. Rick, R. Gray, and C. E. Clarke. 2010. Systematic review of levodopa dose equivalency reporting in Parkinson's disease. *Mov. Disord.* 25:2649–2653.

173 Trinh, J., and M. Farrer. 2013. Advances in the genetics of Parkinson disease. *Nat Rev Neurol* 9:445–454.

174 Uddin, L. Q., K. Supekar, H. Amin, E. Rykhlevskaia, D. A. Nguyen, M. D. Greicius, and V. Menon. 2010. Dissociable connectivity within human angular gyrus and intraparietal sulcus: evidence from functional and structural connectivity. *Cereb. Cortex* 20:2636–2646.

175 Unrath, A., H. P. Müller, A. Riecker, A. C. Ludolph, A. D. Sperfeld, and J. Kassubek. 2010. Whole brain-based analysis of regional white matter tract alterations in rare motor neuron diseases by diffusion tensor imaging. *Hum Brain Mapp* 31:1727–1740.

176 van den Heuvel, M. P., and H. E. Hulshoff Pol. 2010. Exploring the brain network: a review on resting-state fMRI functional connectivity. *Eur Neuropsychopharmacol* 20:519–534.

177 van den Heuvel, M. P., C. J. Stam, R. S. Kahn, and H. E. Hulshoff Pol. 2009. Efficiency of functional brain networks and intellectual performance. *J. Neurosci.* 29:7619–7624.

178 Van Dijk, K. R., T. Hedden, A. Venkataraman, K. C. Evans, S. W. Lazar, and R. L. Buckner. 2010. Intrinsic functional connectivity as a tool for human connectomics: theory, properties, and optimization. *J. Neurophysiol.* 103:297–321.

179 Van Dijk, K. R., M. R. Sabuncu, and R. L. Buckner. 2012. The influence of head motion on intrinsic functional connectivity MRI. *Neuroimage* 59:431–438.

180 van Oort, E. S., A. M. van Cappellen van Walsum, and D. G. Norris. 2014. An investigation into the functional and structural connectivity of the Default Mode Network. *Neuroimage* 90:381-389

181 van Stockum, S., M. R. MacAskill, D. Myall, and T. J. Anderson. 2013. A perceptual discrimination task results in greater facilitation of voluntary saccades in Parkinson's disease patients. *Eur. J. Neurosci.* 37:163–172.

182 Vincent, J. L., I. Kahn, A. Z. Snyder, M. E. Raichle, and R. L. Buckner. 2008. Evidence for a frontoparietal control system revealed by intrinsic functional connectivity. J. *Neurophysiol.* 100:3328–3342.

183 Walls, G. L. 1962. The evolutionary history of eye movements. *Vision Res* 2:69–80.

184 Weissenbacher, A., C. Kasess, F. Gerstl, R. Lanzenberger, E. Moser, and C. Windischberger. 2009. Correlations and anticorrelations in resting-state functional connectivity MRI: a quantitative comparison of preprocessing strategies. *Neuroimage* 47:1408–1416.

185 Whitwell, J. L., R. Avula, A. Master, P. Vemuri, M. L. Senjem, D. T. Jones, C. R. Jack, and K. A. Josephs. 2011. Disrupted thalamocortical connectivity in PSP: a resting-state fMRI, DTI, and VBM study. *Parkinsonism Relat. Disord.* 17:599–605.

186 Wichmann, T., and M. R. DeLong. 2013. The Basal Ganglia. PP. 982–998 *in* Principles of Neural Science. James H. Schwartz, Thomas M. Jessell, Steven A. Siegelbaum, Eric R. Kandel, editor. 5th edition. *McGraw-Hill*, *USA*, New York.

187 Wu, T., P. Chan, and M. Hallett. 2010. Effective connectivity of neural networks in automatic movements in Parkinson's disease. *Neuroimage* 49:2581–2587.

188 Wu, T., and M. Hallett. 2013. The cerebellum in Parkinson's disease. *Brain* 136:696–709.

189 Wu, T., X. Long, L. Wang, M. Hallett, Y. Zang, K. Li, and P. Chan. 2011. Functional connectivity of cortical motor areas in the resting state in Parkinson's disease. *Hum Brain Mapp* 32:1443–1457.

190 Wu, T., X. Long, Y. Zang, L. Wang, M. Hallett, K. Li, and P. Chan. 2009a. Regional homogeneity changes in patients with Parkinson's disease. *Hum Brain Mapp* 30:1502–1510.

191 Wu, T., J. Wang, C. Wang, M. Hallett, Y. Zang, X. Wu, and P. Chan. 2012. Basal ganglia circuits changes in Parkinson's disease patients. *Neurosci. Lett.* 524:55–59.

192 Wu, T., L. Wang, Y. Chen, C. Zhao, K. Li, and P. Chan. 2009b. Changes of functional connectivity of the motor network in the resting state in Parkinson's disease. *Neurosci. Lett.* 460:6–10.

193 Yeo, B. T., F. M. Krienen, J. Sepulcre, M. R. Sabuncu, D. Lashkari, M. Hollinshead, J. L. Roffman, J. W. Smoller, L. Zollei, J. R. Polimeni, B. Fischl, H. Liu, and R. L. Buckner. 2011. The organization of the human cerebral cortex estimated by intrinsic functional connectivity. *J. Neurophysiol.* 106:1125–1165.

194 Yerram, S., S. Glazman, and I. Bodis-Wollner. 2013. Cortical control of saccades in Parkinson disease and essential tremor. *J Neural Transm* 120:145–156.

195 Yugeta, A., Y. Terao, H. Fukuda, O. Hikosaka, F. Yokochi, R. Okiyama, M. Taniguchi, H. Takahashi, I. Hamada, R. Hanajima, and Y. Ugawa. 2010. Effects of STN stimulation on the initiation and inhibition of saccade in Parkinson disease. *Neurology* 74:743–748.

196 Zhang, D., and M. E. Raichle. 2010. Disease and the brain's dark energy. *Nat Rev Neurol* 6:15–28.

197 Zou, Q. H., C. Z. Zhu, Y. Yang, X. N. Zuo, X. Y. Long, Q. J. Cao, Y. F. Wang, and Y. F. Zang. 2008. An improved approach to detection of amplitude of low-frequency fluctuation (ALFF) for resting-state fMRI: fractional ALFF. *J. Neurosci. Methods* 172:137–141.

# Appendix

## Intrinsic Functional Connectivity Networks for all Groups in Detail

The subsequent section illustrates the more complete images of the 10 investigated brain maps according to **Figure 12** in the text. ICNs were identified for the PD-Cu (**Figure 20**) and the PD-CI (**Figure 21**) and the healthy elderly control group (**Figure 22**). In addition, **Figure 23** shows the 10 ICNs as the basis for the covariance analysis that were identified for all PD patients pooled from the PD-Cu and PD-CI group. Details for shown brain maps (**Figure 20**, **Figure 21**, **Figure 22**, **and Figure 23**) are given in **Figure 12**.

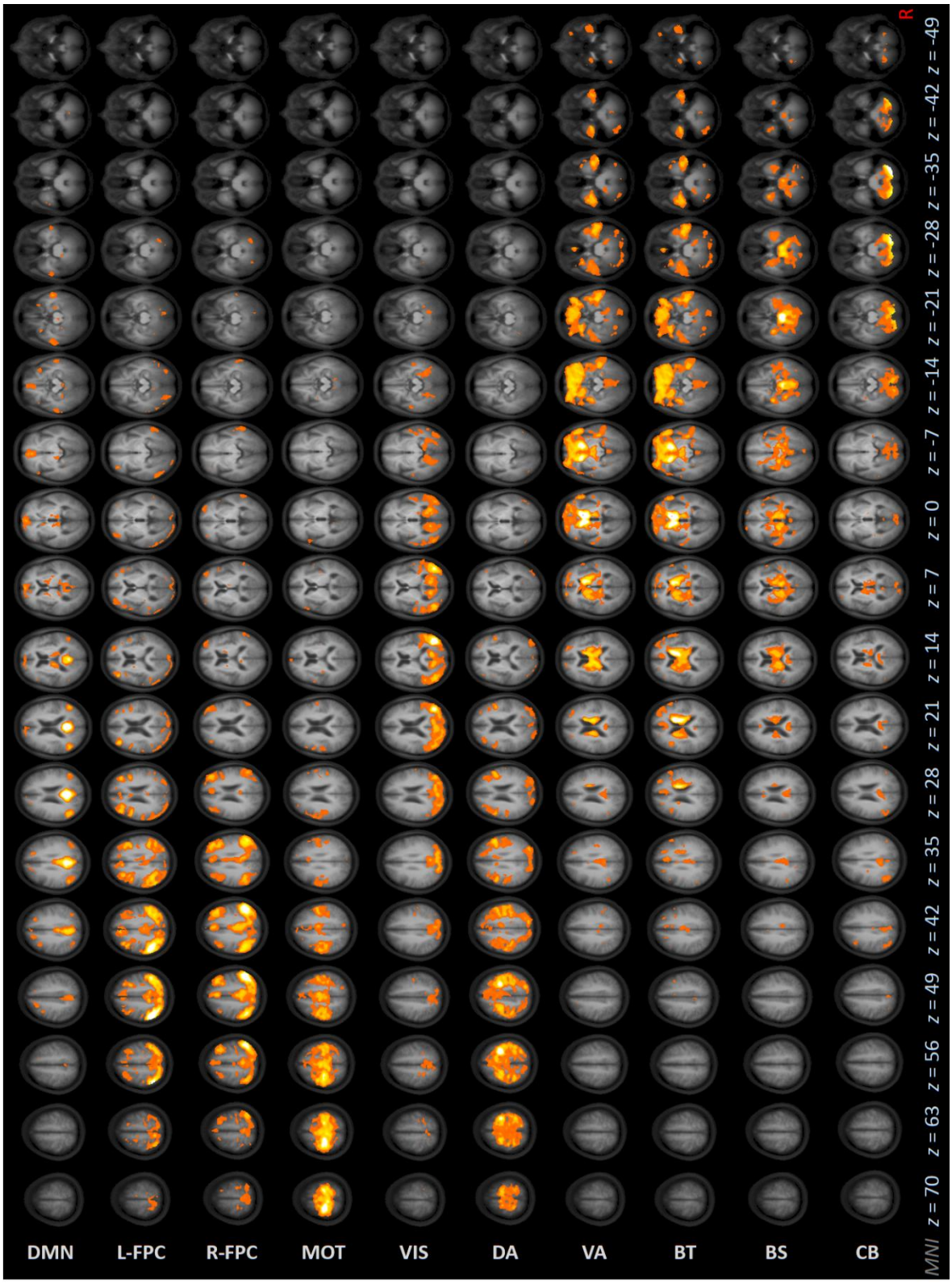


**Figure 20| Axial Slices of 10 Intrinsic Connectivity Networks for Cognitively Impaired Parkinson's Diseases Patients.** Complementary illustration according to **Figure 12**. Abbreviations: DMN, Default Mode; FPC, Frontoparietal Control; VIS, Visuospatial; MOT, Motor; DA, Dorsal Attention; VA, Ventral Attention; BT, Basal Ganglia-Thalamic; BS, Brainstem; CB, Cerebellum; MNI, Montreal Neurological Institute.

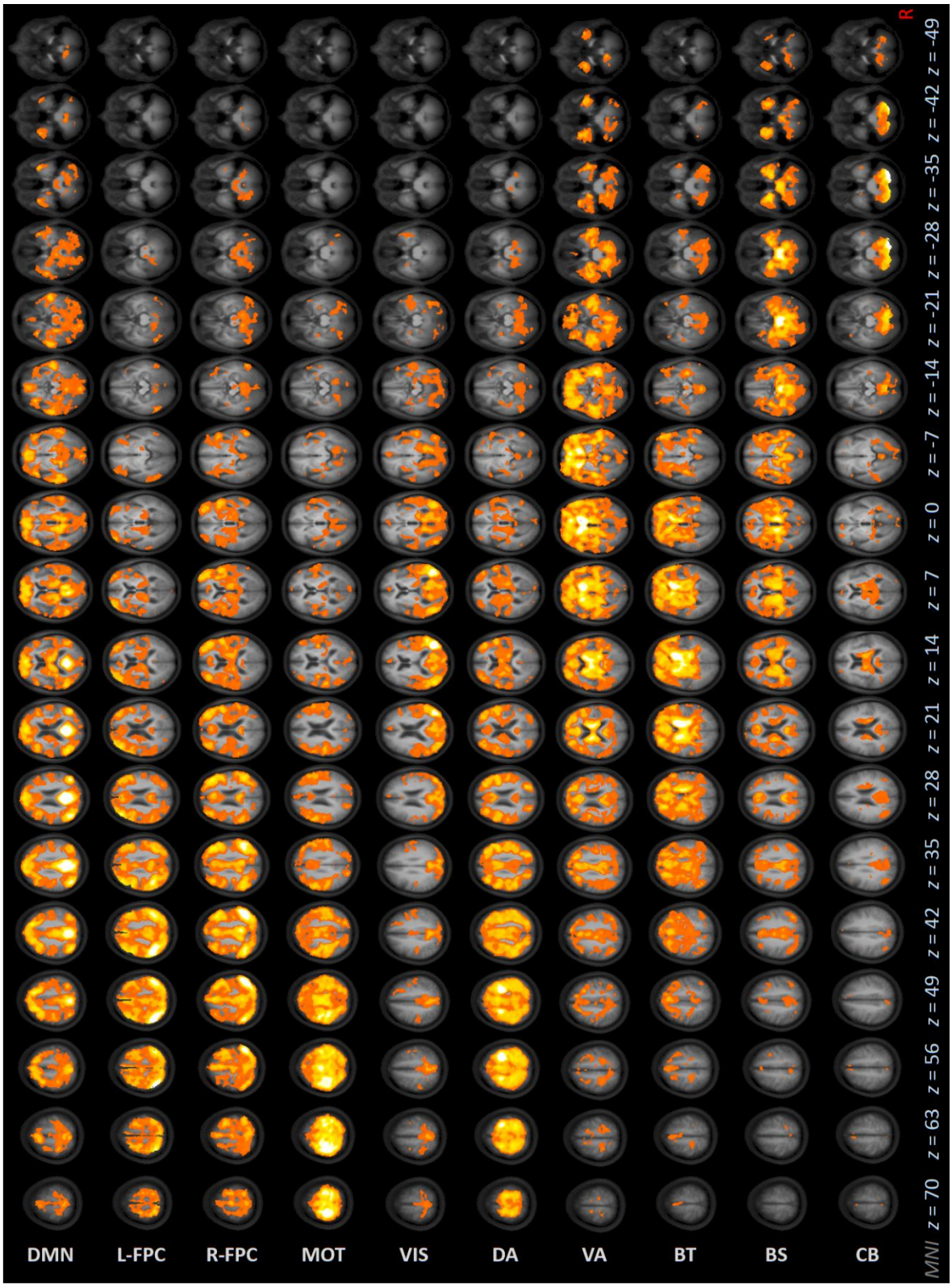


**Figure 21| Axial Slices of 10 Intrinsic Connectivity Networks for Cognitively Unimpaired Parkinson's Diseases Patients.** Complementary illustration according to **Figure 12**. Abbreviations: R, Right; L, Left; DMN, Default Mode; FPC, Frontoparietal Control; VIS, Visuospatial; MOT, Motor; DA, Dorsal Attention; VA, Ventral Attention; BT, Basal Ganglia-Thalamic; BS, Brainstem; CB, Cerebellum; MNI, Montreal Neurological Institute.

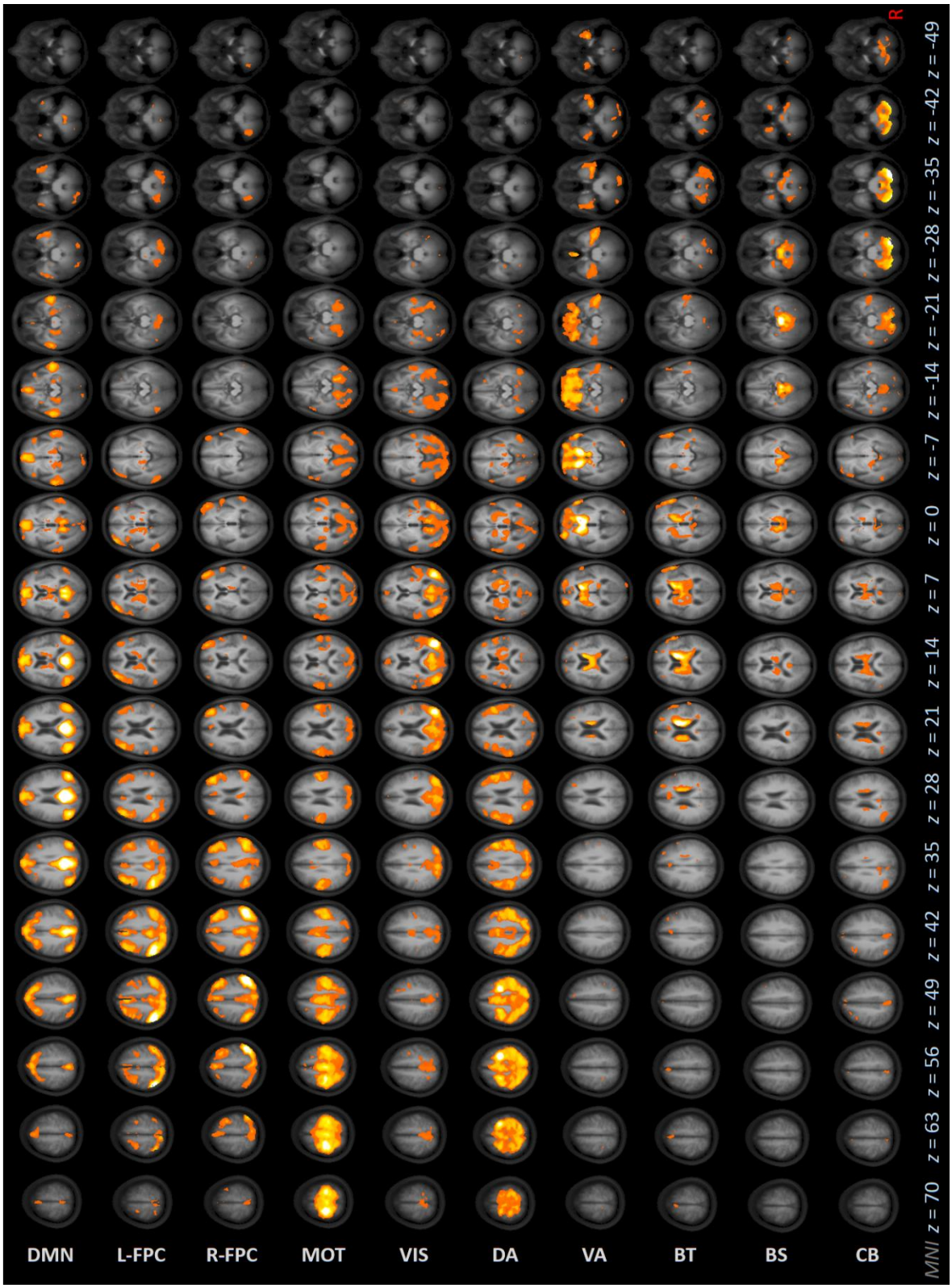


**Figure 22| Axial Slices of 10 Intrinsic Connectivity Networks for Healthy Control Subjects.** Complementary illustration according to **Figure 12**. Abbreviations: R, Right; L, Left; DMN, Default Mode; FPC, Frontoparietal Control; VIS, Visuospatial; MOT, Motor; DA, Dorsal Attention; VA, Ventral Attention; BT, Basal Ganglia-Thalamic; BS, Brainstem; CB, Cerebellum; MNI, Montreal Neurological Institute.

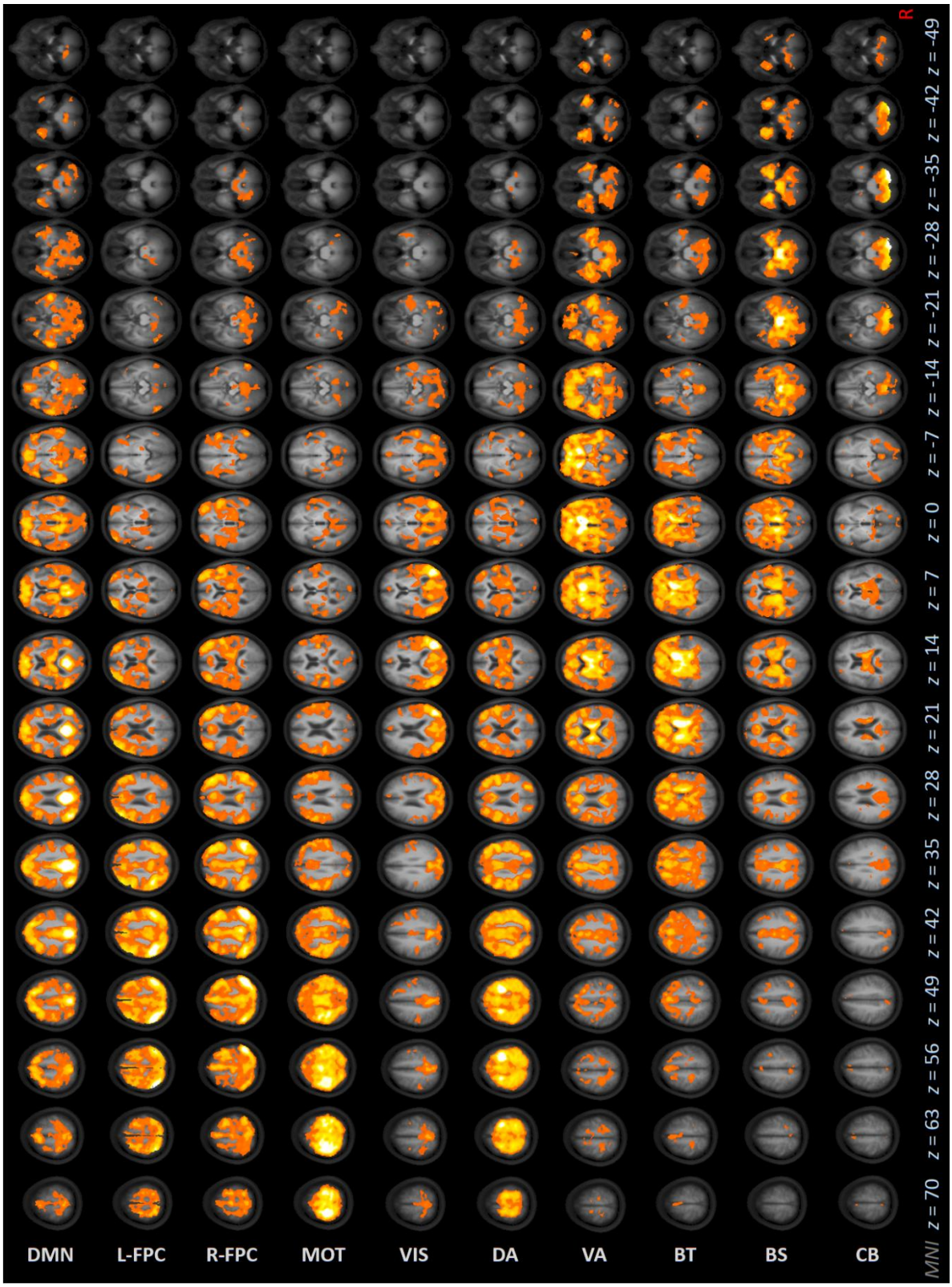


**Figure 23| Axial Slices of 10 Intrinsic Connectivity Networks for All Parkinson's Disease Patients.** Complementary illustration according to **Figure 12**. Abbreviations: R, Right; L, Left; DMN, Default and Mode; FPC, Frontoparietal Control; VIS, Visuospatial; MOT, Motor; DA, Dorsal Attention; VA, Ventral Attention; BT, Basal Ganglia-Thalamic; BS, Brainstem; CB, Cerebellum; MNI, Montreal Neurological Institute.

# Acknowledgement

It is a great pleasure to thank my supervisor Prof. Dr. Jan Kassubek, Vice Chairman of the Department of Neurology, University of Ulm, for both enabling this work and for his fabulous motivation in all aspects. I thank Prof. Dr. Albert C. Ludolph, the Chairman of the Department of Neurology, for his support of the present project. Also, I explicitly thank Priv.-Doz. Dr. Hans-Peter Müller for his brilliant help in the imaging processing. Furthermore, I thankfully acknowledge Prof. Dr. Wolfgang Becker, Dr. Reinhart Jürgens and Priv.-Doz. Dr. Elmar Pinkhardt for their many helpful advices in video-oculographic data analysis. Also, I am indebted to Ralph Kühne for his technical support in the oculomotor lab, Sonja Fuchs for the MRI data acquisition as well as Dorothea Hueske and Sandra Schüle for their great assistance in organizing the investigations. Finally, I want to thank all participants who contributed to this study.

Data were generated within the registry multicenter study “Demenz bei Parkinsonerkrankungen: Zukünftige Herausforderungen (LANDSCAPE)” as a subproject entitled: “Korrelation der MRT Bildgebung mit okulomotorischen Parametern”. The LANDSCAPE study is part of the Competence Network Degenerative Dementias (KNDD) which was funded by the German Federal Ministry of Education and Research (project number 01GI1008C).